CHIMIKA CHRONIKA

NEW SERIES

AN INTERNATIONAL EDITION
OF THE ASSOCIATION OF GREEK CHEMISTS

4/97

CMCRCZ 26(4), 405-604(1997)

ISSN 0366-693X

Volume 26, No 4 p.p. 405-604 October-December 1997

CHIMIKA CHRONIKA

NEW SERIES

AN INTERNATIONAL EDITION

Published by the Association of Greek Chemists (A.G.C.)
27 Kaningos str. Athens 106 82 Greece
Tel. 00301-3821524 FAX: 00301-3833597

Correspondence, submission of papers, subscriptions, renewals and changes of address should be sent to Chimika Chronika-New Series, 27 Kaningos street, Athens 106 82, Greece. The Notice to Authors is published in the first issue of each volume, or sent by request. Subscriptions: 25 USD per year (individuals), 50 USD (libraries)

Phototypesetted and Printed in Greece by EPTALOFOS S.A.
12, Ardittou Str. 116 36 ATHENS Tel. 9217.513

Υπεύθυνος σύμφωνα με το νόμο: Ν. Κατσαρός, Κάνιγγος 27, Αθήνα 106 82.

Responsible under law: N. Katsaros, 27 Kaningos St., Athens 106 82, Greece.

EDITORIAL FAREWELL

More than a quarter of a century elapsed since the journal of "Chimika Chronica - New Series" appeared as the International Edition of the Association of Greek Chemists. Up to that time, 1972, a part of the scientific publications of greek researchers were included in the official organ of the Association, XHMIKA XPONIKA, founded in 1936. The flourishing of chemical science and related fields in Greece, during the last decades, necessitated the separate edition of an international journal where scientific papers, notes, preliminary communications, letters and review articles appeared not only from greek laboratories but from other countries as well.

Now Greece belongs to the European Union since 1981 and as some members of the european family, namely Germany, France, Holland, Italy and Belgium have already proceeded jointly to publish three Chemical Journals, incorporating into these the journals of their six National Chemical Societies, it has been decided for Greece to participate in this effort. Therefore Chimika Chronika - New Series, suspends its separate edition, participating since the 1st of January 1998, in the three European publications. These are: "European Journal of Inorganic Chemistry", "European Journal of Organic Chemistry" and "Chemistry: a European Journal".

The editorial board of Chimika Chronika - New Series, owes grateful thanks to all participated authors during its publication period, especially for their collaboration and for giving an international esteem to this journal.

The Editorial Board

Chimika Chronika, New Series, 26, 405-428 (1997)

SYNTHESIS AND SELF-ASSEMBLY OF MODEL ω-SULFOZWITTERIONIC POLYMERS.

Nikos Hadjichristidis*, Stergios Pispas and Marinos Pitsikalis

University of Athens, Department of Chemistry,

Panepistimiopolis Zografou, 15771 Athens, Greece

(Received: December 23, 1997)

SUMMARY

The synthesis, dilute solution and bulk properties of a variety of polymers of different architectures (linear homopolymers, di- and triblock copolymers, and star homopolymers) having dimethylamine and sulfobetaine end groups are reviewed. The dimethylamine group at the chain-end was introduced by using anionic polymerization and (3-dimethylamino)propyllithium as initiator. The α,ω dimethylamine triblock copolymers and star homopolymers were formed by reacting the ω-functionalized living macromolecular species with the appropriate chlorosilanes. In all preparations high vacuum techniques were applied. The dimethylamine group was converted to sulfozwitterionic by reaction with cyclopropanesultone. Extensive molecular characterization proved the high molecular and compositional homogeneity of these materials. Their aggregation properties in dilute solutions of solvents with different polarity and selectivity, were studied by osmometry, viscometry and static and dynamic light scattering. The homopolymers and block copolymers of styrene have lower association numbers than the homopolymers of isoprene, probably because of the solvating effect of the phenyl rings on the dipolar groups. The bulk properties of end-functionalized homopolymers and diblock copolymers studied by SAXS, rheology and dielectric spectroscopy revealed new features of self organization at this low ionic content and extraordinary phase stability at high temperatures. The adsorption behavior of stars with different number of functionalized arms in dilute solutions was also investigated by ellipsometry showing different behavior compared to linear polymers.

KEY WORDS: ω-sulfozwitterionic polymers, anionic polymerization, (3-dimethylamino)propyllithium, chlorosilanes macromolecular architecture, association, dilute solution properties, adsorption, bulk properties, phase separation.

Introduction

The presence of even a few highly polar groups distributed along or fixed at the ends of nonpolar chains changes dramatically the properties of polymers[1-7]. These changes are caused by the association of the polar groups in the nonpolar environment of the hydrocarbon chains in the bulk or of the aliphatic solvents in solution.

The least complicated examples of polymeric associating species are chains with one polar group[8-9]. These simple materials offer an essential starting point for testing theories and establishing the basic structure-properties relationships, which will help to design associating polymers for practical applications.

Many routes exist for the synthesis of end functionalized polymers[10-12]. However, living anionic polymerization has been proven to be the most efficient method for synthesizing well defined macromolecules[13,14], since it gives the possibility to control many structural variables including placement of the ionic groups.

This review will be focused on the synthesis, the dilute solution and bulk properties of dimethylamine and sulfozwitterionic end-functionalized polymers having different architectures (linear homopolymers, diblock and triblock copolymers and star polymers with different number of functional groups). Emphasis will be given to the ω-functionalized polymers prepared by our group.

Synthesis and Characterization

Homopolymers.

3-Dimethylaminepropyl-lithium (DMAPLi) was used as initiator for the introduction of the dimethylamine group at the end of the polymer chain in all cases. DMAPLi was prepared by the reaction of the (3-dimethylamino)propyl chloride and Li dispersion according to Stewart et al.[15]. Styrene (St), Isoprene (Is) and butadiene (Bd) were polymerized with DMAPLi. The molecular weight distributions are low in the case of polydienes. Stoichiometric molecular weights are in very good agreement with the number average molecular weights, measured by osmometry, These results indicate that DMAPLi is an efficient initiator for the polymerization of isoprene and butadiene.

The microstructure of the polydienes was investigated using ^{1}H-NMR spectroscopy. The results clearly show an increase of the vinyl content with decreasing chain length, due to the presence of the polar dimethylamine group in the initiator.

The slow initiation rate was readily observed during the polymerization of St by the gradual appearance of the orange color[16], which is characteristic of the living polystyllithium chains. This fact in combination with the very fast propagation rate for the polymerization of St resulted in very broad molecular weight distributions (I=1.23-1.27). However when M_s<9300 the number average molecular weights, M_n, measured by SEC, calibrated with PS standards, were much higher than the stoichiometric ones, with the difference being increased as M_s was decreasing. This behavior can be explained by partial consumption of the

initiator. This was verified by the subsequent addition of Is, which produced polymers having bimodal distribution (figure 1). The lower molecular weight peak corresponds to NPI homopolymer, produced by the DMAPLi, which remained unreacted during the polymerization of St. The higher molecular weight peak is attributed to the NPSt-b-PI block copolymer with the amine group at the PSt chain end, produced by the cross-over reaction of NPStLi with Is. Addition of THF to the mixture of St and DMAPLi ([THF]/[Li]>3) gave polymers with close agreement between M_s and M_n and lower polydispersities.

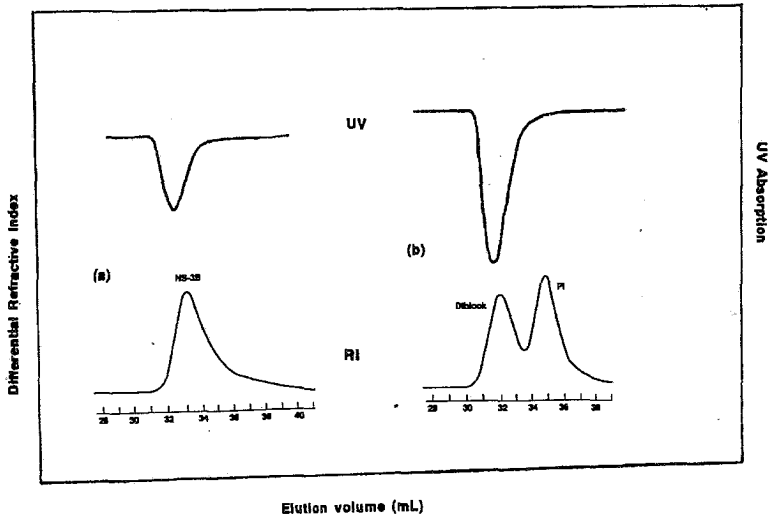

Figure 1. SEC chromatograms of (a) NS-3B (purified DMAPLi; polymerization in pure benzene) and (b) NS-3B after the addition of isoprene (first peak, diblock formed; second peak, homopolyisoprene formed by reaction of isoprene with unreacted DMAPLi). The wavelength of the UV detector was set at 260 nm were only PS absorbs significantly.

Diblock and Triblock Copolymers.

Block copolymers of styrene and isoprene having dimethylamine end-groups at the one or the other chain end were prepared using DMAPLi and sequential addition of monomers[17]. When Is is polymerized first a small amount of THF is added after the polymerization of the diene is completed to accelerate the crossover reaction with St. The reaction scheme is the following:

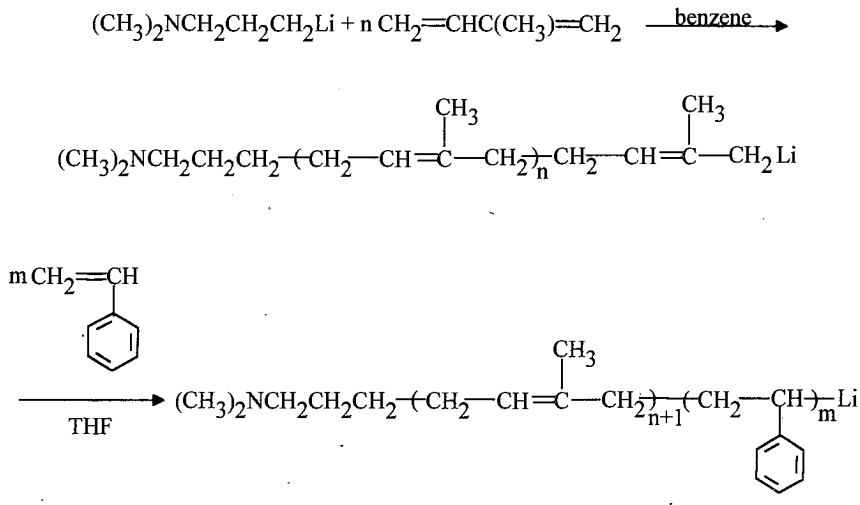

$$\xrightarrow[\text{THF}]{m\ CH_2{=}CH(C_6H_5)}$$

$$\xrightarrow[]{CH_3OH}$$ NIS

Triblock copolymers, having dimethylamine groups at both chain ends were prepared by coupling the diblock living chains with dimethyldichlorosilane, $(CH_3)_2SiCl_2$. The samples are designated with the letter N corresponding to the end-amine group, followed by the sequence of blocks starting with the block at which the functional group is attached.

ω-Functionalized Star Polyisoprenes and Mono-, Di- and Tri-ω-Functionalized Three Arm Star Polybutadienes.

Three and twelve arm PI stars[18] and three arm star PBd with all ends functionalized with dimethylamine groups[19] were synthesized by the reaction of end-functionalized living polymers with suitable chlorosilanes. As an example the reaction scheme for the synthesis of ω-dimethylamine three arm star PBd is given below:

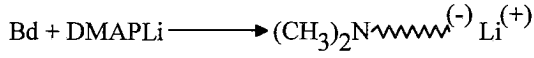

$$\xrightarrow[-3\ LiCl]{3\ NPBdLi + CH_3SiCl_3}$$

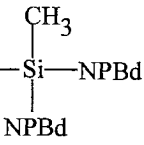

3N-3PBd

Three arm stars PBd with one or two end-amine groups were also prepared using suitable procedures[19]. The presence of one or two functional groups is denoted by the symbols 1N- and 2N- respectively, whereas the symbol 3PBd denotes a three arm star PBd. So 1N-3PBd is a three arm star PBd with one end-amine group. The following numbers differentiate samples of the same series. A schematic representation of the reaction sequence used for the synthesis of samples 1N-3PBd is shown below:

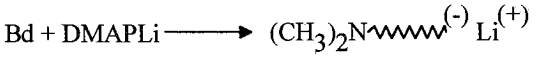

NPBdLi

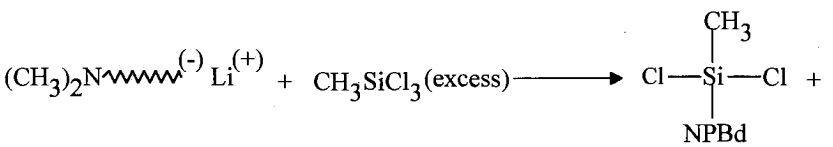

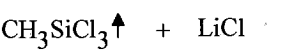

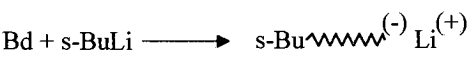

PBdLi

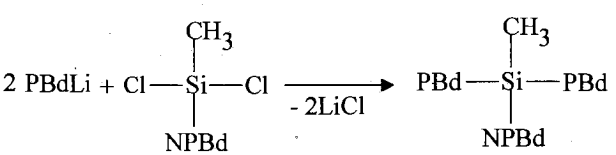

1N-3PBd

A living end-functionalized PBd chain was prepared in benzene using DMAPLi as initiator. The living polymer solution was added to a large excess of methyltrichlorosilane (Si-Cl/C-Li ~100/1) in order to prepare the methyldichlorosilane-capped PBd. Excess linking agent was removed under vacuum line conditions. The polymer was repeatedly redissolved and pumped to extract traces of the silane from the bulk polymer. Finally benzene was distilled into the reactor to dissolve the ω-methyldichlorosilane PBd arm.

The next step involved the synthesis of the unfunctionalized arm, using s-BuLi as initiator. A small excess of this living polymer was coupled with the macromolecular linking agent to produce the final product. Termination of the residual active anions with degassed MeOH and subsequent fractionation to remove the excess Pbd arm gave the pure 1N-3PBd star polymer.

A similar procedure is followed for the synthesis of 2N-3PBd stars, starting from the reaction of the living unfunctionalized arm with excess methyltrichlorosilane followed, after the removal of the excess linking agent, by the coupling reaction of the dichlorosilane-capped arm with a small excess of the amine-functionalized living arm. All these procedures were monitored by SEC.

In the case of samples with low arm molecular weight ($M_n<10^4$), in order to prevent the formation of the diadduct the steric hindrance of the living arm was increased by reaction with diphenylethylene (DPE). A few drops of THF were added to accelerate the crossover reaction. By using this procedure the coupling reaction was minimized using this procedure giving less than 3 % of the byproduct.

The molecular characteristics of representative samples synthesized as described above are given in Table I.

Table I. Molecular characteristics of ω-functionalized polymers of different architectures

Sample	$M_w x10^{-4}$	$M_n x10^{-4}$	$I=M_w/M_n$ (SEC)	%wt PS
NPI	4.56	4.53	1.04	
3NPI	7.2	6.6	1.05	
NIS-3	2.44	2.25	1.06	28
NSI-1	6.96	6.12	1.06	30
NSISN-1	7.63	7.02	1.05	36
NISIN-1	6.98	6.27	1.05	27
1N-3PBd30	11.1	10.4	1.06	
2N-3PBd30	62.4	61.8	1.06	
3N-3PBd40	93.1	91.4	1.06	

All samples indicate high molecular and compositional homogeneity as proved by the combined characterization results (SEC, LALLS, MO, VPO, UVand NMR)

Post-polymerization Reaction of the Amine-Functionalized Polymers.

The amine end groups can be easily transformed to ionic dipoles by reaction with 1,3 cyclopropane sultone[20,21], illustrated in the following scheme:

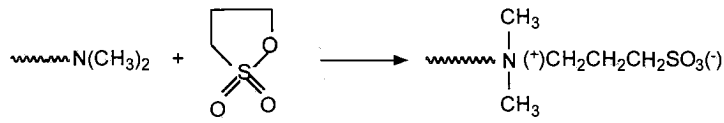

The reaction takes place in dilute THF solutions (2-3 w/v %) at 70 °C for several days using an excess of the sultone over the amine groups (sultone/amine = 10/1). For the PBd samples inert atmosphere was used. Under these conditions this post-polymerization reaction is free of side reactions (crosslinking, degradation etc.) as

was verified by SEC. Similar peaks with the corresponding amine-capped polymers were observed in $CHCl_3$ in all cases.

It is difficult to determine the extent of the conversion of the t-amine groups to sulfobetaine groups due to the low concentration of these groups in the polymer chains. However qualitative results by ^{1}H-NMR show that the reaction yield is very high[17,22]. In figure 2 the ^{1}H-NMR spectra of linear block copolymer NIS-5 and the corresponding zwitterion sample are given. The peak at 2.2 ppm is assigned to the methyl protons of the carbons which are attached to the nitrogen atom. This peak has completely disappeared after the reaction with 1,3 cyclopropane sultone and two new peaks at 3.15 and 2.95 ppm have emerged. These peaks are assigned to the methyl protons attached to the positively charged nitrogen atom of the zwitterionic group and to the methylene protons of the carbon which is attached to the sulfur atom respectively[21,23].

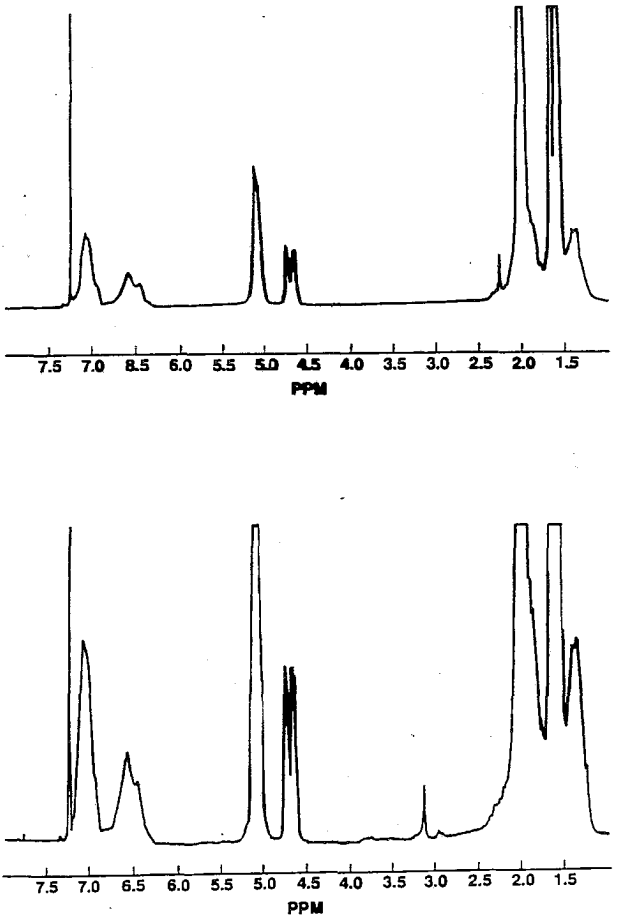

Figure 2. ^{1}H-NMR spectra of samples NIS-5 (top) and ZwIS-5 (bottom) in $CDCl_3$.

Dilute Solution and Bulk Properties

Homopolymers.

The dilute solution properties of ω-functionalized linear homopolymers were studied by membrane osmometry (MO), low angle laser light scattering (LALLS), viscometry and dynamic light scattering (DLS) in various non-polar solvents[18,24,25]. The conclusions obtained from these studiess can be summarized in the following:

a. The dimethylamine-cappped samples present evidence of weak association in non-polar solvents (cyclohexane, CCl_4, toluene) which are good solvents for the polymeric tails.

b. The zwitterion-capped samples form large aggregates in these solvents with aggregation numbers increasing with decreasing molecular weight of the parent material. However, aggregation numbers for PS homopolymers are consistently lower than those obtained for polydiene homopolymers probably because of the solvating effect of the phenyl rings on the dipolar groups.

c. The aggregates are polydisperse as concluded by combination of results from LALLS and MO and independently by DLS measurements.

d. The aggregation numbers decrease when small amounts of alcohol are added to the solution. This has the effect of changing the solvent polarity without changing its quality towards the nonpolar tails. However aggregation persists even at 5% alcohol.

e. The associates behave hydrodynamically as star polymers as evidenced by the increasing k_H values with increasing degree of association and by the good agreement between experimental aggregation numbers and those calculated assuming the star model.

f. The linear head packing model describes fairly well the structures of the aggregates.

Detailed studies by small angle x-ray scattering (SAXS) were performed on low molecular weight zwitterion-capped polyisoprenes[26]. For samples having $14000<M_w<28000$ the scattering profiles show that the aggregates form a body-centered cubic lattice.

Figure 3 shows the corresponding scattering profiles for the lower molecular weight samples ($2200<M_w<4650$). The peaks can be indexed on a two dimensional hexagonal lattice of tubes. In other words the aggregates have a tubular structure with the tubes closed packed on a two dimensional hexagonal lattice with crystalline order. The core is formed by the dipoles which are arranged in an antiparallel configuration as shown in figure 4.

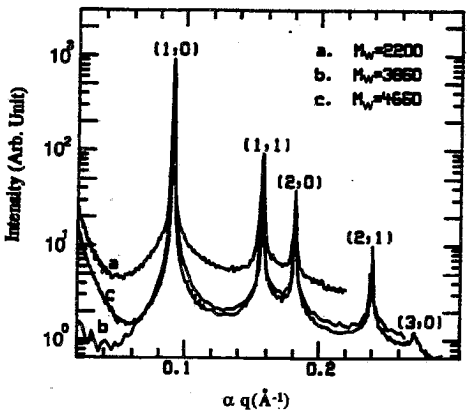

Figure 3. X-ray scattering profiles of zwitterion-capped polyisoprene samples with molecular weights of 4650, 3850, and 2200.The profiles of the last two samples have been shifted by a factor (α) to make the first peak positions overlap.

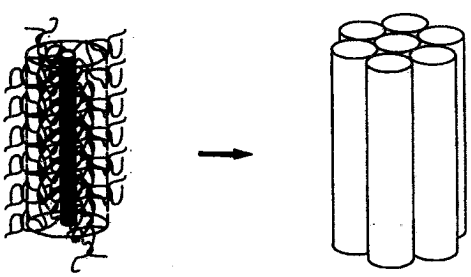

Figure 4. A schematic representation of the formation of two-dimensional lattices of the close-packed tubular aggregates.

It is characteristic that a very small volume fraction of ionic species (<7.5 %) is able to promote a hexagonal cylindrical morphology with long range order in contrast to usual block copolymers.

The viscoelastic behavior in the melt state of end-functionalized polyisoprenes was also investigated[27]. The amine-capped samples behave more or less as conventional polyisoprenes indicating that only weak association may exist in the melt state. The situation is very different for the zwitterion-cappped polymers with the dynamic moduli broadened and shifted to much lower frequencies. For samples with high base molecular weights the viscoelastic behavior more closely resembles the behavior of conventional star polymers.

Samples with intermediate and lower molecular weights show a second relaxation regime at very low frequencies. A characteristic example is given

in figure 5. It is observed that some resemblance exist between the zwitterion and star polymer only at intermediate and high frequencies.

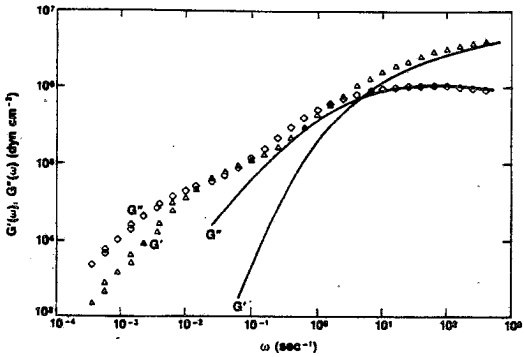

Figure 5. Comparison of dynamic moduli for a four-arm polyisoprene star and a monofunctional zwitterion polyisoprene in the melt state at 25°C . Data for the star (M_a=4.4 x 10^4) are shown by the solid lines; the points are data for a sample with M_o=4.61 x 10^4.

The viscosities of the zwitterion polymers, especially of low and intermediate molecular weights are much larger than those predicted assuming the star model. Consequently it is reasonable to consider that the aggregates have extended morphologies (lamellae, strings etc.). Only in the case of low aggregation numbers, observed for samples of high base molecular weight the behavior is similar to those of star polymers because the core size is rather small and can be considered as the star's center. The extended structures are delicate in a mechanical sense making it possible to explain the remarkable strain sensitivity observed at low frequencies. It is evident that close relation exists between the results obtained by melt rheology and SAXS.

ω-Functionalized Block Copolymers of Styrene and Isoprene.

The association behavior of end-functionalized diblock and triblock copolymers of isoprene and styrene was studied in CCl_4, which is a nonpolar good solvent for both blocks[17,28]. The aggregation numbers, N_w are almost the same whether the zwitterion group is linked at the PI or the PS chain end. Their value depends strongly on the M_w of the base polymer. N_w decreases with increasing molecular weight of the precursor polymer, M_0. The variation of N_w with M_0 for the case of ZwPI in cyclohexane[18] and CCl_4[17], PS in CCl_4*(27)* di- and triblock copolymers in CCl_4[17] is given in figure 6. The aggregation numbers for ZwPI are lower in CCl_4 than in cyclohexane due to the higher polarizability of the former solvent. Another point that deserves attention is that the aggregation numbers of the copolymers are closer to those determined for the ZwPS samples than the ZwPI samples in CCl_4. The aromatic rings, due to their high polarizability cause some kind of solvation, thus leading to reduced N_w values. The aggregation

numbers are almost the same for the monofunctional and difunctional samples of the same molecular weight. This is rather surprising, since the difunctional polymers form gels at concentrations lower than c_{gel} (c_{gel}=0.5 c*). A higher aggregation number would be expected for these samples due to the higher probability of forming aggregates as the result of the existance of two polar groups per chain. The result can be seen as evidence of intramolecular association in dilute solutions since intermolecular aggregation at higher concentrations is the reason for the formation of gels.

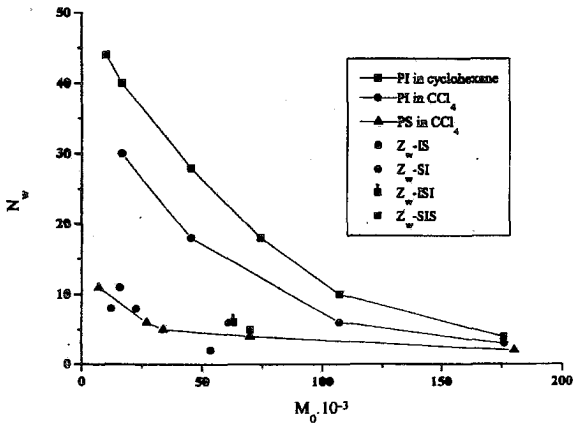

Figure 6. Dependence of the weight average aggregation number, N_w from the base molecular weight, M_o for various polymer series.

DLS was used to study the hydrodynamic properties of the end-functionalized copolymers. The zwitterionic polymers have a substantially different behavior than their precursors, due to the formation of aggregates in CCl_4. The values of the diffusion coefficient at infinite dilution, D_0 are lower, the R_H values higher and the polydispersity values are higher leading to the conclusion that aggregates are polydisperse. The k_D values are negative in most cases, due to the aggregation process and is consistent with the low A_2 values obtained by LALLS.

Viscosity measurements were also performed to complement the DLS data. The [η] values for the zwitterionic samples are considerably higher than those for the amine-capped samples and the reduced viscosity vs concentration plots are not always linear. The Huggins plots are concave upwards in some cases and especially for the difunctional samples.

The nonlinear dependence of the reduced viscosity on concentration is an indication that the association number changes by increasing concentration, something which is expected to be more pronounced in the case of the difunctional triblocks.

The stability of the aggregates was tested by adding small amounts of an alcohol, namely 2-methylcyclohexanol (at 1% and 5% content), which is isorefractive with CCl_4. The association is reduced in the presence of the alcohol,

but even at 5% alcohol content there are samples remained aggregated. With increasing alcohol content the aggregation numbers are reducing, the A_2 values are increasing and the k_H values are decreasing. LALLS experiments on solutions prepared long before (more than one year) measurement showed that the aggregation numbers remain the same leading to the conclusion that the association process is an equilibrium one.

SAXS, rheology and dielectric spectroscopy were used to study the statics and dynamics of the end-functionalized block copolymer[29,30]. SAXS profiles from the amine and the corresponding zwitterion-capped samples confirm the existence of ionic aggregation and two kinds of microphase separation. One between the ionic and nonpolar phase and one between the PI and PS. A characteristic example is given in figure 7. The following features were observed: a) a background originating from density and concentration fluctuations, b) an excess intensity at low Q which is related to heterogeneities with long correlation lengths in the case of ionomers[31], c) the microdomain peak[32] characteristic of the microphase separation process between PI and PS phases and d) the peak related to the polar groups, which has emerged in the case of the zwitterionic sample.

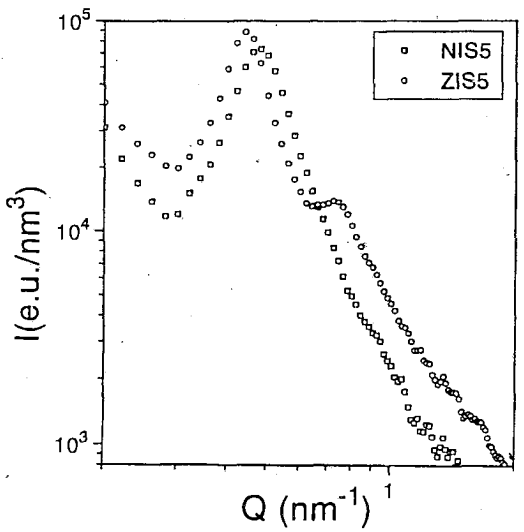

Figure 7. SAXS profiles for two ω-functionalized IS diblock copolymers at T=303 K. Data have been corrected for the density fluctuations, and the intensities are given in absolute units.

The last three characteristics are temperature dependent with the aggregate peak intensity being much less sensitive to changes of temperature for the specific temperature range used for the experiment. The microdomain peak intensity has a

similar temperature dependence for both the amine and the zwitterion-capped copolymers.

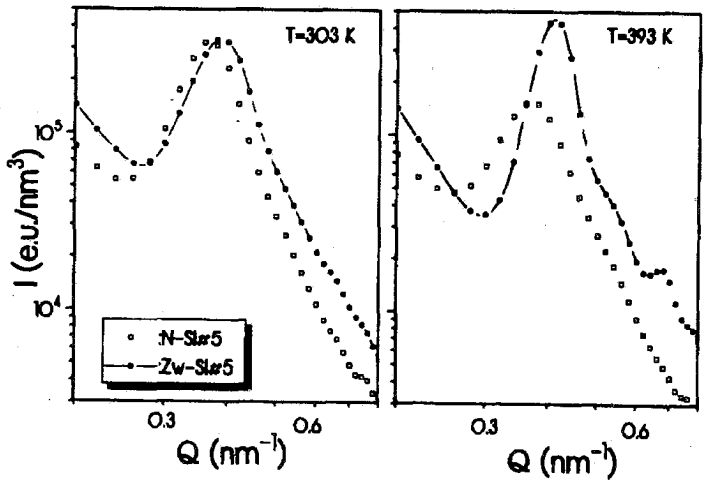

Figure 8. Comparison of the SAXS profiles for the dimethylamino- and zwitterion-substituted ω-functionalized copolymers at two temperatures.

A completely different behavior is observed when the functional group is attached to the PS chain-end, as shown in figure 8. The microdomain peak dominates the scattering pattern in this case. The peak increases in intensity, sharpens and moves to slightly higher Q values with increasing temperature. The absence of any dissolution process clearly indicates that the microdomain structure is stabilized by the ionic aggregates. In the case of ZwSI samples the ionic groups are trapped within the PS phase without being able to aggregate. The increase of temperature increases the mobility of the polar groups leading to the formation of aggregates within the "hard" phase. This is schematically illustrated in figure 9 for both systems, ZwIS and ZwSI. As a concequence the incompatibility of PI and PS is enhanced and a completely different phase behavior is observed. In this way by only changing the position of the polar group, from the PI to the PS chain-end it is possible to change the phase diagram of block copolymers[30].

The conclusions derived from SAXS experiments were confirmed by rheology. In the case of the zwitterionic copolymers an extension of the rubbery plateau is observed. This behavior is explained considering that the aggregates act as physical crosslinks within the PI phase. Furthermore within the temperature range investigated no sign of an order-disorder transition was observed in agreement with SAXS results, meaning that the cubic microdomain structure is stable up to high temperatures.

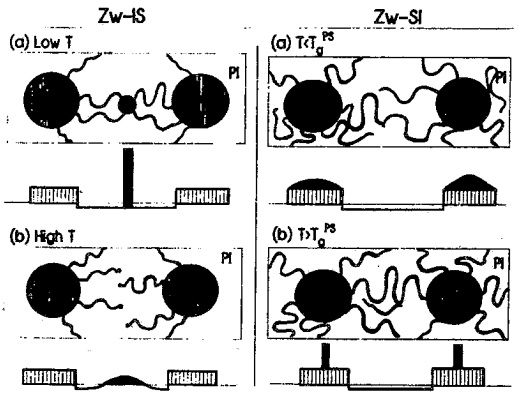

Figure 9. Schematic illustration of the microstructures in ω-functionalized SI block copolymers, showing the Zw-IS (left) and Zw-SI (right) cases at low (upper) and high (lower) temperatures. The corresponding electron density distributions are also shown.

Dielectric spectroscopy also offers the means to verify the conclusions drawn so far through the selective probing of the PI chains. In the case of ZwIS copolymers in addition to the fast segmental and the slow normal mode an intermediate process, with activation parameters which are reminiscent of the segmental process is observed. This intermediate process arises from the regions of the reduced mobility created around the aggregates impending the motion of the PI chains in their immediate environment. An intermediate Tg value could not be detected by differential scanning calorimetry, since DSC is not so sensitive and the size of these regions is very small in order to detect, however an increase on the Tg of the polyisoprene block has been observed at low molecular weights[33].

The combination of the association of polar groups in a nonpolar solvent with the micellization process, promoted in selective solvents leads to interesting solution behavior. The dilute solution properties of ω-functionalized diblock copolymers having dimethylamine or zwitterion groups at the PS chain-end were studied in n-decane a nonpolar selective solvent for the PI blocks[34].

The presence of the polar groups introduces another factor capable to enhance the aggregation numbers for the zwitterionic samples in n-decane, a selective solvent for PI. Much lower N_w, comparable to ones found for unfunctionalized diblocks, were observed for the amine-capped copolymers, meaning that the amine groups are not polar enough to bring any changes to the association process. Typical LALLS plots are given in figure 10.

From DLS measurements negative k_D values were obtained for the amine-capped polymers as expected having in mind the negative A_2 values. For the

zwitterionic samples the k_D values were positive meaning that the equilibrium is shifted in favor of the micelles.

Viscometry measurements were also conducted. The Huggins coefficients increase with increasing molecular weight for the amine-capped polymers. This behavior is consisted with a star-like structure. For the zwitterionic samples constant k_H values, around 1.1 were obtained, meaning that rather compact structures exist in solution.

The R_v and R_H values are identical within experimental error for the amine polymers but for the zwitterionic polymers R_H is much higher than R_v. The former result is consistent with star-like structures, whereas the latter can be explained considering the high sensitivity of DLS to large structures and/or to the development of shear forces in the capillary tube able to disrupt the larger aggregates. The fact that the polar core probably has an elongated structure with antiparallel placement of the zwitterionic groups is able to support the above assumption, since a break of the association at one point can cause a large reduction of the micelle's size.

Intensity vs temperature measurements at concentrations where micelles are the dominant species revealed that the micelles formed by the zwitterionic copolymers are stable at much higher temperatures than the ones made of amine-capped precursors. It seems that in the former case the high temperature resistive ionic cores stabilise the micelles (figure 10(c)).

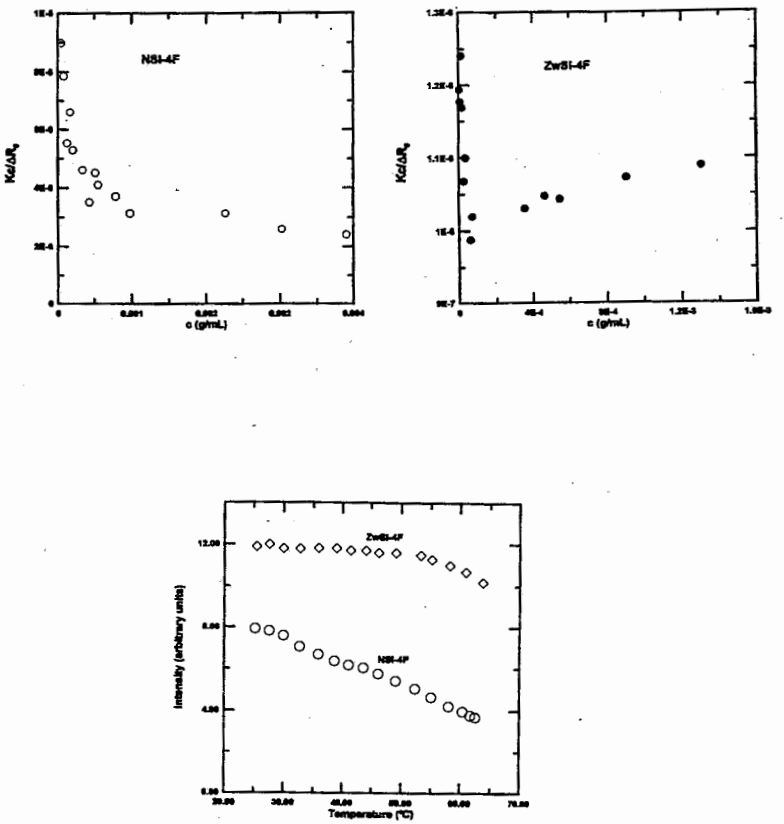

Figure 10. $Kc/\Delta R_\theta$ vs concentration plots given for (a) sample NSI-4F and (b) sample ZwSI-4F in n-decane at 25°C. (c) Intensity vs temperature plot for the same samples at c= 2.800 x 10^{-3} g/mL for NSI-4F and c= 1.629 x 10^{-3} g/mL for ZwSI-4F.

3-Arm Star Polybutadienes with End-Functional Groups.

The amine-capped star polymers provide no evidence of association in cyclohexane, whereas strong association is observed in the case of zwitterionic samples. It is evident that (a) among the different series of polymers the aggregation number decreases with increasing number of functional groups and (b) among the samples with the same number of polar groups the degree of association decreases with increasing molecular weight of the precursor polymer, due to excluded volume repulsions. These results are given schematically in figure 11.

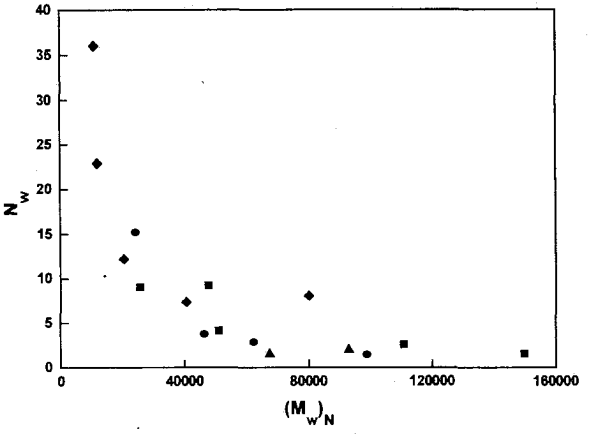

Figure 11. Weight-average aggregation number, Nw vs base molecular weight (Mw)N of the star polymers: Zw-1N-3PBd (■), Zw-2N-3PBd (●), and Zw-3N-3PBd (▲). The data for linear polybutadienes are also given (◆).

The multifunctional samples, especially the trifunctional stars form gels even at low concentrations. This result connected with the low aggregation numbers for these samples leads to the conclusion that in very dilute solution intramolecular association dominates and by increasing concentration there is a rather sharp transition from intramolecular to intermolecular association, able to produce stable gels.

The degrees of association of the monofunctional stars are lower than those measured for the linear ω-functionalized PBd, meaning that the star structure prevents the association due to the steric hindrance caused by the unfunctionalized arms.

The hydrodynamic behavior of the functionalized stars was studied by DLS and viscometry[35]. The increased values of polydispersity (μ_2/Γ^2>0.2) indicate that the aggregates produced by the zwitterionic samples are polydisperse in agreement with the MO and LALLS results. Low k_D values were observed in most cases as a consequence of the decreased second virial coefficients.

The strongly negative k_D values for the trifunctional stars indicate the existence of strong hydrodynamic interactions between the macromolecular chains eventhough these samples have low aggregation numbers and show only small increases in R_H compared to their precursors. This behavior can be seen as evidence of intramolecular association in very dilute solutions. For the case of difunctional stars the above analysis is not straightforward. It is clear that intermolecular association cannot be ruled out.

For the monofunctional samples there is no possibility of intramolecular association. The star model can be used for these samples considering that the aggregates correspond to star polymers and their precursors to the arms of these stars. Consequently it is possible to calculate the aggregation numbers from DLS measurements, N_{DLS}. The results show that the aggregates formed from the monofunctional samples behave hydrodynamically as star polymers with functionality equal to $2N_w$. It seems that the two unfunctionalized arms anchored at the periphery of the aggregates are responsible for the overall size of the micelles.

The conclusions drawn by DLS are verified by viscometry for the amine-capped polymers. The zwitterionic trifunctional samples have lower intrinsic viscosities than their precursors but the k_H values are extremely high, indicating the presence of strong hydrodynamic interactions. This behavior implies that in very dilute solutions compact structures are formed through intramolecular association. This result is in agreement with LALLS and DLS data.

Comparative examination of R_v and R_H values show that $R_v<R_H$ for the zwitterionic polymers, meaning that the aggregates dessociate to some extent in the capillary tube, due to the shear forces applied therein. These forces are not very strong indicating that the critical shear rate is very small. Only for samples with low N_w there is good agreement between R_v and R_H. It seems that the increased steric repulsions introduced by the unfunctionalized arms lead to the formation of not so strong associates as in the case of linear polymers.

The adsorption behavior of functionalized linear and three arm star PBd was studied by ellipsometry at 20°C in a mixed solvent of cyclohexane and toluene (50 % by volume)[36]. Both solvents are good for PBd but cyclohexane promotes association of the polar groups. Consequently it cannot be used for the adsorption measurements due to the absence of a large quantity of free chains able to be adsorbed on silicon wafers. On the other hand association is not promoted by toluene but the refractive index difference with PBd is too low to give accurate measurements. Therefore a mixture of cyclohexane and toluene was used. In this mixture association is not detected up to the concentration of 2.0 mg/ml from DLS measurements and the dn/dc values (0.050 ml/g at 589.4 nm at 20.0 °C) provide enough contrast for accurate measurements.

Characteristic adsorption isotherms are given in figure 12 for the linear ω-functionalized polymers and in figure 13 for the ω-functionalized stars, whereas various parameters of the adsorption behaviour of the samples are reported in Table II. The adsorbed amount A is increased with decreasing molecular weight for the linear samples. The longer the adsorped PBd chains the bigger space they occupy and the stronger the repulsion between them. The ratio $\delta=D_{inter}/D_{over}$ of the interchain distance (D_{int}) over the space needed to accomodate a swollen polymer

coil in a good solvent in it's unperturbed state on the surface (D_{over}) is much lower than unity. This indicates that the adsorped chains are stretched adopting a brush-like conformation.

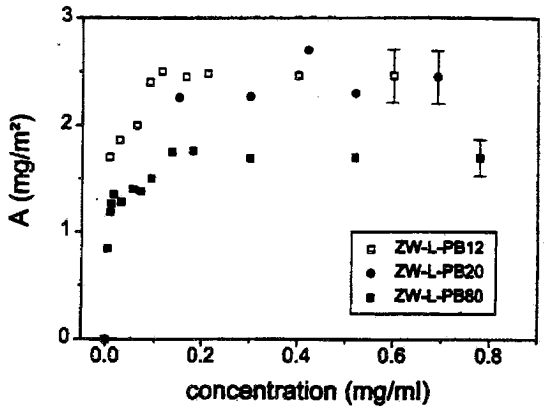

Figure 12. Adsorption isotherms for three linear end-functionalized PBds from cyclohexane-toluene (50/50) mixture at 20°C.

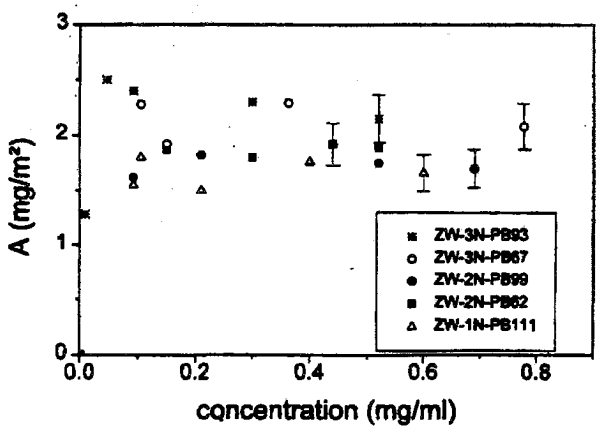

Figure 13. Adsorption isotherms for five 3-armed star PBds with different number of functionalized arms from cyclohexane-toluene (50/50) mixture at 20°C.

In the case of the zwitterionic stars the adsorped amount increases with increasing number of functionalized arms. The grafting density σ, defined as $\sigma=AN_A/M_w$, where A is the adsorped amount, N_A the Avogadro number and M_w the weight average molecular weight of the star seems to present stronger dependence on the molecular weight than the functionality of the stars. The σ values of the samples Zw-2N-3PBd30 and Zw-3N-3PBd25 are very close indicating that despite the fact

that the adsorption energy is high the entropic loss involved in the attachment of the third arm when two arms are already attached may be very high.

Table II. Various adsorption parameters of ω-functionalized linear (L) and mono-(1N)-, Di-(2N)-, and tri-(3N)-ω-functionalized polybutadienes.

Sample	$A_{plateau}$ (mg/m^2)	σ ($chains/nm^2$)	D_{inter} (nm)	D_{over} (nm)	$\delta=D_{inter}/D_{over}$
Zw-L-PBd12	2.47+0.01	0.125	2.8	10.5	0.27
Zw-L-PBd20	2.410+.25	0.07	3.8	14.5	0.26
Zw-L-PBd80	1.69+0.18	0.012	9.1	33.3	0.27
Zw-1N-3PBd30	1.77+0.17	0.0096	10.2	25.2	0.4
Zw-2N-3PBd30	1.86+0.06	0.0179	7.5	19.1	0.39
Zw-2N-3PBd40	1.90+0.12	0.0128	8.8	25.2	0.35
Zw-3N-3PBd25	2.14+0.18	0.0191	7.2	19.7	0.37
Zw-3N-3PBd40	2.3+0.2	0.0148	8.2	24.3	0.34

Schematic illustrations of all possible attachments of the chains with different architectures are given in figure 14. Configurations f and g are less favored than configuration e for entropic reasons. This conclusion is also supported by the similar D_{inter} values obtained for stars with two and three polar groups.

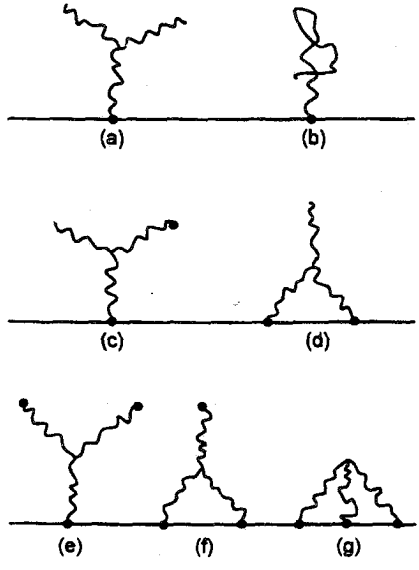

Figure 13. Schematic representation of the possible conformational states of the adsorbed end-functionalized stars and linear molecules. Different conformational states may contribute very differently to the total adsorbed amount.

The adsorption kinetics, studied by time-resolved ellipsometry show two processes. At the initial stages the adsorption is diffusion controled. At longer times the polymers must penetrate the barrier formed by the initially adsorbed chains. It was found that the star polymers penetrate this barrier faster than the linear chains, due to the different conformations adopted by the stars.

ΠΕΡΙΛΗΨΗ

Στο άρθρο αυτό γίνεται ανασκόπηση των μεθόδων σύνθεσης ομο- και συμπολυμερών διαφόρων αρχιτεκτονικών (γραμμικά ομοπολυμερή, δισυσταδικά και τρισυσταδικά συμπολυμερή, αστεροειδή ομοπολυμερή) με ακραίες ομάδες διμεθυλαμίνης και σουλφοβεταίνης καθώς επίσης και των ιδιοτήτων τους σε αραιά διαλύματα και σε συμπυκνωμένη φάση. Έμφαση δίνεται στα πολυμερή που παρασκευάστηκαν στο Εργαστήριο Βιομηχανικής Χημείας του Πανεπιστημίου Αθηνών. Τα ακροδραστικά πολυμερή παρασκευάστηκαν με την μέθοδο του ανιοντικού πολυμερισμού, υπό υψηλό κενό, χρησιμοποιώντας τον απαρχητή 3-διμεθυλαμινοπροπυλολίθιο για την εισαγωγή της διμεθυλαμινομάδας στην άκρη της μακρομοριακής αλυσίδας. Για την παρασκευή των α,ω-διδραστικών συμπολυμερών και των αστεροειδών ομοπολυμερών η σύζευξη των ζωντανών μακρομορίων έγινε με χρήση κατάλληλων χλωροσιλανίων. Η διμεθυλαμινομάδα μετατράπηκε σε σουλφοδιπολική μέσω αντίδρασης με κυκλοπροπανοσουλτόνη. Εκτενής χαρακτηρισμός των πολυμερών (ωσμωμετρία μεμβράνης και τάσης ατμών, σκέδαση φωτός, χρωματογραφία αποκλεισμού μεγεθών, διαφορική διαθλασιμετρία, NMR και UV φασματοσκοπία) απέδειξε ότι τα πρότυπα αυτά μακρομόρια κατέχουν υψηλό βαθμό ομοιογένειας τόσο ως προς το μοριακό βάρος, όσο και ως προς τη σύσταση. Οι ιδιότητες συσσωμάτωσής τους σε αραιά διαλύματα διαλυτών με διαφορετική πολικότητα και εκλεκτικότητα απέναντι σε διαφορετικά τμήματα των μορίων μελετήθηκαν με ιξωδομετρία, στατική και δυναμική σκέδαση. Ο βαθμός συσσωμάτωσης των πολυμερών που περιέχουν στυρένιο είναι κατά πολύ μικρότερος από αυτόν των ομοπολυδιενίων, ίσως λόγω της επιδιαλύτωσης των ιοντικών διπόλων από τις φαινυλομάδες. Οι ιδιότητες των ακροδραστικών γραμμικών ομοπολυμερών και συμπολυμερών σε συμπυκνωμένη φάση (στερεά και τήγματα) μελετήθηκαν με σκέδαση ακτίνων Χ σε μικρές γωνίες, ρεολογία και διηλεκτρική φασματοσκοπία. Παρά το μικρό ποσοστό ιοντικών ομάδων παρουσιάστηκαν καινούργια χαρακτηριστικά αυτοοργάνωσης στα ομοπολυμερή καθώς και εξαιρετικά ενδιαφέρουσα σταθερότητα φάσεων σε υψηλές θερμοκρασίες στα συμπολυμερή. Τέλος μελετήθηκε η προσρόφηση των αστεροειδών ομοπολυμερών, με διαφορετικό αριθμό ακροδραστικών κλάδων, από αραιά διαλύματα με ελλειψομετρία, η συμπεριφορά των οποίων παρουσιάζει διαφορετικά χαρακτηριστικά από εκείνη των γραμμικών.

References

1. Lundberg, R.D.; Phillips, R.R. J. Polym. Sci. Polym. Phys. Ed., 1982, 20, 1143.
2. Hegedus, R.D.; Lenz, R.W. J. Polym. Sci., Part A: Polym. Chem., 1988, 26, 367.
3. Hara, M.; Wu, J. Multiphase Polymers: Blends and Ionomers, Utracki L.A., Weiss R.A Eds., ACS Symposium Series 395, American Chemical Society: Washington, DC, 1988; Chapter 19.
4. Nagata, N.; Kobatake, T.; Watanabe, H.; Veda, A.; Yoshioka, A. Rubber Chem. Technol., 1987, 60, 837.
5. Zhou, Z.; Chu, B.; Wu, G.; Peiffer, D.G. Macromolecules, 1993, 26, 2968.
6. Fitzgerald, J.J.; Weiss, R.A. J. Macromol. Sci., Rev. Macromol. Chem. Phys., 1988, C28, 1.
7. Mauritz, K.A.; J. Macromol. Sci., Rev. Macromol. Chem. Phys., 1988, C28, 65.
8. Broze, G.; Jerome R.; Teyssie, P. Macromolecules, 1981, 14, 224.
9. Broze,G.; Jerome R.; Teyssie, P. Macromolecules, 1982, 15, 1300.
10. Lenz, R.W. Organic Chemistry of Synthetic High Polymers, Interscience: New York, 1967.
11. Kennedy, J.P. Rubber Chem. Technol. Reviews, 1983, 56, 639.
12. Sogah, D.Y.; Webster, O.N. J. Polym. Sci. Polym. Lett. Ed., 1983, 21, 927.
13. Young, R.N.; Quirk, R.P.; Fetters, L.J. Adv. Polym. Sci., 1984, 56, 1.
14. Bywater, S. Anionic Polymerization in Encyclopedia of Polymer Science and Engineering, Vol. 2.
15. Stewart, M.J.; Shepherd, N.; Service, D.M. Br. Polym. J., 1990, 22, 319.
16. Pispas, S.; Pitsikalis, M.; Hadjichristidis, N.; Dardani, P.; Morandi, F. *Polymer*, 1995, 36, 3005.
17. Pispas, S.; Hadjichristidis, N. Macromolecules, 1994, 27, 1891.
18. Davidson, N.S.; Fetters, L.J.; Funk, W.G.; Graessley, W.W.; Hadjichristidis, N. Macromolecules, 1988, 21, 112.
19. Pitsikalis, M.; Hadjichristidis, N. Macromolecules, 1995, 28, 3904.
20. Bahr, U.; Weiden, H.; Rinkler, H.-A.; Nische, G. Makromol. Chem., 1972, 161, 1.
21. Monroy Soto, V.M.; Galin, J.C. Polymer, 1984, 25, 121.
22. Pitsikalis, M. Ph. D. Thesis, University of Athens, 1994.
23. Schulz, D.N.; Peiffer, D,G.; Agarwal, P.K.; Larabee, J.; Kaladas, J.J.; Soni, L.; Handwerker, B.; Garner, R.T. Polymer, 1986, 27, 1734.
24. Borlenghi, A.; Pitsikalis, M.; Pispas, S.; Hadjichristidis, N. Macromol. Chem. Phys., 1995, 196, 4025.
25. Pitsikalis, M.; Siakali-Kioulafa, E.; Hadjichristidis, N.; J. Polym. Sci., Part B: Polym. Phys. Ed., 1996, 34, 249.
26. Shen, Y.; Safinya, C.R.; Fetters, L.J.; Adam, M.; Witten T.; Hadjichristidis, N. Phys. Rev., 1991, 43, 1886.
27. Fetters, L.J.; Graessley, W.W.; Hadjichristidis, N.; Kiss, A.D.; Pearson D.S.; Younghouse, L.B. Macromolecules, 1988, 21, 1644.
28. Pispas, S.; Hadjichristidis N.; Mays, J.W. Macromolecules, 1994, 27, 6307.

29. Floudas, G.; Fytas, G.; Pispas, S.; Hadjichristidis, N.; Pakula, T.; Khokhlov, A.R.; Macromolecules, 1995, 28, 5109.
30. Floudas, G.; Fytas, G.; Pispas, S.; Hadjichristidis, N.; Pakula,T.; Khokhlov, A.R.; Macromol. Symp., 1996, 106, 137.
31. Chu, B.; Wang, J.; Li, Y.; Peiffer, D. Macromolecules, 1992, 25, 4229.
32. de Gennes, P.-G. Scaling Concepts of Polymer Physics, Cornell University Press, Ithaca, New York, 1979.
33. Pispas, S.; Hadjichristidis, N.; Mays, J.W. Polymer Comm., 1996, 37, 3989.
34. Pispas, S.; Allorio, S.; Hadjichristidis, N.; Mays, J.W. Macromolecules, 1996, 29, 2903.
35. Pitsikalis, M.; Hadjichristidis, N.; Mays, J.W. Macromolecules, 1996, 29, 179.
36. Siqueira, D.F.; Pitsikalis, M.; Hadjichristidis, N.; Stamm, M. Langmuir, 1996, 12, 1631.

Chimika Chronika, New Series, 26, 429-440 (1997)

Aqueous Bath Dyeing of Vinylferrocene Copolymers with C.I. Disperse Blue 165

ALEXANDROS A. VASSILIADIS*

Department of Chemistry, The University of Athens, Panepistimiopolis, 157 71 Athens, Greece

(Received: February 12, 1997 In final form: September 9, 1997)

Summary

Vinylferrocene–styrene and vinylferrocene–methyl methacrylate random copolymers synthesized by free radical polymerization, were characterized by size exclusion chromatography and membrane osmometry. The vinylferrocene content was determined by visible spectroscopy. The glass transition temperature of the polymers was measured by differential scanning calorimetry. The dyeability of the polymers, for aqueous bath dyeing with C.I. Disperse Blue 165, was examined by determining the exhaustion of the dye-liquor. It was found that by incorporating more vinylferrocene units into the copolymers an increase in glass transition temperature and dye uptake occurred.

Key Words: Carrier dyeing, vinylferrocene copolymers, glass transition temperature, differential scanning calorimetry.

INTRODUCTION

The synthesis and properties of vinyl-n^5-dicyclopentadienyliron (vinylferrocene) were first described by Arimoto and Haven **[1]** and vinylferrocene ho-

---

* Present address: T.E.I. of Piraeus, 122 41 Athens, Greece

mopolymers and copolymers with olefinic compounds **[2-6]**, styrene **[7]** and methyl methacrylate **[8]** have been extensively studied. However, the dyeability of these copolymers, and the influence, on the dye adsorption, of vinylferrocene introduction into the homopolymers of styrene and methyl methacrylate has not been investigated. Vinylferrocene is an electron rich monomer and does not obey normal vinyl-polymerization kinetics. Intramolecular electron transfer termination of a polymer chain radical has been reported **[9]** and this is the reason why it is unique in comparison with other vinyl-monomers.

The presence of the ferrocene nucleus can play a decisive role, influencing the segmental mobility of the macromolecular chain. In this work the dyeing of vinylferrocene–styrene and vinylferrocene–methyl methacrylate copolymers with C.I. Disperse Blue 165 dye, in the presence of a carrier, is reported and the dependence of the exhaustion of the dyebath upon glass transition temperature is discussed.

EXPERIMENTAL

Free Radical Polymerization and Characterization

Vinylferrocene (VF) was copolymerized free–radically with styrene (S), and methyl methacrylate (MM) in degassed benzene solutions, with the use of 2,2'-azobisisobutyronitrile (AIBN) as the initiator. Copolymerization reactions were performed at three different initial VF/comonomer weight ratios of 5/95, 10/90 and 15/85 to give copolymers of type 5, 10 and 15 respectively.

Details on the synthesis, characterization and estimation of composition of the copolymers are recorded elsewhere **[10]** and will be given in a forthcoming paper. The number-average molecular weights ($\overline{M}_n$) determined by membrane osmometry and the polydispersity ($\overline{M}_w/\overline{M}_n$) values are summarized in *Table I.*

The content of vinylferrocene as a function of absorbance was determined in the region of 440nm **[8, 11]** and is shown in *Table I* for the different samples of copolymers used in this study.

Table I. AIBN - Initiated Copolymerization of VF with Styrene and with Methyl Methacrylate at 60 °C in Benzene Solution[a]

Polymer	$\overline{M}_w/\overline{M}_n$[b]	$\overline{M}_n \cdot 10^{-3}$	VF in copolymer, % w/w
S/A[c,d]	1.61	18.3	—
SVF/A5	1.61	17.8	2.58
SVF/A10	1.65	14.9	4.68
SVF/A15	1.66	19.2	7.06
S/B[d]	1.63	58.8	—
SVF/B5	1.82	53.6	2.16
SVF/B10	1.87	53.4	4.22
SVF/B15	1.71	48.7	6.06
MM/A[c,e]	1.74	49.3	—
MMVF/A5	1.51	56.6	5.87
MMVF/A10	1.37	46.7	10.70
MMVF/A15	1.47	47.6	15.40
MM/B[e]	1.60	140.0	—
MMVF/B5	1.48	123.0	6.04
MMVF/B10	1.97	107.0	12.90
MMVF/B15	1.67	92.2	19.70

[a] 0.1% w/w AIBN (series A); 0.01% w/w AIBN (series B)
[b] Obtained from size exclusion chromatography measurements
[c] Prepared at 50 °C
[d] Poly(styrene)
[e] Poly(methyl methacrylate)

Glass Transition Temperature

The glass transition temperature (T_g) was determined by differential scanning calorimetry. Transition temperatures at heating rates of 5, 10, 20 and (in one case) 40 K·min^{-1} were obtained. The measurements were performed on a Du Pont 990 DSC differential calorimeter. Indium was used to calibrate the instrument prior to all measurements. The calibration was also checked when the heating rate was changed. True glass transition values extrapolated to zero heating rate were calculated from a least-squares analysis of linear plots of transition temperature against heating rate.

Carrier Dyeing Procedure

The visible spectrum of C.I. Disperse Blue 165 (Hoechst) was examined from aqueous dispersions with a Hitachi U-2000 spectrophotometer. A linear calibration curve that related absorbance to concentration was constructed at the

wavelength of maximum absorbance (λ_{max}). The dye obeyed the Beer–Lambert law up to a concentration of 0.05 $g \cdot l^{-1}$. The least-squares method was used to get the best fit to the experimental data.

The polymers, being in granular form, were separated before dyeing by sieving into fractions using a Fritsch Analysette apparatus and grains ranging in size from 355 μm to 1000 μm were obtained. Thus, samples of similar particle size of the polymers to be dyed were prepared, so that the dye could be uniformly distributed on the samples during dyeing.

The following method of dyeing was used for polymer samples in a liquor ratio of 1:10.

The dyebath was set with

5 $g \cdot l^{-1}$ Samaron - Blau GSL 400 dye (C.I. Disperse Blue 165)

1 $g \cdot l^{-1}$ Eganal PS dispersing agent (Hoechst) and

3 $g \cdot l^{-1}$ Remol NTG carrier (Hoechst)

in distilled water. The dye was dispersed in water and this dispersion was filtered through a fine sieve into the dyebath. The pH of the dye-liquor was adjusted to 5 with acetic acid. The temperature was raised to 97 °C and dyeing was carried out in a thermostatically controlled glycerol bath for 90 min. The dye-liquor was circulated throughout the whole dyeing cycle. On completion of dyeing, the samples were taken out by filtration (to remove all polymer particles) through a metallic sieve, in order to avoid loss of dye.

The filtered liquors were studied by visible spectroscopy and the absorbance of their dilute aqueous suspensions was measured at λ_{max} on a Hitachi U-2000 spectrophotometer.

RESULTS AND DISCUSSION

Differential Scanning Calorimetry

Typical results of T_g measurements are given in *Table II*.

Table II. Glass Transition Temperatures at Different Heating Rates

	Glass Transition Temperature, K			
Polymer	T_g [a]	5[b]	10[b]	20[b]
S/A	363.3	364.2	365.0	366.7
SVF/A15	370.6	371.7	372.5	374.7
SVF/B5	372.2	372.9	373.7	375.0
SVF/B10	372.6	373.6	374.6	376.7
MMVF/A5	388.8	389.1	389.4	390.0
MMVF/A10	390.1	390.7	391.2	392.5
MM/B	394.6	395.3	396.2	397.8
MMVF/B15	397.4	398.1	399.1	400.6

[a] Determined by extrapolation to a heating rate of 0 K·min^{-1}
[b] Heating rate, K·min^{-1}

The linearity in the plots of the observed transition as a function of heating rate suggests a reasonable degree of confidence in the results. The transition temperatures of all polymers at zero heating rate found by the least-squares method are listed in *Table III*.

The DSC and compositional analysis results show that, within any given series of polymers, the T_g increases steadily as the percentage of vinylferrocene incorporated in polymers is raised, with the exception of MMVF/ A15. In the case of this polymer a T_g value of 378.4 K was estimated, which is considerably lower than those of other series A methyl methacrylate polymers prepared under similar experimental conditions. It has been shown **[12–15]** that the low flexibility of polymethacrylates with aromatic side groups is due to interactions between the aromatic rings. Accordingly, further work seems necessary particularly with MMVF/A15 and probably with MMVF/B15, which also has a relatively low glass transition temperature. Taken altogether **[10]** the viscosity, solubility and polydispersity data for these polymers show that they may be branched **[16]**. This is not unexpected, since the high transfer activity of VF **[9,17]** suggests a high transfer activity with the polymer; thus branching will probably occur **[18]**.

Dye Absorption

Samaron Blau GSL 400 dye (C.I. Disperse Blue 165) absorbs light in the visible range with λ_{max} at 673 nm. A typical spectrum of the dyestuff measured

from dispersion in water is shown as a plot of absorbance against wavelength in *Figure 1.*

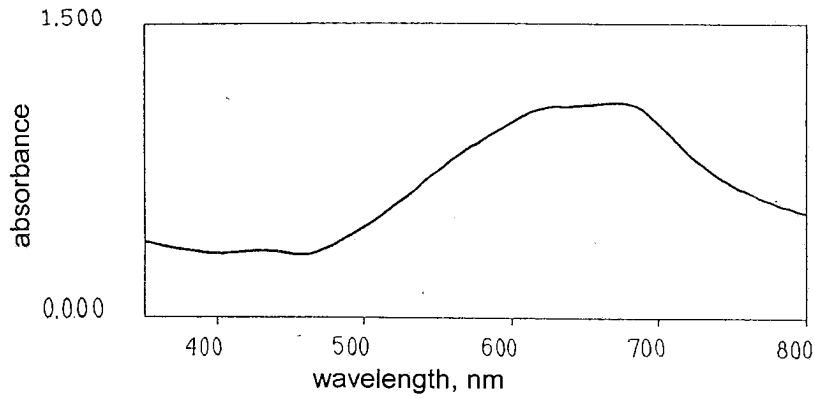

Figure 1. Plot of absorbance as a function of wavelength for C.I. Disperse Blue 165 in water

A calibration curve was prepared by plotting dye absorbance at 673 nm against six known dye concentrations. The straight line obtained is presented in *Figure 2.*

The degree of exhaustion is known to be a measure of the total dyestuff that resides on the sample as opposed to the dyestuff in solution in the dye-liquor. Exhaustion (expressed as a percentage) is defined by eq. (1) :

$$\text{Exhaustion} = 100\,\frac{C_i - C_f}{C_i} \qquad (1)$$

where C_i is the initial concentration of dye in the dye-liquor at the commencement of dyeing (C_i=5 $g \cdot l^{-1}$ according to the above dyeing recipe) and C_f is the final concentration of dye at the end of the dyeing process.

After dyeing, the liquid residues were diluted with water to a hundredfold volume. The purpose of this was to prepare suspensions whose dye concentrations are within the linearity limits of the calibration curve (*Figure 2*). Care was taken not to waste any amount of the residues. The dye content was determined spectrophotometrically as already mentioned. In the final dye concentration calcula-

tions, account was taken of the dilutions described above. The exhaustion of the dyebath was then obtained from eq. (1).

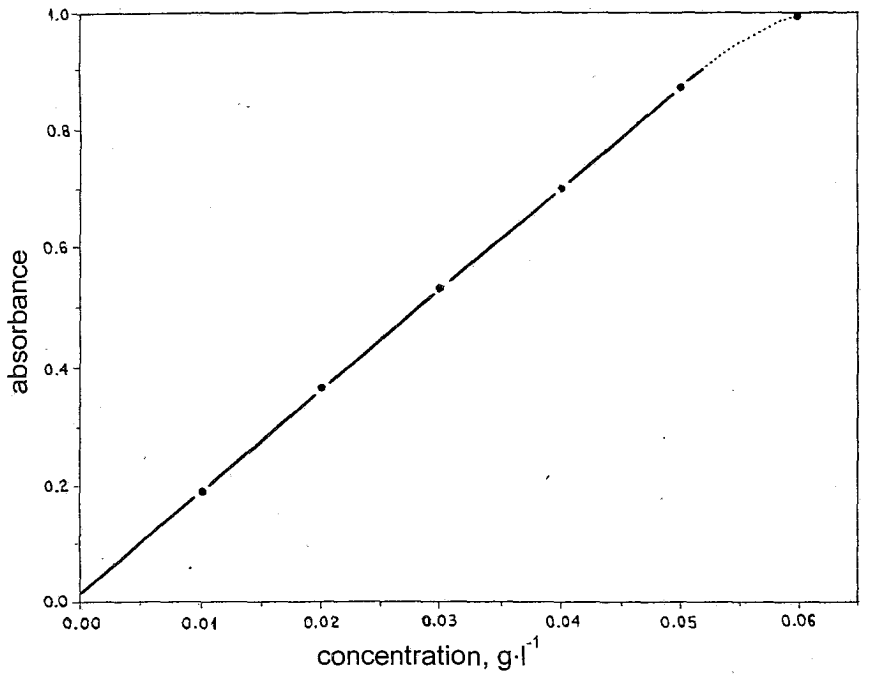

Figure 2. Calibration line for C.I. Disperse Blue 165 between absorbance and dye concentration

The absorbances of dilute suspensions at 673 nm and the final dye concentrations together with the exhaustions of the dye-liquors are recorded in *Table III.*

In this study the dyeing was performed using a carrier in the dye-liquor. In general, the carrier can increase the accessibility, facilitating the diffusion of dye and, also, can plasticize the polymer, bringing down the T_g. Here it must be noted that the influence of temperature on diffusion of dye is represented by the well-known Williams–Landel–Ferry equation **[19]** which applies to amorphous polymers above T_g. It needs particular consideration that all polymers reported in this paper, with only three exceptions, exhibited values of T_g higher than the actual dyeing temperature given above (370.2 K).

Table III. Exhaustion of Dyebaths Obtained from Polymers with Different Glass Transition Temperatures

Polymer	T_g, K	Absorbance	C_f,g·l^{-1}	Exhaustion, %
S/A	363.3	0.50	2.83	43.4
SVF/A5	368.6	0.54	3.06	38.8
SVF/A10	370.0	0.52	2.94	41.2
SVF/A15	370.6	0.50	2.83	43.4
S/B	370.8	0.39	2.18	56.4
SVF/B5	372.2	0.53	3.00	40.0
SVF/B10	372.6	0.46	2.59	48.2
SVF/B15	372.9	0.40	2.24	55.2
MM/A	388.6	0.52	2.94	41.2
MMVF/A5	388.8	0.58	3.30	34.0
MMVF/A10	390.1	0.55	3.12	37.6
MMVF/A15	378.4	0.53	3.00	40.0
MM/B	394.6	0.46	2.59	48.2
MMVF/B5	395.4	0.53	3.00	40.0
MMVF/B10	397.1	0.52	2.94	41.2
MMVF/B15	397.4	0.52	2.94	41.2

Attempts were made to dye the polymers without adding carrier in the dye-liquor. In all these experiments it was observed that the yield of the disperse dye on the samples used for dyeing was limited in the absence of carrier. Consequently, the exhaustion of the dye on them is not sufficient unless a carrier is used. On this basis, the results in *Table III* support the suggestion that the carrier increases the dyeability and this may arise because a reduction in T_g would have the same effect as an increase in the temperature of dyeing **[20,21]**. In all cases, however, the exhaustion of the dyebath is below 56.5%. The data clearly show that the polymers used for these results are dyeable with non-ionic dyes such as C.I. Disperse Blue 165 employed in the dyeing experiments and the uptake of the disperse dye varies from polymer to polymer.

Relationship Between T_g and Exhaustion of Dyebath

Table III indicates that the exhaustion of the dyebath for each homopolymer is higher compared to that for its copolymers (equal in the case of SVF/A15). It can be seen that introduction of a few percent vinylferrocene units into each of four homopolymers leads to a sudden drop in dye adsorption. These results show,

also, that in this case the exhaustion rapidly decreases with increasing glass transition temperature, and this can be ascribed to that, at least to a first approximation, the rate of dye diffusion into a polymer is a direct function of the temperature difference ($T-T_g$), where T is the actual dyeing temperature. To the extent to which the diffusion of dye molecules in the amorphous regions is determined by the segmental motions of the polymer chains, the free volume theories can be expected to be important **[22,23]**. Therefore, the observed behavior appears to be in accord with the free volume model of dye diffusion.

A second feature notable in *Table III*, however, is that for each series of copolymers the value of exhaustion is increased as further increase in the vinylferrocene content occurs. An explanation could be that, as more vinylferrocene is incorporated into the copolymers, the amount of the non-crystalline regions present in the polymer is raised. This will cause an increase in the rate of dyeing, since the crystals can be considered completely inaccessible to the dye molecules and dyeing takes place only in the amorphous domains. Furthermore, a small increase in glass transition temperature is noted, with only one exception, in the higher vinylferrocene content copolymers. Thus, the free volume model is inapplicable and this is probably due to the fact that both an increase in glass transition temperature and a decrease in crystallinity occur in competition. Obviously these must be viewed with caution, since the dyeing system is an extremely complicated one and some interactions within the dyebath might be expected. For example, the existence of hydrophilic ester groups in methyl methacrylate polymers may influence the dye diffusion into the samples. Additionally, electrical interactions between the diffusing dye molecules and the substrate such as dipole interactions, dispersion forces and so on are ignored, but they may be important. Further work is required to clarify this point.

CONCLUSIONS

The vinylferrocene–styrene and vinylferrocene–methyl methacrylate copoly-

mers were found to be dyeable with a commercial disperse dye using a carrier dyeing method. The copolymer samples used for dyeing exhibited values of exhaustion between 34 and 55%. The carrier plays a rather positive role in lowering the T_g of these polymers acting as a plasticizer and facilitates the adsorption of dye, thus improving the exhaustion of the dyebath. Introduction of vinylferrocene into the poly(styrene) and poly(methyl methacrylate) chains reduces the exhaustion, but as the T_g is increased in the copolymers of higher vinylferrocene contents the exhaustion of the dyebath increases, approaching the value determined for the homopolymers.

Βαφή Συμπολυμερών του Βινυλοφερροκενίου σε Υδατικό Λουτρό με το C.I. Disperse Blue 165

Περίληψη

Τυχαία συμπολυμερή βινυλοφερροκενίου–στυρενίου και βινυλοφερροκενίου–μεθακρυλικού μεθυλεστέρα παρασκευάστηκαν με πολυμερισμό ελευθέρων ριζών. Τα πολυμερή χαρακτηρίστηκαν με χρωματογραφία αποκλεισμού μεγεθών και ωσμωμετρία μεμβράνης. Η περιεκτικότητα των συμπολυμερών σε βινυλοφερροκένιο προσδιορίστηκε με φασματοσκοπία ορατού. Η θερμοκρασία υαλώδους μεταπτώσεως των πολυμερών μετρήθηκε με διαφορική θερμιδομετρία σαρώσεως. Στα πολυμερή που παρασκευάστηκαν επιχειρήθηκε – για πρώτη φορά σε ανάλογες ενώσεις – και πραγματοποιήθηκε με επιτυχία βαφή με χρώμα διασποράς. Εξετάστηκε η ικανότητα βαφής των πολυμερών σε υδατικό διάλυμα με το C.I. Disperse Blue 165 και υπολογίστηκε η εξάντληση του λουτρού βαφής, ώστε να διαπιστωθεί η επίδραση του – χημικά ενωμένου με το μακρομόριο – σιδήρου στην απορρόφηση χρώματος απο τα πολυμερή. Τα δείγματα συμπολυμερών που μελετήθηκαν, κατά την βαφή με χρησιμοποίηση φορέα, έδωσαν τιμές εξάντλησης μεταξύ 34 και 55%. Ο φορέας φαίνεται πως ελαττώνει τη θερμοκρασία υαλώδους μεταπτώσεως των πολυμερών ενεργώντας ως πλαστικοποιητής και διευκολύνει τη διάχυση του χρώματος βελτιώνοντας την

εξάντληση του λουτρού βαφής. Η ενσωμάτωση περισσότερων μορίων βινυλοφερροκενίου στα συμπολυμερή είχε ως αποτέλεσμα αύξηση της θερμοκρασίας υαλώδους μετάπτώσεως αλλά και της απορρόφησης του χρώματος, πιθανότατα λόγω μείωσης της κρυσταλλικότητας των πολυμερών κατά την αύξηση της περιεκτικότητάς τους σε βινυλοφερροκένιο.

Acknowledgements

The author is greatly indebted to Professor N. Hadjichristidis, Department of Chemistry, The University of Athens, and to Dr. R. N. Young, Department of Chemistry, The University of Sheffield, England, for valuable discussion and advice. Financial support by the Greek General Secretariat of Research and Technology and by the Royal Society is gratefully acknowledged. Thanks are also due to the Hoechst Company for gifts of chemicals.

References

1. Arimoto, F. S., and Haven, A. C., Jr., J. Am. Chem. Soc., **77**, 6295 (1955).
2. Pittman, C. U., Jr., and Grube, P. L., J. Polym. Sci., A–1, **9**, 3175 (1971).
3. Pittman, C. U., Jr., Grube, P., and Hanes, R. M., J. Paint Technol., **46**, 597, 35 (1974).
4. Pittman, C. U. Jr., and Grube, P. L., J. Appl. Polym. Sci., **18**, 2269 (1974).
5. Pittman, C. U., Jr., Marlin, G. V., and Rounsefell, T. D., Macromolecules, **6**, 1, 1 (1973).
6. Tada, K., Higuchi, H., Yoshimura, M., Mikawa, H., and Shirota, Y., J. Polym. Sci., Polym. Chem. Ed., **13**, 1737 (1975).
7. Diaz–Barrios, A., and Howard, G. J., Makromol. Chem., **182**, 1081 (1981).
8. Lai, J. C., Rounsefell, T., and Pittman, C. U., Jr., J. Polym. Sci., A–1, **9**, 651 (1971).
9. George, M. H., and Hayes, G. F., J. Polym. Sci., Polym. Chem. Ed., **13**, 1049 (1975).
10. Vassiliadis, A. A., Ph. D. Thesis, University of Athens, 1991.
11. Tinker, A. J., George, M. H., and Barrie, J. A., J. Polym. Sci., Polym. Chem. Ed., **13**, 2005 (1975).

12. Hadjichristidis, N., and Desreux, V., J. Macromol. Sci.—Chem., **A6**(7), 1227 (1972).

13. Hadjichristidis, N., Devaleriola, M., and Desreux, V., Eur. Polym. J., **8**, 1193 (1972).

14. Alexopoulos, J. B., Hadjichristidis, N., and Vassiliadis, A., Polymer, **16**, 386 (1975).

15. Niezette, J., Hadjichristidis, N., and Desreux, V., Makromol. Chem., **177**, 2069 (1976).

16. Roovers, J. E. L., and Bywater, S., Macromolecules, **5**, 384 (1972).

17. Tinker, A. J., George, M. H., and Barrie, J. A., J. Polym. Sci., Polym. Chem. Ed., **13**, 2133 (1975).

18. Sasaki, Y., Walker, L. L., Hurst, E. L., and Pittman, C. U., Jr., ibid., **11**, 1213 (1973).

19. Williams, M. L., Landel, R. F., and Ferry, J. D., J. Am. Chem. Soc., **77**, 3701 (1955).

20. McGregor, R., and Peters, R. H., J. Soc. Dyers Colourists, **84**, 267 (1968).

21. Ingamells, W. C., Thornton, S. R., and Peters, R. H., J. Appl. Polym. Sci., **17**, 3733 (1973).

22. Rosenbaum, S., ibid., **7**, 1225 (1963).

23. Rosenbaum, S., J. Polym. Sci., A, **3**, 1949 (1965).

Chimika Chronika, New Series, 26, 441-458 (1997)

KINETIC SPECTROPHOTOMETRIC STUDY OF THE OXIDATION REACTION OF N-ACETYLNEURAMINIC ACID BY PERIODATE.

(Received: April 18, 1997 In final form: September 30, 1997)

Maria -Helen E. Spyridaki and Panayotis A. Siskos*

Laboratory of Analytical Chemistry, Department of Chemistry, University of Athens, Panepistimiopolis - Kouponia, 157 71 Athens, Greece

The oxidation reaction of N-acetylneuraminic acid (NANA) by periodate was studied kinetically using spectrophotometry at 244 nm. The following reaction rate law, which is independent of the ionic strength, at pH 6.0, $\theta = 25$ °C, is proposed: $NANA + IO_4^- \overset{K}{\longleftrightarrow} [NANA.IO_4^-]$, $[NANA.IO_4^-] \xrightarrow{k} \text{products}$, $\upsilon = kK\,[NANA].[IO_4^-]$. Values for the reaction rate constant, k, and the equilibrium constant, K, were found to be $k = 0.239 \pm 0.011\ s^{-1}$ and $K = 0.100 \pm 0.005\ M^{-1}$, respectively. The reaction order with respect to NANA and to periodate were obtained using the Guggenheim method and the initial-rate method using a least-squares parameter estimation. The activation energy, $E_a = 4.0 \pm 0.2$ kcal/mol, was calculated from Arrhenius plots, which corresponds to a temperature variation of about 3% per °C.

Key Words: N-acetylneuraminic acid, periodate oxidation, kinetics

Introduction

Sialic acids are the common terminal saccharides of glycoproteins and glycolipids, which form the major components of the cell membrane. The linkage of single sialyl units to oligosaccharide chains involves α-glycosidic bonds between the C-2 anomeric hydroxyl group of sialic acid and the C-3, C-4 or C-6 hydroxyl groups of the penultimate non-sialic acid monosaccharide moiety. These linkages may involve D-galactose, N-acetyl-D-glucosamine, N-acetyl-D-galactosamine and in some unique gangliosides D-glucose. The most common linkages found are α(2-3) to D-galactose and α(2-6) to D-galactose or N-acetyl-D-galactosamine [1]. N-acetylneuraminic acid (NANA, 5-acetamido-3,5-dideoxy-D-glycero-D-galacto-2-nonulopyranos-1-onic acid, Figure 1) is one of the mainly naturally occurring sialic acids primarily observed in man. NANA is recognised as a tumour marker used for prognosis and monitoring response to therapy in different types of cancer [2]. In addition, increased urinary levels of free NANA were found in some inherited storage diseases such as sialuria and Salla disease [3].

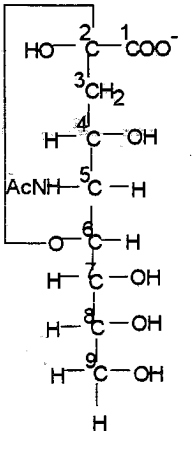

Figure 1. Structure of NANA.

Spectrophotometric methods [4,5], enzymatic methods [6], fluorimetric methods [7], gas-liquid chromatography [8] alone or in combination with mass spectrometry [9] and high-performance liquid chromatography [10], have been reported for the determination of NANA.

Periodic acid and its salts are highly specific oxidising agents under mild reaction conditions for various classes of organic compounds [11]. Periodate oxidation of NANA has been used for the first time in the periodate-thiobarbituric acid method [4] for the determination of free NANA in serum and then in the periodate-resorcinol method [5]. Years later, the periodate-resorcinol method has been automated [12] using the Technicon Autoanalyzer II, adapted to a microassay using microtiter plate reader [13] and improved recently for the determination of free, bound and total NANA in biological fluids [14].

Another analytical application of the oxidation reaction of NANA by periodate consists the establishment of the structures of isolated oligosaccharides, including NANA. In addition, the anionic properties of the sialic acid residues were therefore utilised to separate the periodate oxidation products and thereby establish the position of the sialic acid in the oligosaccharide chain [15]. On the other hand, in histochemistry, methods based upon the selective oxidation of sialic acid residues have been devised for the simultaneous visualisation of neutral sugars and sialic acids [16].

Although the wide use of the periodate oxidation reaction of NANA, there is very limited kinetic and mechanistic information [17,18]. It seems that there is a need for the kinetic study of the oxidation of NANA by periodate which may help in improvement of analytical methods related to this reaction. For example, quality kinetic results of the oxidation of NANA glycoconjugates, such as glycolipids and gly- coproteins, have been used for the improvement of the periodate-resorcinol method for the determination of NANA in serum and urine [14].

In the present work, the reaction of NANA by periodate was studied spectrophotometrically by monitoring the decrease of absorbance at 244 nm, due to the consumption of periodate. To the best of our knowledge, this is the first systematic kinetic study, proposing the following reaction rate law, which is independent of the ionic strength, at pH 6.0, θ = 25 °C: NANA + IO_4^- $\overset{K}{\longleftrightarrow}$ [NANA.IO_4^-], [NANA.IO_4^-] $\xrightarrow{k}$ products, $\upsilon = kK[NANA][IO_4^-]$, where the reaction rate constant, k = 0.239 ± 0.011 s^{-1}, and the equilibium constant, K = 0.100 ± 0.005 M^{-1}. The activation energy, E_a, was found to be 4.0 ± 0.2 kcal/mol.

Experimental

Apparatus

The measuring and recording system was a double beam spectrophotometer, Hitachi model U2000, with 2 nm slit width and photometric accuracy ± 0.002 A (0-0.5 A) and ± 0.004 A (0.5-1.0 A). All measurements were made at 244 nm, with quartz cuvettes with a 1.000-cm light path. The runs were performed at 25.0 ± 0.2 °C, unless otherwise stated, the temperature being controlled with a Tectron 3000543 water-bath.

Reagents

All reagents used were of analytical-reagent grade and distilled water was used.

Stock aqueous solutions of NANA (Sigma Chemical Company, approx. 98%, M_r 309.3) 20.0 mM and paraperiodic acid (H_5IO_6, > 99.0%) 2.00 mM, were prepared. The stock reagents were stable for several weeks if stored in the dark at -4°C.

Working solutions of paraperiodic acid and NANA were prepared daily from the stock solutions by dilution with the appropriate buffer solution and distilled water, respe-

ctively.

Buffer solutions: The buffers used were $NaH_2PO_4.2H_2O$ 0.100 M-CH_3COOH 0.100 M adjusted with NaOH solution for pH 3.2-7.5 and $NaH_2PO_4.2H_2O$ 0.100 M for pH 6.0.

Na_2SO_4 solutions 0.100, 0.500 and 1.00 M were also prepared with buffer solution pH 6.0.

Measurement Procedure

Set the instrument for kinetic studies by selecting the mode "time scan" on the "main menu" screen: a graph is displayed with time increments on the abscissa and photometric values are printed out at the specified time interval.

Mix 0.400 ml of NANA working solution with 2.00 ml paraperiodic acid working solution into the sample cell and press promptly the button "start". Record the reaction curve for 5 min. Keep all working solutions in a water bath at the appropriate temperature.

Results and Discussion

General considerations concerning the study of kinetic parameters are based on previous studies [19,20]. Reasons for the choice of various features of the procedure and results of the kinetic study are given below.

Choice of wavelength

Initial measurements of absorbance for monitoring the reaction NANA + IO_4^- were done at 222 nm, the absorption maximum of periodate. The results were no satisfa-

ctory for several reasons. Firstly, there was interference by coexisting acetates in used buffers. Secondly, the high molar absorptivity of IO_4^- (ε_{222nm} = 10065 $M^{-1}cm^{-1}$) has restricted the use of periodate concentrations larger than 0.100 mM in the reaction mixture, in order to maintain absorbance ≤ 1.2 absorbance units. Thus, the kinetic study of the oxidation of NANA by periodate was carried out by monitoring the decrease of absorbance at 244 nm, the second isosbestic point of periodate species, due to their consumption, (ε_{244nm} = 3700 M^{-1} cm^{-1}) (Figure 2). NANA solutions, buffer solutions of $NaH_2PO_4.2H_2O$-CH_3COOH and iodate, product of the periodate reduction, do not interfere at this wavelength.

Moreover, at 244 nm there were no changes of molar absorptivity of periodate solutions with pH, because this wavelength is one of the two isosbestic points of periodate species.

Since ultraviolet radiation has been shown to decompose photochemically periodate [21], control experiments have been run to demonstrate that the short exposure of ultraviolet radiation at 244 nm used to take the readings did not cause significant decomposition of periodate.

Effect of pH on the reaction rate

The effect of pH on the reaction rate was studied in nine different pH values. Experiments were performed with 1.02 mM of NANA and 0.250 mM of paraperiodic acid in buffer solutions NaH_2PO_4 0.100 M-CH_3COOH 0.100 M in the pH range 3.2-7.5 (Figure 3). The findings show that the reaction rate increases from pH 3.2, reaches the maximum at pH 6.0 and then decreases down to pH 7.5. Thus, pH control is needed. The kinetic study of the oxidation of NANA was done preferably in the region of maximum reaction rate, that is at pH 6.0. At this pH, the monovalent periodate species IO_4^- predominates in equilibrium with the $H_4IO_6^-$ species (equation 1) and small variations of pH have a negligible effect on the reaction rate.

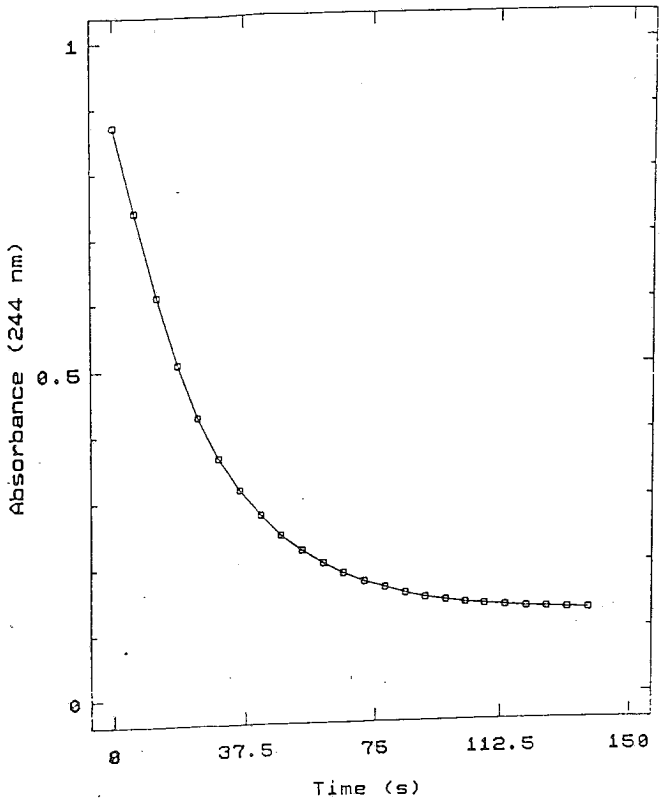

Figure 2. Typical reaction rate curve of absorbance-time signal. [NANA] = 0.875 mM, $[IO_4^-]$ = 0.250 mM, pH 6.0 $NaH_2PO_4.2H_2O$ buffer 0.100 M, θ = 25 °C.

$$H_4IO_6^- \xleftrightarrow{K_D} IO_4^- + 2\,H_2O,\ K_D = 40 \qquad (1)$$

Effect of Temperature on the Reaction Rate

At pH 6.0 and over the temperature range of 12.0-34.5 °C (five different temperatures), data were produced in order to create Arrhenius plots, according to the

equation: $\ln k = \ln A - (E_a/R)(1/T)$ (*2*), where k is the reaction rate constant, A is the frequency factor, E_a is the activation energy of the chemical reaction and T is the absolute temperature.

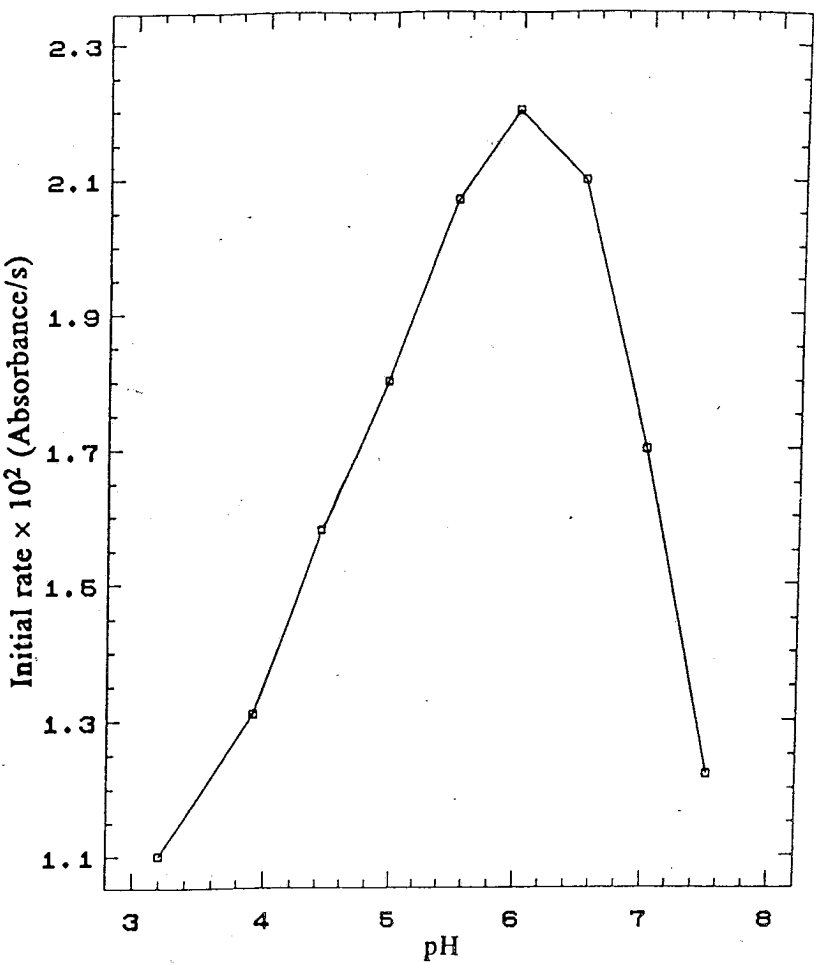

Figure 3. Effect of pH buffer values ($NaH_2PO_4.2H_2O$, 0.100 M-CH_3COOH 0.100 M) on the initial reaction rate. [NANA] = 1.02 mM, $[IO_4^-]$ = 0.250 mM, θ = 25 °C.

From the equation $\ln(dA/dt)_{init} = (1.51\pm0.45) - (2.03\pm0.13)\ (1000/T)$ (3), activation energy was found to be 4.0 ± 0.2 kcal/mol. The exceptionally low activation energy is an additional advantage for the kinetic determination of NANA because of the small temperature effect on the reaction rate; a temperature variation of about 3% per °C was found. Low activation energy has been noticed also for the tartaric acid-periodate reaction [22].

Kinetic and Mechanistic Studies

Determination of the Reaction Rate Constant, k, and the Equilibrium Constant, K

The oxidation reaction proceeds, as it is known from other organic compounds [11,23], via a reversible formation of a negatively charged intermediate between NANA and periodate, followed by a rapid decomposition of the intermediate to the final products. This mechanism is also supported by studying the effect of ionic strength on the reaction rate. Experiments have shown that the rate of the reaction is independent of ionic strength for five different concentrations over the range 0.100-1.00 M Na_2SO_4 at pH 6.0. This provides evidence that the rate-determining step takes place between species that at least one should be uncharged: this is attributable to the fact that formation of the cyclic intermediate would involve an initial attack of a first mole of the negatively charged periodate ion upon the uncharged hydroxyl groups at carbon atoms 8 and 9 of NANA molecule. Probably, the bond between carbon atoms 7 and 8 is susceptible to further oxidation by a second mole of periodate. The uptake of a third mole by NANA points to the opening of the pyranose ring as a requisite for the third phase of the oxidation, which presumably concerns the rupture between carbon 6 and 7 (Figure 4). The second and the third phase of the oxidation occurs when periodate are in large excess.

In the case of NANA, a N-acetylated polyhydroxy-amino keto acid, the following scheme is proposed:

$$NANA + IO_4^- \overset{K}{\longleftrightarrow} [NANA.\ IO_4^-] \quad (4)$$

$$[NANA.\ IO_4^-] \xrightarrow{k} \text{products} \quad (5)$$

where $[NANA.IO_4^-]$ represents the intermediate NANA-periodate complex and K and k are the equilibrium and rate constants, respectively. The kinetics of the reaction are based on the studies of Duke et al. [24] and if NANA is present in large excess over a constant concentration of periodate at pH 6.0, the following equation is proposed:

$$-d[IO_4^-]/dt = - (kK[NANA][IO_4^-])/(1+K[NANA]) \quad (6)$$

where [NANA] is the concentration of the uncoordinated NANA.

From equation (6), equation (7) is obtained

$$d\ln[IO_4^-]/dt = -(kK[NANA])/(1+K[NANA]) \quad (7)$$

From Beer's law for IO_4^- species, equation (8) is obtained

$$A = \varepsilon.b.[IO_4^-] \Leftrightarrow \ln A = \ln(\varepsilon.b) + \ln[IO_4^-] \quad (8)$$

Differentiating equation (8) with respect to time and combining with equation (7), equation (9) is obtained, where Q is an experimentally determinable quantity.

$$d\ln A/dt = -(kK[NANA])/(1+K[NANA]) = Q \quad (9)$$

Rearranging equation (9),

$$-1/Q = (1/k) + (1/kK).(1/[NANA]) \quad (10)$$

Thus, by a plot of 1/Q vs 1/[NANA], the constants k and K can be determined from the intercept and the slope of the curve using the least squares method. The linearity of the experimental curves confirms the validity of the overall reaction scheme. Calculated values for the equilibrium constant K, ($K = 0.100 \pm 0.005\ M^{-1}$, $n = 6$) and the rate constant k, ($k = 0.239 \pm 0.011\ s^{-1}$, $n = 6$) are given in Table I. Because of the low value of K the term K[NANA] is omitted from the denominator in the equation (9) and there is a good approach to an overall reaction according to the following reaction scheme:

$$IO_4^- + NANA \xrightarrow{k'} IO_3^- + \text{products} \quad (11)$$

where k′ is the overall reaction rate constant, equal to kK.

Table I. Results for the determination of equilibrium and rate constants for the reactions: $NANA + IO_4^- \xleftrightarrow{K} [NANA.IO_4^-]$, $[NANA.IO_4^-] \xrightarrow{k}$ products. $[IO_4^-] = 0.0454$ mM, pH 6.0, 25 °C.

[NANA], mM	0.456	0.545	0.636	0.726	0.816	0.906
-dlnA/dt (=-Q[a,b])	0.0109	0.0142	0.0182	0.0191	0.0202	0.0223

[a] Mean values of triplicate runs

[b] Regression equation: 1/Q = -4.19+41.8(1/[NANA]), n = 6, r = 0.975

Consecutive reactions between the primary product and periodate are unlikely because of the large excess of NANA.

Determination of the Reaction Order

The general reaction-rate equation can be expressed by equation (12)

$$-d[IO_4^-]/dt = k' [IO_4^-]^a[NANA]^b \quad (12)$$

By keeping the concentration of one of the two reagents constant and in large excess and varying the concentration of the second, pseudo-first-order conditions were achieved with respect to each reagent in turn. For example, by keeping [NANA] in large excess, equation (12) can be written as follow:

$$\upsilon = -d[IO_4^-]/dt = k_{obs}[IO4^-]^a \quad (13)$$

where k_{obs} is: $k_{obs} = k'[NANA]^b$ (14)

Under these conditions, the initial slope, $\Delta A/\Delta t$, is directly proportional to the periodate

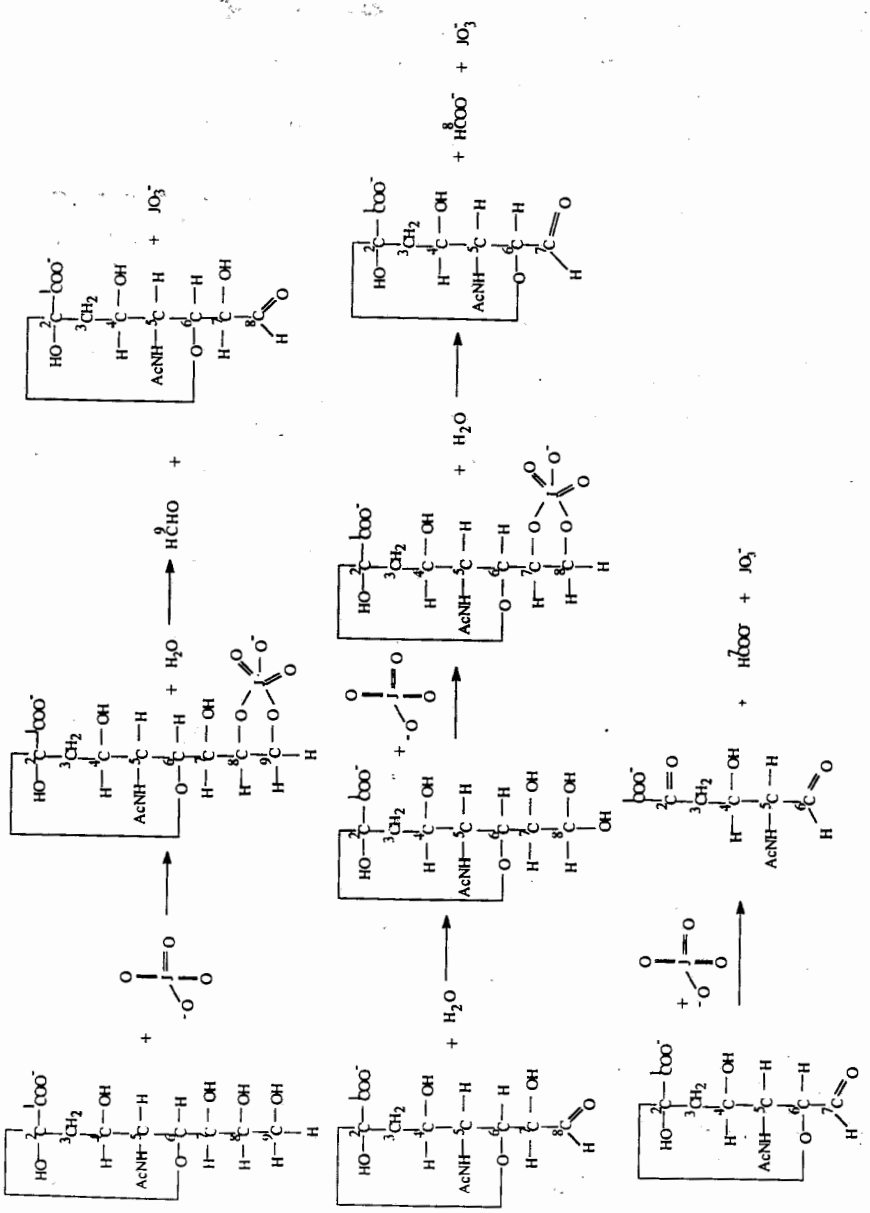

Figure 4. The proposed reaction scheme for the oxidation of NANA (5-acetamido-3,5-dideoxy-D-glycero-D-galacto-2-nonulopyranos-1-onic acid) by periodate at pH 6.0 ($NaH_2PO_4.2H_2O$, 0.100 M). Periodate is in larger excess over NANA concentration.

concentration. Equation (13) can be tranformed to:

$$\log \upsilon_{init} = \log \left| -dA/dt \right|_{init} = \log k_{obs} + a \log [IO_4^-]_{init} \qquad (15)$$

Table II shows the kinetic results for the determination of the reaction order with respect to periodate. From recorded kinetic curves for runs with different concentrations of periodate, a mean value for a was found to be 1.19 ± 0.04, $n = 5$, using linear regression for equation (15).

On the other hand, equation (14) could also be applied for the determination of the reaction order with respect to NANA. Table III presents the kinetic results for the determination of the reaction order, b, by using the Guggenheim method for pseudo-first-order reaction. In this way, k_{obs} can be determined from the recorded reaction curves by plotting $\ln [A_t - A_{t+\tau}]$ vs. time (Figure 5). A_t and $A_{t+\tau}$ are the absorbances at times t and $t+\tau$ respectively. τ is a constant interval that is taken approximately half the time during which the reaction is followed. So, a series of k_{obs} values was obtained for different NANA concentrations. The reaction order, b, can be obtained by plotting $\log k_{obs}$ vs. $\log$ [NANA], as it follows from equation (12).

Table II. Kinetic results of the oxidation reaction of NANA with IO_4^- for the determination of the reaction order with respect to periodate using the initial-rate method. [NANA] = 2.50 mM, optimum pH 6.0, $\theta = 25$ °C.

$[IO_4^-]$, mM	0.128	0.203	0.250	0.292	0.340
$-(dA/dt)_{init}$ [a,b]	-0.00942	-0.0167	-0.0218	-0.0260	-0.0296

[a] Mean values of triplicate runs

[b] Regression equation: $\log \left| -dA/dt \right|_{init} = (2.62 \pm 0.14) + (1.19 \pm 0.04) \log [IO_4^-]$, $n = 5$, $r = 0.999$.

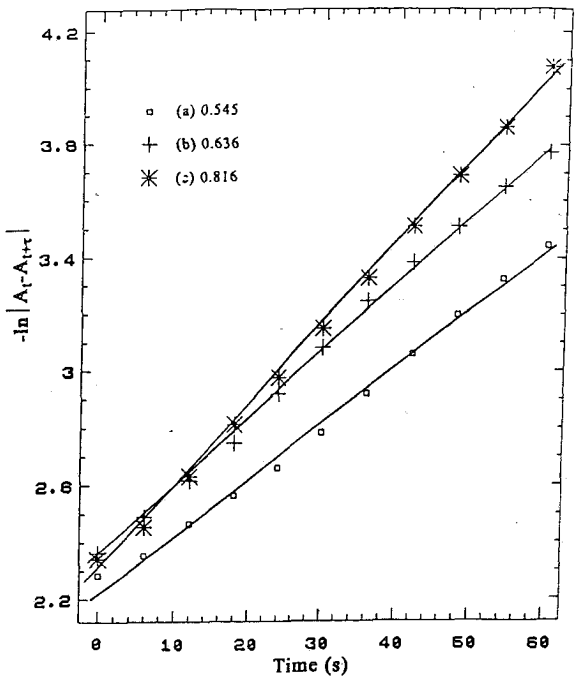

Figure 5. First-order plots for a reaction mixtures of NANA + IO_4^-. [IO_4^-] = 0.0454 mM, pH = 6.0, θ = 25 °C and [NANA] = 0.545 (a), 0.636 (b), 0.816 (c).

By regression analysis a value of 0.98 ± 0.04 was obtained for b (n = 6), indicating that the reaction is first-order with respect to the organic reagent.

Table III. Kinetic results of the oxidation reaction of NANA with IO_4^- for the determination of the reaction order with respect to NANA using Guggenheim method. [IO_4^-] = 0.0454 mM, optimum pH 6.0, θ = 25 °C.

[NANA], mM	0.456	0.545	0.636	0.726	0.816	0.906
k_{obs}, s^{-1} [a,b]	0.0157	0.0200	0.0237	0.0256	0.0295	0.0308

[a] Mean values of triplicate runs

[b] Regression equation: log k_{obs} = - (1.47±0.20) + (0.98±0.06) log [NANA], n = 6, r = 0.991

In conclusion, we present the first systematic kinetic investigation of the oxidation reaction of NANA by periodate. The kinetic study was carried out successfully by monitoring the decrease in absorbance at 244 nm, the isosbestic point of periodate, at 25 °C in phosphate buffer solution pH 6.0. The proposed reaction rate equation is: $\upsilon = kK[\text{NANA}].[IO_4^-]$, where $k = 0.239 \pm 0.011$ s^{-1} and $K = 0.100 \pm 0.005$ M^{-1}. The activation energy was found to be 4.0 ± 0.2 kcal/mol.

Acknowledgements- The authors wish to thank Dr. C.E. Efstathiou for constructive criticism. M. E. S. is grateful to the State Scholarships Foundation for awarding her a scholarship for Ph.D. studies.

References

1. Corfield, A.P. and R. Schauer, Sialic acids, Chemistry, Metabolism and Function, Springer-Verlag: Vienna, 1982; Vol. 10, pp. 33-40.
2. Waters, P I.; Lewry, E. and C.A. Pennock, Ann. Clin. Biochem., 1992, 29, 625-630.
3. Cardo, P.P.; Lombardo, C. and Gatti, R. Clin. Chim. Acta, 1985, 150, 129-135.
4. Warren, L. I. Biol. Chem., 1959, 234, 1971-1975.
5. Iourdian, G.W.; Dean L. and Roseman, S. I. Biol. Chem., 1971, 246, 430-435.
6. Horiuchi, T. and Kurokawa, T. Clin. Chim. Acta, 1989, 182, 117-122.
7. Hammond, K.S. and Papermaster, D.S. Anal. Biochem., 1976, 74, 292-297.
8. Casals-Stenzel, I.; Buscher, H-P. and Schauer, R. Anal. Biochem., 1975, 65, 507-524.
9. Sugiyama, N.; Saito, K-I.; Mizu, H.; Ito, M. and Nagai, Y. Anal. Biochem., 1988, 170, 140-144.
10. Manzi, A.E.; Diaz, S. and Varki, A. Anal. Biochem., 1990, 188, 20-32.
11. Dryhurst, G. In Belcher, R. and Anderson, D.M.W. (Eds.) Periodate Oxidation of Diol and other Functional Groups. Analytical and Structural Applications, Pergamon Press: London, 1970, pp. 24-72.
12. Oegema, T.R. Ir and Cooper, K.M. Anal. Biochem., 1983, 133, 233-238.
13. Bhavanandan, V.P. and Sheykhnazari, M. Anal. Biochem., 1993, 213, 438-440.
14. Spyridaki, M.E. and. Siskos, P.A Anal. Chim. Acta, 1996, 327, 277-285.
15. Gathmann, W.D. and Aminoff, D. Biochem. Biophys. Res. Commun. 1981, 100, 1453-1458.

16. Volz, D.; Reid, P.E.; Park, C.M.; Owen, D.A. and Dunn, W.L. Histochemical Journal, 1987, 19, 249-256.
17. Spiro, R.G. J. Biol. Chem., 1964, 239, 567-573.
18. Peters, B.P. and Aronson, N.N. Jr. Carbohydr. Res., 1976, 47, 345-353.
19. Karayannis, M.I. and Siskos, P.A. Anal. Chim. Acta, 1982, 136, 339-346.
20. Cox, B.G. Modern Liquid Phase Kinetics, Oxford University Press: Oxford, 1994, pp. 4-22.
21. Head, F.S.H. and Standing, H.A. J. Amer. Chem. Soc., 1952, 74, 1457-1462.
22. Hartofylax, V.H.; Efstathiou, C.E. and Hadjiioannou, T.P. Microchem. J., 1986, 33, 9-17.
23. Efstathiou, C.E. and Hadjiioannou, T.P. Reviews in Analytical Chemistry, 1995, 14, 253-277.
24. Duke, F.R. and Bulgrin, V.C. J. Amer. Chem. Soc., 1954, 76, 3803-3806.

ΚΙΝΗΤΙΚΗ ΦΑΣΜΑΤΟΦΩΤΟΜΕΤΡΙΚΗ ΜΕΛΕΤΗ ΤΗΣ ΑΝΤΙΔΡΑΣΗΣ ΟΞΕΙΔΩΣΕΩΣ ΤΟΥ Ν-ΑΚΕΤΥΛΟΝΕΥΡΑΜΙΝΙΚΟΥ ΟΞΕΟΣ ΜΕ ΥΠΕΡΙΩΔΙΚΑ.

Τα σιαλικά οξέα, μια σειρά παραγώγων του νευραμινικού οξέος, απαντώνται ευρέως στους ζωικούς οργανισμούς και βρίσκονται συνήθως ενωμένα στο τελικό άκρο της σακχαρικής αλυσίδας των γλυκοπρωτεϊνών και των γλυκολιπιδίων. Στην παρούσα εργασία, παρουσιάζεται για πρώτη φορά η κινητική φασματοφωτομετρική μελέτη της αντίδρασης οξειδώσεως του κυριότερου παραγώγου των σιαλικών οξέων, του Ν-ακετυλονευραμινικού οξέος (NANA) με υπεριωδικά, στο μήκος κύματος απορρόφησης των υπεριωδικών ιόντων, στα 244 *nm*, παρακολουθώντας την ταχύτητα καταστροφής τους. Οι αντιδράσεις που λαμβάνουν χώρα είναι: $NANA+IO_4^- \overset{K}{\longleftrightarrow} [NANA.IO_4^-]$, $[NANA.IO_4^-] \xrightarrow{k}$ προϊόντα, ενώ η συνολική ταχύτητα αντιδράσεως είναι: $\upsilon = kK[NANA].[IO_4^-]$, όπου k, η σταθερά ταχύτητας διάσπασης του συμπλόκου $[NANA.IO_4^-]$, $k = 0.239 \pm 0.011\ s^{-1}$ και K η σταθερά ισορροπίας σχηματισμού του συμπλόκου, $K = 0.100 \pm 0.005\ M^{-1}$. Η τάξη αντίδρασης ως προς το NANA και τα υπεριωδικά βρέθηκε με τη βοήθεια της μεθόδου Guggenheim και της μεθόδου αρχικής ταχύτητας, χρησιμοποιώντας τη μέθοδο ελαχίστων τετραγώνων. Η ενέργεια ενεργοποίησης, E_a = 4.0 ± 0.2 kcal/mol, υπολογίστηκε από τα διαγράμματα Arrhenius και αντιστοιχεί σε μεταβολή θερμοκρασίας περίπου 3% ανά °C.

Chimika Chronika, New Series, 26, 459-474 (1997)

CONDUCTANCE AND ELECTROSTRICTION OF LIPID BILAYER SUPPORTED ON CONDUCTING POLYMER AND METAL SURFACE

Tibor Hianik[1], Zuzana Červeňanska and Tadeusz Krawczynski vel Krawczyk[2]

[1]Department of Biophysics and Chemical Physics, Comenius University, Mlynska dolina F1, 842 15 Bratislava, Slovakia

[2]Department of Chemistry, University of Warsaw, Pasteura 1, 02093 Warsaw, Poland

(Received: May 10, 1996 In final form: December 23, 1997)

SUMMARY

We studied the conductance and electrostriction of supported bilayer lipid membranes (s-BLM) in dependence on the kind of solid support and concentration of ammonia. Increasing of concentration of ammonia resulted in increase of dc current flowing across polypyrrole (PPY) layer adjacent to metal surface and that covered by lipid bilayer from crude ox brain fraction (COB). No effect on dc conductance has been observed for s-BLM formed on metal support of stainless steel. Electrostriction and membrane capacitance of s-BLM depended on the kind of support onto which s-BLM has been formed. s-BLM formed on PPY layers were characterized by lower compressibility and less expressed dependence of electrostriction parameters upon application of external dc voltage. This evidence that s-BLM on PPY layers are more smooth and as a result more homogeneous than those formed on metal support. Membrane stability characterized by breakdown voltage also depended on the kind of support. s-BLM formed on PPY layers were characterized by about 2 time higher breakdown voltage than that formed on metal support.

Key words: lipid bilayers, polypyrrole, metal support, ammonia, conductance, electrostriction

Acknowledgements

This work was financially supported by The Commission of the European Communities (project No CIPA-CT94-0231) and partly by USAID (project No 12.039 E) and by Slovak Grant Agency project No 1/2190/95. We also thank to Dr. M. Šnejdárková and Dr M. Rehák for generous gift of phospholipids.

Abbreviations and Terminology

A	area of the membrane
ac	alternating current
BLM	bilayer lipid membrane
s-BLM	supported bilayer lipid membrane
C	electrical capacitance
C_s	specific electrical capacitance
COX	crude ox brain fraction
d	thickness of the hydrophobic part of the membrane
dc	direct current
E_0	amplitude of ac voltage
$E_\perp$	Young modulus of elasticity
f	frequency
FI	flow injection method
I	amplitude of dc current
I_0	amplitude of the background dc current
I_1	amplitude of the first harmonic of ac current
I_3	amplituded of the third harmonic of ac current
p	electrostriction pressure
PPY	polypyrrole
SD	standard deviation
U	amplitude of dc voltage

Introduction

Bilayer lipid membranes supported on the metal surface (s-BLM) have been shown as extremely stable and useful for construction of biosensors, e.g. for glucose detection [1,2], xanthine [3] or as a suitable system for development of immunosensors [4]. Application of s-BLM is most powerful in the case, when red-ox reaction takes place on the s-BLM electrode modified by enzyme (e.g. oxidation of glucose by glucose oxidase), i.e. when detected output of reaction represents the current of electrons. However, for detection of ions (e.g. in the case of using s-BLM system as ion selective electrode, or enzymatic electrode with ion output) this system in configuration, when dc current represents the detected signal, is less sensitive. Ions, in principle, can flow through the membranes, but their further movement is stopped at bilayer-metal interface. This gap can be get over using multilayer system consisting of BLM, conducting polymer and metal. The system consisting of conducting polymer - polypyrrole (PPY) - and metal has been already successfully used for construction of biosensor (e.g. for determination of concentration of ammonia [5]).

Polypyrrole is one of the most widely studied conducting polymers because of its high electrical conductivity, useful stability in the conducting form, interesting electrochemical properties, and its relative ease of synthesis on chemical way [6] as well as by anodic electropolymerization method [7] on various conducting substrates from either non-aqueous [8] or aqueous [9] solution containing the monomer and a supporting electrolyte. The PPY properties such as electroactivity, morphology and conductivity are influenced by electropolymerization conditions: e.g. the electrolyte solution (anion species [10] and solvent [11]), temperature [12], current density [13], or potential [9]. Polymerization occurs mainly by α-substitution [14] and the resulting PPY is a linear chain of pyrrole molecules jointed by 5,2 linkages, however, it was also proposed that, at least in certain polymerization conditions, PPY with a macrocyclic (e.g. fullerene-like [15]) structure is formed.

Conducting PPY with cation radical sites (polarons [16], bipolarons [17] or mixed contribution of both [18]) can be charged and discharged reversibly with incorporation and expulsion of small anions maintaining electroneutrality [19]. However, when large immobile anions are incorporated during electropolymerization, electroneutrality during this so called "redox switching" is preserved by movement of electrolyte cations. Depending on the nature of dopant PPY can exhibit different ion-exchange properties [20]. It is also known that electroactivity of PPY is lost upon irreversible oxidation at extreme potentials [21]. Overoxidized PPY is electrochemically non-conductive but ionically conductive and ion-exchange properties are retained.

The interaction of PPY with ammonia gives analytical signal due to change of conductance, capacitance or admittance [22], resistance [23], potential [24] or current [5,25] proportional to ammonia concentration change and therefore PPY can be used in biosensors for detection of ammonia produced in enzymatic reaction. The mechanism of this reaction is not fully known, however, it was broadly discussed [26].

In spite of usefulness of the sensors containing PPY, even for development of biosensors with PPY with immobilized molecules of enzyme, in certain cases the presence of lipid bilayer could be obligatory. This is mainly due to possibility of effective immobilization of enzyme on bilayer surface as well as to provide the optimal condition of enzymatic activity. For example the enzyme electrode containing s-BLM with immobilized glucose oxidase has been more close to native system in respect to its activity then that immobilized on glassy carbon surface and containing ferrocene derivatives [27]. The coexistence of the stable free standing lipid bilayer containing lecithin and polypyrrole (PPY) has been reported by Kotowski and Tien [28]. They showed that free standing BLM containing PPY are more stable than those without PPY, however the presence of PPY did not influence their resistance.

In this paper we report the study of new membrane system containing lipid bilayer, PPY layer and metal surface of the tip of freshly cut Teflon coated stainless steel wire. We compared the conductivity and electrostriction of several systems and

have shown that lipid bilayer can be formed on PPY layer polymerized on metal surface as well as that system provides sufficient sensitivity for detection of ammonia in configuration of measurement dc current. In contrast to PPY supported membranes, s-BLM formed on metal surface had no sensitivity to ammonia.

Materials and Methods

2.1. Preparation of BLM on metal support and reagents

Supported bilayer lipid membranes (s-BLM) were formed on the freshly cut tip of Teflon coated stainless steel wire of diameter 0.33 mm (Leico Industries, Inc. USA). The preparation procedure for s-BLM consisted of two steps [29]. First, one end of a Teflon-coated stainless steel wire was immersed into the lipid solution for a few minutes and then, while still immersed, the tip was cut off. In order to achieve a nice clean cut with the reproducible results, a small guillotine was developed for the cutting procedure. Second, the fresh tip of the wire, having become coated with lipid solution was placed in a 50 mM borate buffer (pH 9.4). Upon immersion of the lipid coated wire in the aqueous solution, the lipid film spontaneously thins, forming a self-assembled lipid bilayer. The existence of lipid bilayer of s-BLM was really proved by Tien and Salamon [29] by means of electrical capacitance measurement of this layer. Such s-BLM are adsorbed onto the metal substrate, have a surrounding Plateau - Gibbs border (torus), and expose polar groups of the lipid molecules to the aqueous phase. The procedure of formation BLM on polypyrrol layer was similar. First the wire was placed into the electrolyte 0.1 M NaCl containing 0.1 M pyrrole (Sigma). Then, in order to form polypyrrole layer the dc voltage U = +0.8 V has been applied to the wire through saturated calomel electrode (SCE) served as reference (positive terminal was on the wire). After 3 min of the application of the voltage the thin PPY layer has been formed due to the polymerization reaction. The tip of the wire with PPY layer has been then put into the chloroform and after dried on the air it has been put into the

lipid solution for a short time (1 min) and subsequently into the electrolyte. The self assembled process of bilayer lipid membrane formation then took place analogically as in the case of metal surface. s-BLM were formed from crude ox brain fraction (COX), prepared according to Folch et al. [30]. Lipid solution contained n-decane:butanol (8:1, v/v) in concentration of 20 mg lipids per 1 ml n-decane.

2.2. DC current measurements

DC current through s-BLM has been measured by simple electrometrical amplifier with high input resistance, based on hybrid integrated circuit WSH 223 (Tesla) [31,32]. Positive terminal was applied to the mini electrode, negative terminal of the potential was applied to the solution via reference SCE.

2.3. Measurements of elasticity modulus $E_\perp$ and membrane capacitance C

The macroscopic parameters of s-BLM supported on metal and-or PPY surface have been checked by simultaneous measurement of two parameters: the Young modulus of elasticity in the direction perpendicular to the membrane surface ($E_\perp$) and membrane capacitance (C) [33-35]. To measure the values of $E_\perp$ and C according to the above methods, an ac voltage $E=E_0\sin 2\pi ft$ with an amplitude of E_0 and frequency f is applied to the lipid bilayer. The membrane is compressed due to electrostriction, and this is reflected in its thickness. According to Hianik and Passechnik [33], this results in the generation of a component of the membrane current with frequency 3f and amplitude I_3, in addition to the first harmonic (with frequency f and amplitude I_1). I_1 and I_3 can be used to calculate the electrical capacitance C of a membrane and the modulus of elasticity in the direction normal to the membrane surface, $E_\perp=-p/(\Delta d/d)$, where $\Delta d/d$ is the relative change in membrane thickness and p is the pressure induced by the electrostriction voltage ($p=C_sE_0^2/2d$). $C_s=C/A$ is the

specific BLM capacitance per unit area and A is the membrane area. In terms of the measured quantities

$$C=I_1/2\pi fE_0 \quad (1)$$

$$E_\perp=3C_sE_0^2I_1/4dI_3 \quad (2)$$

This means that to obtain the parameters $E_\perp$ and C it is sufficient to measure the amplitudes I_1 and I_3. The values of the above parameters can be obtained using standard electronic equipment including resonance amplifiers [33]. In the present work, an alternating voltage with amplitude E_0=40 mV and frequency f=1kHz was applied to the membranes. For calculations the $E_\perp$ of s-BLM we used $C_s=4x10^{-3}$ F/m^2 and d = 4.6 nm (average values of C_s and d according to [29]). C_s and d represent values for "final state" of s-BLM.

Measurements were carried out under the control of an IBM PC/AT 286 computer. All experiments were done at room temperature ($T=20^0$ C).

3. Results and Discussion

3.1. Study of s-BLM conductance

In the first sets of experiments we have studied the conductance of s-BLM formed on metal and/or PPY substrate as well as conductance of PPY layer on metal support (without bilayer) in dependence on concentration of ammonia. We applied to the minisensor the potential of +0.3 V (vs. SCE). This potential has been shown as the optimal for the anodic polarization of the working platinum electrode with PPY layer [5]. Fig. 1 shows the dependence of the changes of dc current $I-I_0$ (I_0 is the current at zero concentration of ammonia) on the concentration of ammonia for five s-BLM formed on metal support. We can see that changes of dc current for both membranes are similar and very low sensitive to the concentration of ammonia (the maximal changes were about ±50 pA). In contrast to s-BLM on metal support, dc current for s-BLM formed on PPY layer adjacent to the metal surface increased following addition

of ammonia into the electrolyte (Fig. 2). For comparison at the Fig. 3 is also shown the plot of the changes of dc current ($I-I_0$) in dependence on the concentration of ammonia for polypyrrole layer on metal support for three independently prepared wires with PPY layers. We can see that with increasing concentration of ammonia the changes of dc current increased, however from c=0.1 mM ammonia saturation takes place. For two electrodes with PPY layers we even observed the decrease of the current at concentrations above 0.2 mM. It is interesting to compare the results presented on Fig. 3 with those obtained in the paper [5]. Using the flow injection method (FI) the authors showed that the ammonium sensor consisting PPY layer formed on platinum electrode with diameter ranging from 1.5 to 3.5 mm revealed linear response up to 0.1 mM concentration of ammonia and the saturation takes place at higher concentrations. In this respect, the results presented in Fig. 3 are similar to that presented in [5]. More pronounced saturation effect and decrease of the current observed for PPY layers on stainless steel wire can be attributed to irreversible changes in PPY layers due to reaction of ammonia with PPY. Irreversibility of reaction is less expressed in FI experiments, when PPY is exposed to ammonia only for short time (approximately 2 min). The presence of s-BLM on PPY layer preserves the minielectrode from the pronounced saturation. Phospholipid bilayer can in this case play the role of the specific filter. The molecules of ammonia are electrically neutral and can penetrate across the membrane to the PPY. The concentration of NH_3 at the s-BLM/PPY interface is less but comparable with that in the electrolyte. This is proved by similar current response of the PPY and s-BLM/PPY systems following addition of ammonia. Principal effect of s-BLM consists in the barrier of the membrane against penetration to the PPY layer the charged ions, i.e. OH^- and Cl^-. Especially chloride has been shown as ion influencing the conductance of PPY layer (see [5]). For PPY layers adjacent to platinum electrode, several possible reactions were proposed for anodic process (Fig. 4, scheme 1,2 [5]). In our case the scheme 1 is more appropriate for explanation of increasing anodic current with increasing concentration of ammonia. This modified scheme is presented as scheme 3 on Fig.4. We can assume that due to

none or negligible concentration of OH^- in the s-BLM/PPY interface the anodic reaction consists in binding of NH_3 with PPY and in production of two electrons and two protons per one molecule of ammonia. Electrons are moving toward anode, while protons are moving to the electrolyte through the structural defects in the membrane.

3.2. Study of membrane electrostriction

In order to check how macroscopic parameters of supported membranes depend on the kind of support we have measured the elasticity modulus in direction perpendicular to the membrane place $E_\perp$ and membrane electrical capacitance C.

Fig. 5 (a) shows the typical example of kinetic of $E_\perp$ (curve 1) and C (curve 2) following application to s-BLM an ac voltage with small amplitude (E_0=40 mV). We can see that both values reached the steady state after ~ 30-50 min. The values of $E_\perp$ for these membranes were (2.38±1.32)x10^6 Pa (n=5, ±SD) and C=(109±81) pF (n=5, ±SD). The membrane capacitance was in average about 3.5 time less than the geometrical capacitance calculated from diameter of wire and using value of specific capacitance C_s=4x10^{-3} F/m^2. This evidences about considerable Plateau-Gibbs border and a number of inhomogeneities in these membranes filled with hydrocarbon solvent [35]. Similar kinetics and values of $E_\perp$ were obtained also for s-BLM formed from crude ox brain fraction on PPY layers adjacent to metal support (Fig 5b). These s-BLM were, however, formed faster and the steady state values of $E_\perp$ and C have been reached after ~ 15 min. The values of $E_\perp$ for these membranes were (2.66±2.9)x10^6 Pa (n=5, ±SD), however the average capacitance reached considerably higher values C=(650±290) pF (n=5, ±SD). This evidences, that s-BLM formed on PPY layers are more homogeneous and are characterized by lower Plateau-Gibbs area.

A complicated dependence of electromechanical parameters of s-BLM on externally applied dc voltage has been found in previous studies [34,35]. This phenomenon holds also for s-BLM formed on metal support studied in this work. Fig. 6 a,b shows the dependence of $E_\perp$ (a) and C (b) on dc voltage applied to the s-BLM

formed in 50 mM borate buffer (pH 9.4) on metal support with rate 500 mV/min in the case of cyclic application of the voltage from 0 to 500 mV and 500 to 0 mV (the direction of voltage is shown by arrows). We can see that while membrane capacitance changes monotonously, the elasticity modulus is represented by curves with maximum around 220 mV. The nature of dependence of $E_{\perp}$ and C on dc voltage as well as hysteresis of these parameters has been discussed in detail earlier [34]. We have shown that shape of the dependence of these parameters on dc voltage can be connected with solvent redistribution in rather inhomogeneous s-BLM. In such a membrane solvent plays certain structuralized role in contrast to the situation in free standing BLM. Moving the solvent out of this region in s-BLM leads to a decrease of the membrane ordering and thus to a decrease of $E_{\perp}$, whereas in BLM $E_{\perp}$ is increased. Capacitance has minimum just in the region of the maximal value of $E_{\perp}$ (see [34]).

s-BLM formed on PPY layer adjacent to metal support were characterized by less expressed extreme for C and $E_{\perp}$ (Fig. 7 a,b). Moreover the decrease of capacitance with voltage correspond to decrease of $E_{\perp}$ similarly like in planar free standing BLM. This phenomenon can be due to smoother surface of PPY adjacent to metal in comparison with metal surface [36] (see schematic representation of the s-BLM structure at Figs. 6 and 7) and as a consequence the electrostriction properties of s-BLM formed on PPY layers become closer to planar free standing BLM. Smoother surface of s-BLM formed on PPY layer can also explain better stability of these membranes upon breakdown by dc voltage. While amplitude of breakdown voltage for s-BLM on metal support was U = (1077±178) mV (n=3, ±SD) for s-BLM formed on PPY layer this value was higher than 2 V.

Conclusion

s-BLM formed on PPY layers adjacent to metal support represent stable system allowing detection of ammonia with detection limit lower than 50 μM. In contrast to electrodes with PPY layers but without lipid bilayer, the new developed system

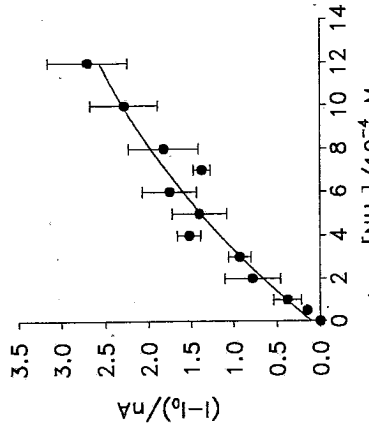

Fig. 1

Fig. 2

Fig. 1 The plot of $(I-I_0)$ versus concentration of ammonia for five s-BLM of the same composition formed on the tip of stainless steel wire. I_0 is the background current at concentration of ammonia c=0. U=300 mV (positive terminal on the wire).

Fig. 2 The plot of $(I-I_0)$ versus concentration of ammonia for s-BLM formed on the PPY layer adjacent to the metal surface at the tip of stainless steel wire. U=300 mV (positive terminal on the wire). The error bars represent SD obtained on 3 s-BLM.

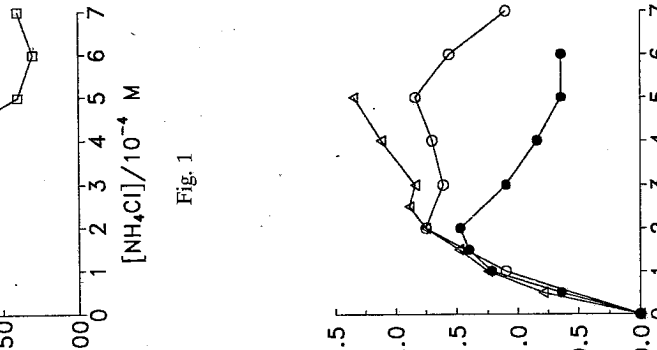

Fig. 3

Fig. 3 The plot of $(I-I_0)$ versus concentration of ammonia for three independently prepared PPY layers formed on the tip of stainless steel wire. U=300 mV (positive terminal on the wire).

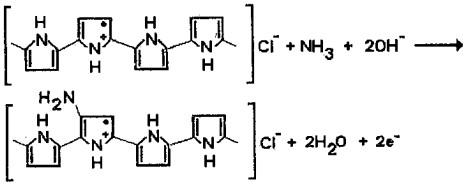

Scheme 1

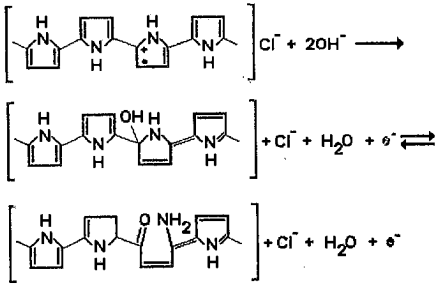

Scheme 2

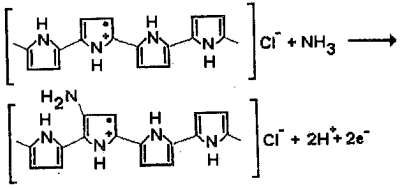

Scheme 3

Fig. 4 The schemes of anodic processes taking place between PPY and electrolyte (schemes 1,2) (according to [5]) and on lipid bilayer/PPY interface (scheme 3) (for explanation see the text).

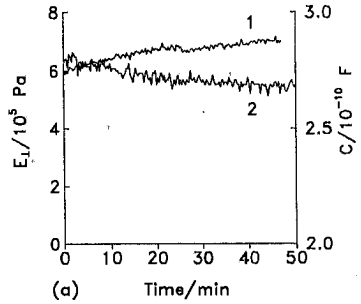

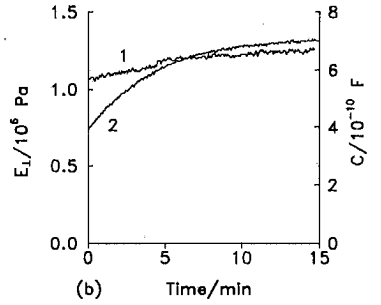

Fig. 5 Kinetics of elasticity modulus $E_{\perp}$ (curve 1) and membrane capacitance (curve 2) following application of ac voltage of small amplitude (E_0=40 mV) for: (a) s-BLM formed on metal support; (b) s-BLM formed on polypyrrole layer adjacent to metal support.

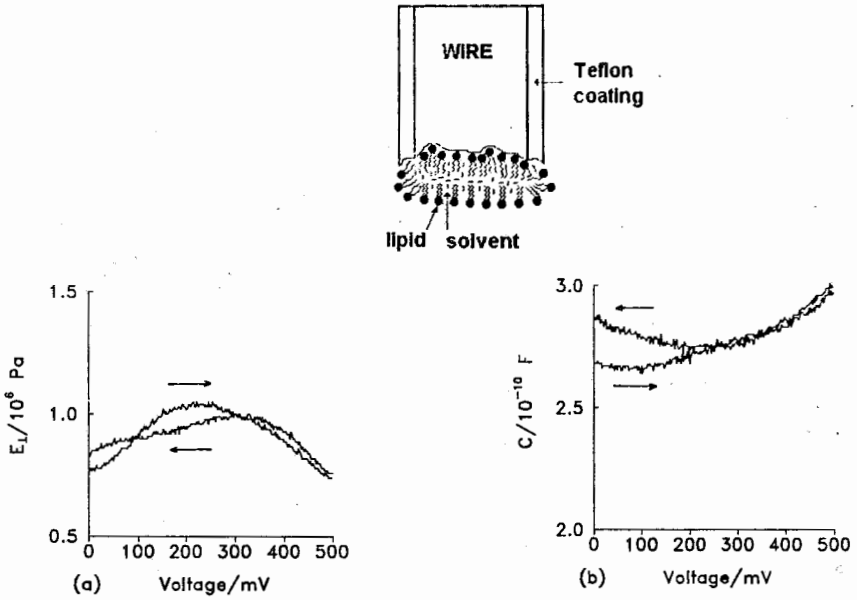

Fig. 6. Dependence of elasticity modulus E1 (a) and membrane capacitance C (b) on magnitude of dc voltage cyclically applied on s-BLM formed on metal support. Scan rate 500 mV/min, direction of voltage is shown by arrows. Electrolyte side was positive. A schematic representation of the structure of bilayer.

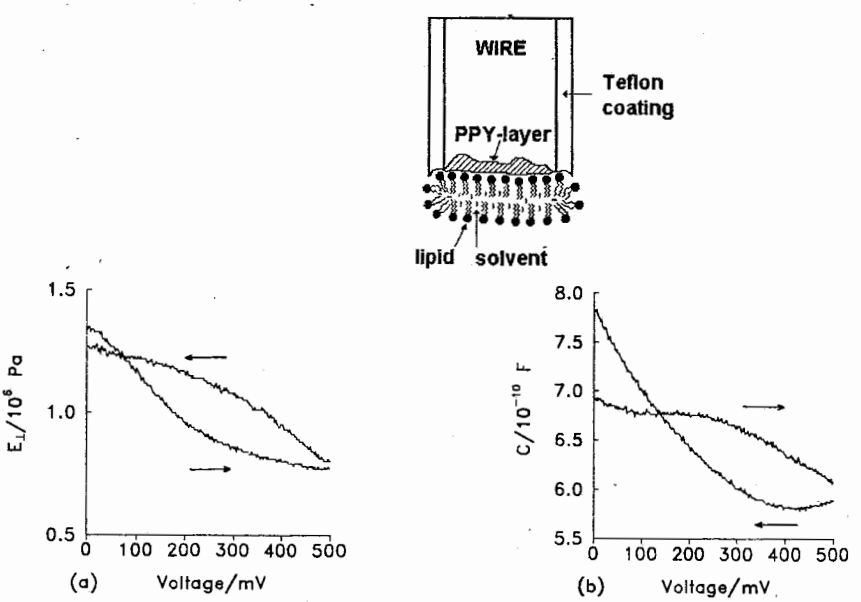

Fig. 7. Dependence of elasticity modulus E1 (a) and membrane capacitance C (b) on magnitude of dc voltage cyclically applied on s-BLM formed on PPY layer adjacent to metal support. Scan rate 500 mV/min, direction of voltage is showed by arrows. Electrolyte side was positive. A schematic representation of the structure of bilayer.

ΠΕΡΙΛΗΨΗ

ΑΓΩΓΙΜΟΤΗΤΑ ΚΑΙ ELECTROSTRICTION ΔΙΠΛΟΣΤΙΒΑΔΑΣ ΛΙΠΙΔΙΩΝ ΕΠΙ ΑΓΩΓΙΜΟΥ ΠΟΛΥΜΕΡΟΥΣ ΚΑΙ ΕΠΙ ΜΕΤΑΛΛΙΚΗΣ ΕΠΙΦΑΝΕΙΑΣ

Μελετήθηκε η αγωγιμότητα και η electrostriction υποστηριγμένης μεμβράνης διπλοστιβάδας λιπιδίων (S-BLM) σε συνάρτηση με το είδος του στερεού υποστηρίγματος και της συγκέντρωσης της αμμωνίας. Η αύξηση της συγκέντρωσης της αμμωνίας είχε ως αποτέλεσμα την αύξηση της ροής του ρεύματος dc δια μέσου της στιβάδας της πολυπυρρόλης (PPY) επί της μεταλλικής επιφάνειας και της επικαλυμένης με διπλοστιβάδα λιπιδίων από ακατέργαστο κλάσμα από μυαλά βοδιού (COB). Δεν παρατηρήθηκε επίδραση επί της αγωγιμότητας dc για την S-BLM που σχηματίσθηκε επί μεταλλικού υποστηρίγματος από ανοξείδωτο χάλυβα. Η electrostriction και η ηλεκτρική χωρητικότητα της μεμβράνης S-BLM εξαρτάται από το είδος του υποστηρίγματος επί του οποίου έχει σχηματισθεί η S-BLM. Η S-BLM που σχηματίσθηκε επί στιβάδας PPY χαρακτηρίσθηκε από χαμηλότερη συμπιεστότητα και μικρότερη εκφρασμένη εξάρτηση των παραμέτρων της electrostriction κατά την εφαρμογή εξωτερικής τάσης dc. Απόδειξη ότι η S-BLM επί στιβάδας PPY είναι περισσότερο λεία και ως αποτέλεσμα περισσότερο ομοιογενής απ' ότι αυτές που σχηματίζονται επί μεταλλικών υποστηριγμάτων. Η σταθερότητα της μεμβράνης που χαρακτηρίζεται από τη διακοπή της τάσης επίσης εξαρτάται από το είδος του υποστηρίγματος. Η S-BLM που σχηματίσθηκε επί στιβάδας PPY χαρακτηρίσθηκε από 2 φορές περίπου υψηλότερη τάση διακοπής σε σύγκριση με αυτήν επί μεταλλικού υποστηρίγματος.

References

1. Šnejdárková, M., Rehák, M. and Otto, M.: *Anal. Chem.* **65** 665 (1993).
2. Hianik, T., Šnejdárková, M., Passechnik, V.I., Rehák, M. and Babincová, M.: *Bioelectrochem. Bioenerg.* (1996) (in press).
3. Rehák, M., Šnejdárková, M. and Otto, M.: *Biosensors and Bioelectronics* **9**, 337 (1994).
4. Nikolelis, D.P., Tzangelis, M.G. and Krull, U.J.: *Anal. Chim. Acta* **282**, 527 (1993).
5. Trojanowicz, M., Lewenstam, A., Krawczynski vel Krawczyk, T., Lahdesmaki, I., Szczepek, W.: *Electroanalysis* (1996) (in press).
6. Ractliffe, N.M.: *Anal. Chim. Acta* **239**, 256 (1990).
7. Diaz, A.F., Kanazawa, K.K. and Gardini, G.P.: *J. Chem. Soc. Chem. Commun.* 635 (1979).
8. Genies, E.M., Bidan, G. and Diaz, A.F.: *J. Electroanal. Chem.* **149**, 101 (1983).
9. Asavapiriyanont, S., Chandler, G.K., Gunawardena, G.A. and Pletcher, D.: *J. Electroanal. Chem.* **177**, 229 (1984).
10. Kuwabata, S., Nakamura, J. and Yoneyama, H.: *J. Electrochem. Soc.* **137**, 2147 (1990).
11. Diaz, A.F. and Castillo, J.I.: *J. Chem. Soc. Chem. Commun.* 397 (1980).
12. Ogasawara, M., Funahashi, K., Demura, T., Hagiwara, T. and Iwata, K.: *Synth. Met.* **14**, 61 (1986).
13. Schmeisser, D., Naarmann, H. and Gopel, W.: *Synth. Met.* **59**, 211 (1993).
14. Street, G.B., Clarke, T.C., Krounbi, M., Kanazawa, K., Lee, V. and Pfluger, P.: *Mol. Cryst. Liq. Cryst.* **83**, 253 (1982).
15. van Eyk, S.J. and Naarmann, H.: *Synth. Met.* **58**, 233 (1993).
16. Waller, A.M. and Compton, R.G.: *J. Chem. Soc., Faraday Trans. I.* **85**, 977 (1989).
17. Lippe, J. and Holze, R.: *Synth. Met.* **41-43**, 2987 (1991).

18. Zotti, G. and Schiavon, G.: *Synth. Met.* **41-43**, 445 (1991).
19. Kawai, K., Mihara, N., Kuwabata, S. and Yoneyama, H.: *J. Electrochem. Soc.* **137**, 1793 (1990).
20. Li, Y. and Qian, R.: *Synth. Met.* **26**, 39 (1988).
21. Krische, B. and Zagorska, M.: *Synth. Met.* **28**, C257 (1989).
22. Yon Hin, B.F.Y., Sethi, R.S. and Lowe, C.R.: *Sens. Actuators* **B1**, 550 (1990).
23. Nylander, C., Armgart, M. and Lundstrom, L.: *Anal. Chem. Symp. Ser.* **17**, 203 (1983).
24. Adeloju, S.B., Shaw, S.J. and Wallace, G.G.: *Anal. Chim. Acta* **281**, 611 (1993).
25. Pandey, P.C. and Mishra, A.P.: *Analyst* **113**, 329 (1988).
26. Gustafsson, G., Lundström, I., Liedberg, B., Wu, C.R., Inganäs, O. and Wennerström, O.: *Synth. Met.* **31**, 163 (1989).
27. Bartlett, P.N., Bradford, V.Q. and Whitaker, R.G.: *Talanta* **38**, 57 (1991).
28. Kotowski, J. and Tien, H.T.: *Bioelectrochem. Bioenerg.* **22**, 277 (1989).
29. Tien, H.T. and Salamon, Z.: *Bioelectrochem. Bioenerg.* **22**, 211 (1989).
30. Folch, J., Lees, M. and Stanley, G.S.H.: *J. Biol. Chem.* **226**, 497 (1957).
31. Dostál, J.: Operational Amplifiers, (1st edition), p. 118, Elsevier, Amsterdam, Oxford, New York (1981).
32. Hianik, T., Laputková, G. and Bajci, A.: *Gen. Physiol. Biophys.* **7**, 191 (1988).
33. Hianik, T. and Passechnik, V.I.: Bilayer Lipid Membranes. Structure and Mechanical Properties, (1st edition), p. 26, Kluwer Academic Publishers, Dordrecht (1995).
34. Hianik, T., Dlugopolsky, J. and Gyepessova, M.: *Bioelectrochem. Bioenerg.*, **31**, 99 (1993).
35. Hianik, T., Passechnik, V.I., Sargent, D.F., Dlugopolsky, J. and Sokolíková, L.: *Bioelectrochem. Bioenerg.* **37**, 61 (1995).
36. Hianik, T., Dlugopolsky, J., Passechnik, V.I., Sargent ,D.F. and Ivanov, S.A.: *Coll Surf. A* **106**, 109 (1996).

Chimika Chronika, New Series, 26, 475-486 (1997)

BINDING OF AROMA VOLATILES TO BIOPOLYMERS

C.J. ISRAILIDES[1*], A.VLYSSIDES[2] , R.S.T. LINFORTH[3]

AND A. J. TAYLOR[3]

1. Institute of Technology of Agricultural Products. National Agricultural Research Foundation
   1. S. Venizelou St., Lycovrissi 141 23 Athens Greece.
2. National Techical University of Athens
   Dept. of Chemical Engineering, Division IV
   Laboratory of Organic and Environmental Technology
   Polytechnioupoli Zographou, Athens 157 80
3. University of Nottingham
   Dept. of Applied Biotechnology and Food Science.
   Sutton Bonigton Campus, Loughborough
   Leics, LE 12 5RD. U.K.

(Received: February 11, 1997 In final form: December 23, 1997)

SUMMARY

The release of aroma volatiles from aqueous solutions and their binding to biopolymers contained therein was studied. The methods were traditional headspace analysis using Tenax trapping followed by GC-MS analysis and an Atmospheric Pressure Chemical Ionisation technique (APCI) that allows a novel approach to headspace analysis.

The biopolymers studied were the polysaccharides starch, pullulan and dextran along with two proteins, bovine serum albumin (BSA) and casein.

In the case of polysaccharides there was no evidence of any positive binding for any of the volatiles tested, while salting out effects have been manifested with some of the volatiles.

Of the proteins, BSA showed a significant binding effect to diacetyl and benzaldehyde. On the other hand casein bound positively to dimethylpyrazine and to benzaldehyde.

Key Words: Aroma, Volatiles, Binding, Proteins, Polysaccharides

* corresponding author:

INTRODUCTION

Aroma compounds are very significant in the food industry particularly when they bind to biopolymers important in human nutrition. Foods with added flavour have been produced and consumed for thousands of years and their use has been in constant increase in recent decades.

Main reasons for such a trend is the increase in use of processed foods which demand flavour, the introduction of new raw materials and the production of food substitutes on the market.

Binding of volatile aroma compounds to proteins and polysaccharides is probably achieved with the aid of hydrogen bonds.

The binding of aroma compounds by biopolymers may involve one or more binding sites of those occuring in the polymer.

The sorption of aroma volatiles on the biopolymer is based on the law of mass action (one binding site)[1].

$$K = \frac{[BA]}{C_f[B]} = \frac{[BA]}{KC_f[B]}$$

Where K= a single binding constant

Cf= concentration of free aroma compound

[B] = " of biopolymer

[BA] = " of aroma - biopolymer complex

The average number of aroma molecules bound to a biopolymer is given by the specific binding capacity (r).

$$r = \frac{[BA]}{([B]+[BA])} = \frac{K\,C_f[B]}{([B]+K[B]C_f)} = \frac{KC_f}{1+KC_f}$$

When several binding sites (n) are involved equal in binding capacity and independent of each other

$$\text{then } r = \frac{nKC_f}{1+KC_f} = nk = K' \text{ overall binding constant}$$

The binding regions may be located in the inner space of the macromolecule as in the case of starch which can trap the volatiles inside its helical structure after gelatinization. There can also be binding regions located in the outer surface of the helix. However within the helix the

trapped aroma compound can not fulfill an active role as an aroma constituent.

In proteins there is a large number of binding groups (or sites) involved in aroma binding. The greater binding affinity indicated by higher binding constants (K') with aldehydes like butanal or benzaldehyde implies reactions with free amino or SH-groups., while compounds such as di-methylpyrazine and butyric acid are practically unable to bind[2].

MATERIALS AND METHODS

The release of five volatile compounds from aqueous solution containing biopolymers was studied. The volatiles were:

1) Diacetyl
2) Pentanol
3) Hexanal
4) 2,5 - Dimethyl Pyrazine
5) Benzaldehyde

The biopolymers studied were three polysacharides, namely: potato starch, pullulan, and dextran (avg. MW 250.000), along with two proteins, namely: bovine serum albumin (BSA) and casein.

The methods used were traditional headspace analysis using Tenax trapping followed by GC-MS and a new on line MS technique namely: Atmospheric Presure Chemical Ionization, (APCI) that allows a novel approach to headspace analysis[3,4].

Tenax trapping is a method which effectively separates the volatile compounds of interest from air and, to a great extent, from water. The volatiles can subsequently be desorbed and chromatographed, thereby allowing the identification and quantification of compounds present. APCI is a technique where compounds can be ionised in air containing water vapour at atmospheric pressure. Ions are subsequently collected into the high vacuum region of the analyser which allows easier interfacing. This technique is designed for analysis of aqueous samples. It adds a proton (in positive ionisation mode) to the compound of interest and does not normally induce

fragmentation [4,5,6,7,8].

ANALYTICAL PROCEDURE

The solution of volatiles was prepared by adding 750µl of an aqueous solution (containing 150 µl of dimethyl pyrazine, 10µl hexanal, 90 µl diacetyl, 130 µl pentanol and 20µl benzaldehyde per 100 ml H_2O) to 100 ml of water in a 1 l flask. The amounts of the volatiles were chosen so that the concentration of the compounds in the headspace would be roughly equal based on their partition coefficients.

The volatiles were allowed to equilibrate for 5 min before samples were taken.

In both methods of analyses, Tenax trapping and APCI, the headspace of aqueous solutions (control) was compared to that of the solution containing the biopolymers. In the case of Tenax trapping starch was the only biopolymer.

A. Tenax Trapping

Fifty ml of head space (HS) were collected each time into a tenax trap using a vacuum pump. Compounds were desorbed from traps and cryofocused on column (N_2 cold trap). GC analysis was performed using a temperature programme with initial temperature 30°C and then 8°C per min ramp up to 150°C. The column, BP-1, was 25m x 0.22 mm I.D.

B. APCI

After equilibration of the volatiles the head space was sampled into the MS (flow rate 25 ml/min). The ions monitored corresponded to the molecular ion plus a proton (MH^+), except for pentanol which lost water during ionisation (MH^+-H_2O monitored).

The signal produced by the volatiles in the headspace was constant, indicating that the dilution of the headspace as a result of continuous sample removal was insufficient to cause a significant disruption of the air/water equilibrium.

Blanks of solutions of each of the biopolymers were run to confirm that these were not associated with ions of a similar mass to the ions of interest.

RESULTS AND DISCUSSION

Table I and Figures 1 and 2 show average values and standard error from three replicates of volatile compounds released in the headspace of

water and 1% (w/v) aqueous solutions of starch measured by Tenax trapping. The results are also expressed as normalized values relative to pentanol.

TABLE I: Comparison of the peak areas of volatiles present in the headspace of water and 1% (w/v) aqueous solution of starch. (Tenax trapping).

Compound	water Av.area		Starch Av.area		% Binding
Diacetyl	241+87	(44+3)	241+72	(49+12)	0.00 (-9.88)
Pentanol	537+167	(100+0)	495+210	(100+0)	7.79 (0.00)
Hexanal	503+211	(91+15)	412+192	(82+9)	18.09 (9.00)
2,4 Dimethyl pyrazine	827+200	(158+20)	1004+498	(206+72)	-21.47 (-30.50)
Benzaldexyde	1096+294	(212+59)	1077+407	(226+50)	1.75 (-6.50)

Numbers in brackets are normalised relatively to pentanol

Table II and Figures 3 & 4 show the average values and standard error from three replicates of volatiles released (peak heights) in the headspace of solutions of polysaccharides by the APCI method.

TABLE II: Mean values of volatile peak heights in the headspace of solutions of polysaccharides. (APCI method).

Compound	Control	Starch	Dextran	Pullulan
2,4 Dimethyl pyrazine	14.4+1.1[a]	15.4+0.7	15.5+1.8	17.5+0.1[a]
Benzaldehyde	60.8+1.9	64.2+0.4	65.9+7.0	66.5+2.8
Hexanal	43.7+0.5[b]	48.3+1.6[b]	43.7+3.7	44.2+4.1
Diacetyl	16.8+1.2	18.5+0.5	19.3+1.6	17.4+0.7
Pentanol	63.9+2.5	62.6+1.3	55.7+7.4	66.9+3.5

Means bearing the same superscripts are significantly different ($p<0.05$)

There was a significant salting out effect (negative binding) in the case of pullulan with 2,4 dimethylpyrazine and in the case of starch for hexanal Interestingly enough this latter effect was not verified with tenax trapping where there were no real differences detected in starch for binding with any of the volatiles tested probably due to the great variability in the results. It should be kept in mind that starch binds the volatiles only after gelatinization by trapping them in its helical structure (Belitz and Grosch, 1985).

Table III and Figures 5 & 6 show the average and standard error from three replicate runs of volatiles released (peak heights) in the headspace of protein solutions by the APCI method.

TABLE III: Mean values of volatile peak heights in the headspace of protein solutions.

Compound	Control	BSA	Casein
2,4 Dimethyl pyrazine	13.3+1.0[a]	12.4+1.1	6.5+2.5[a]
Benzaldehyde	57.6+1.1[b]	34.3+3.1[b]	48.6+5.9[b]
Hexanal	40.8+1.9	0.0+0.0	40.4+3.9
Diacetyl	15.3+0.6[c]	9.1+0.7[c]	13.1+1.8
Pentanol	67.0+14.6	54.8+12.8	49.1+5.6

Means bearing the same supercripts are significantely different

a: $p<0.01$

b: $p<0.01$ (for BSA) $p<0.05$ (for casein)

c: $p<0.001$

The BSA solution was the only solution to produce a significant contaminating ion. The ion produced (m/z 100.8) made it impossible to observe the interaction of hexanal with BSA. The presence of this ion may have been due to hexanal itself since BSA preparation is often associated with lipid, and it might have contained hexanal in the initial state.

There was a significant binding effect of diacetyl ($p<0.001$) and

benzaldehyde ($p<0.01$) to BSA and of 2.4 dimethyl pyrazine ($p<0.01$) and benzaldehyde ($p<0.05$) to casein.

CONCLUSIONS

There was no evidence for any positive binding of volatives to polysaccharides in solution as compared to blanks in aqueous solutions with all the volatiles tested.

Proteins appear to have stronger affinities for aroma volatiles compared to polysaccharides probably due to more binding sites and hydrophobic interactions which result in aroma binding.

ACKNOWLEDEMENTS

The authors would like to acknowledge the European Commission DGXII/B1 for supporting this research through the COST 96 programmes.

ΠΕΡΙΛΗΨΗ

ΔΕΣΜΕΥΣΗ ΠΤΗΤΙΚΩΝ ΑΡΩΜΑΤΙΚΩΝ ΕΝΩΣΕΩΝ ΣΕ ΒΙΟΠΟΛΥΜΕΡΗ

Στην εργασία αυτή μελετήθηκε η δέσμευση διαφόρων πτητικών οσμηρών ενώσεων σε υδατικά διαλύματα που περιείχαν μακρομοριακές ενώσεις όπως πολυσακχαρίτες και πρωτεΐνες. Σαν μάρτυρας χρησιμοποιήθηκε νερό με τις ίδιες πτητικές ενώσεις και σε ίσες συγκεντρώσεις. Η απελυθέρωσή τους στην υπερκείμενη αέρια φάση και κατά συνέπεια η δέσμευσή τους από μακρομοριακές ενώσεις είναι μεγάλης σημασίας για τις βιομηχανίες τροφίμων λόγω της διαρκώς αυξανόμενης τάσης για προσθήκη διαφόρων αρωματικών ιδίως στα μεταποιημένα τρόφιμα.

Οι μέθοδοι που χρησιμοποιήθηκαν ήταν η ανάλυση με τη χρήση παγίδας Tenax και συνέχεια ανάλυση με αέρια χρωματογραφία και φασματογραφία μάζης. Επίσης χρησιμοποιήθηκε μια νέα τεχνική που ονομάζεται χημικός ιονισμός ατμοσφαιρικής πίεσης (APCI). Οι μακρομοριακές ενώσεις που μελετήθηκαν ήταν τρείς πολυσακχαρίτες, δηλ. άμυλο, πουλλουλάνη, και δεξτράνη και δύο πρωτεΐνες, αλβουμίνη ορού βοοειδών (BSA) και καζεΐνη.

Οι πτητικές αρωματικές ενώσεις που χρησιμοποιήθηκαν ήταν: Διακετύλιο, πεντανόλη, εξανάλη, 2,5 δι-μεθυλ-πυραζίνη και βενζαλδεΰδη.

Στην περίπτωση των πολυσακχαριτών δεν υπήρξε θετική δέσμευση με καμία από τις πτητικές αρωματικές ουσίες που μελετήθηκαν ενώ με μερικές από αυτές παρατηρήθηκαν φαινόμενα αρνητικής δέσμευσης (salting out effects). Αυτό συνέβη στην περίπτωση της πουλλουλάνης με τη 2,4 δι-μεθυλ-πυραζίνη και στην περίπτωση του αμύλου με την εξανάλη.

Στις πρωτεΐνες η BSA έδειξε σημαντική επίδραση δέσμευσης με το διακετύλιο και την βενζαλδεϋδη. Επίσης η καζεΐνη δέσμευσε την δι-μεθυλ-πυραζίνη και την βενζαλδεϋδη.

Γενικά οι πρωτεΐνες εμφανίζουν ισχυρότερη τάση δέσμευσης αρωματικών πτητικών ενώσεων σε σύγκριση με τους πολυσακχαρίτες, πιθανόν λόγω του μεγαλύτερου αριθμού των ενεργών κέντρων και υδρόφοβων αλληλεπιδράσεων που ευθύνονται για την δέσμευση οσμηρών ενώσεων στις πρωτεΐνες.

REFERENCES

[1]. Belitz, H.D. and Grosch, W.: Food Chemistry, 2nd ed. Springer Verlag, New York (1985).

[2]. Solms, J.: Aromastoffe als Liganden. Geruch-und Geschmackstoffe (Ed:Drawert, F.) Verlag Hans Carl, Nurnberg (1975).

[3]. Linforth, R.S.T. and Taylor A.J.: Food Chem. 48, 115(1993).

[4]. Ingham, K.E., Linforth, R.S.T. and Taylor, A.J: Food Chem, 54, 283 (1995).

[5]. Ketkar, S.N, Dulak, J.G., Fite, W.L., Buchner, J.D. and Dheandhanoo, S.: Anal. Chem., 61, 260 (1989).

[6]. Linforth, R.S.T. and Taylor, A.J.: Apparatus and methods for the analysis of trace constituents in gases. Patent application (U.K). 9615303.6 (1966).

[7]. Linforth, R.S.T. and Taylor, A.J.: Improvement relating to volatile compound detection. Patent application (U.K) 9615304, 4 (1966).

[8]. Linforth, R.S.T.: Ingham, K.E.: Taylor, A.J.: Flavour Science: Recent Developments. Royal society of chemistry, pp.361-368. ISBN 0854047026 (1977).

FIG.1. Comparison of peak heights of compaounds in the headspace of pure water or 1% starch solutions (determined by Tenax trapping)

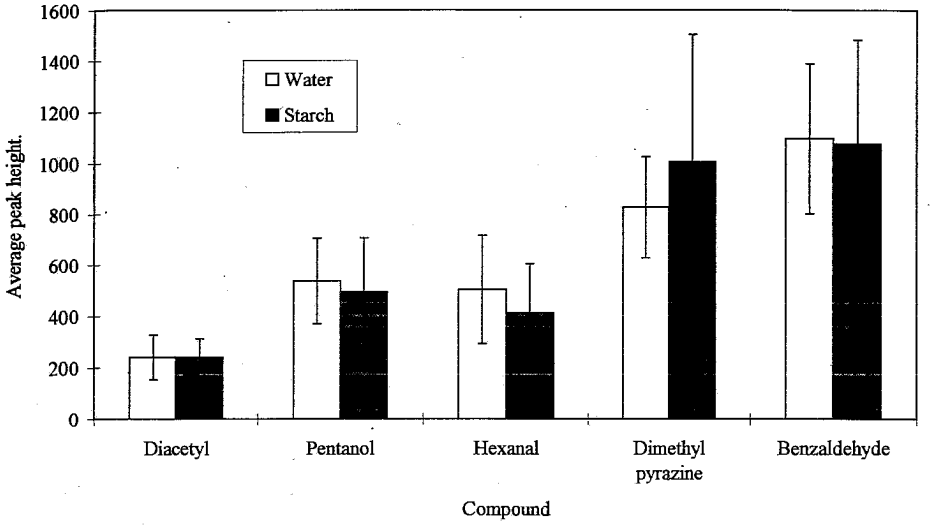

FIG.2. Comparison of peak heights (normalised relative to pentanol) of compounds in the headpspace of pure water or 1% starch solution (determined by Tenax trapping).

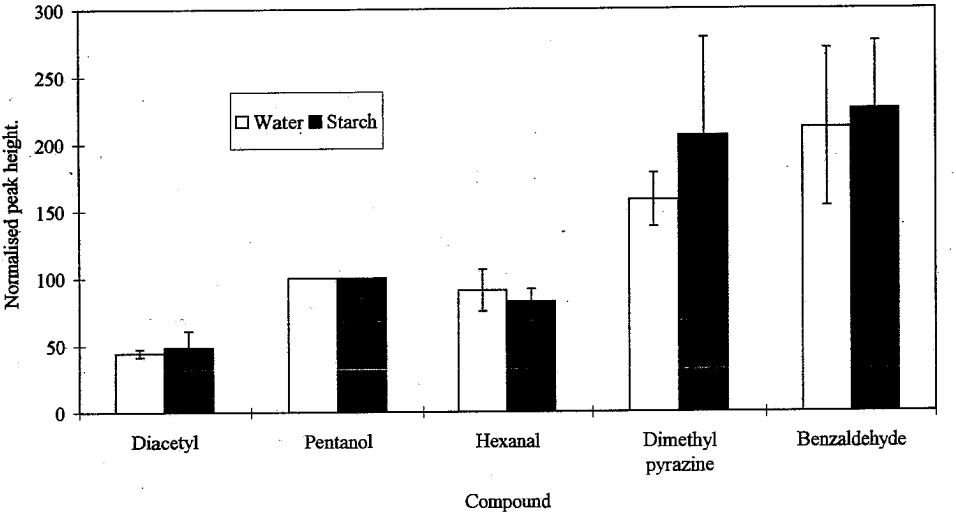

FIG.3. Peak height for volatiles compounds in headspace of 0.5% polysaccharide solutions.

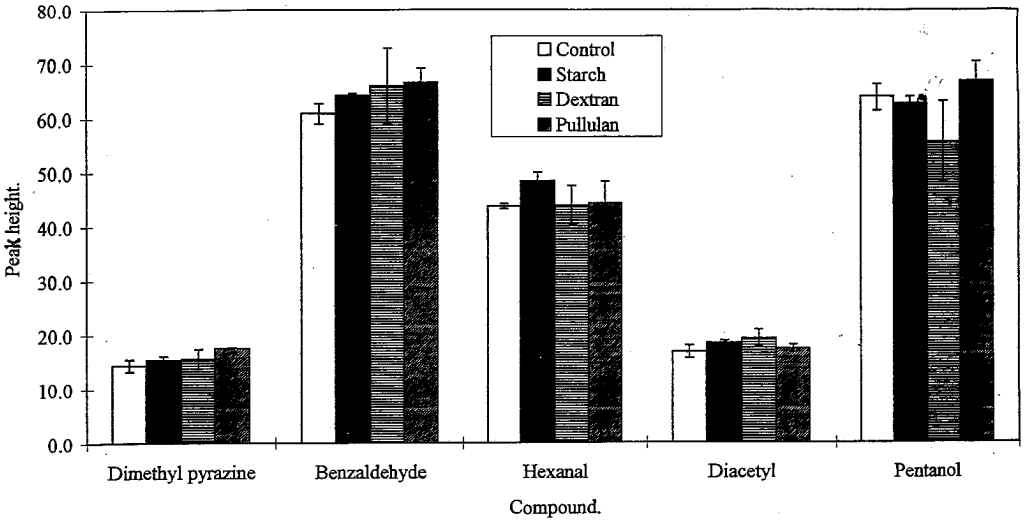

FIG.4. Percentage binding of volatiles by 0.5% polysaccharide solutions

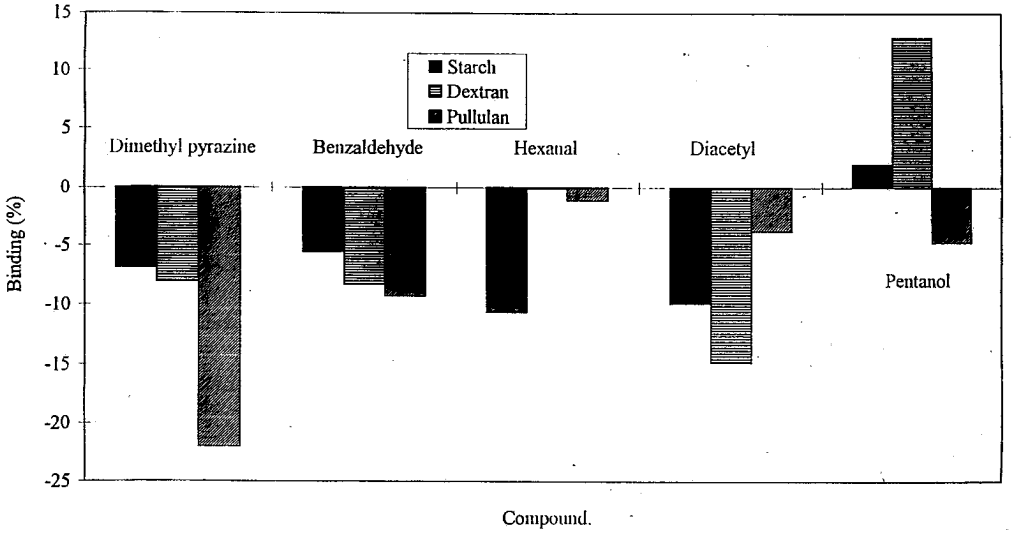

FIG.5. Peak height for volatile compounds in headspace of 0.5% protein solutions.

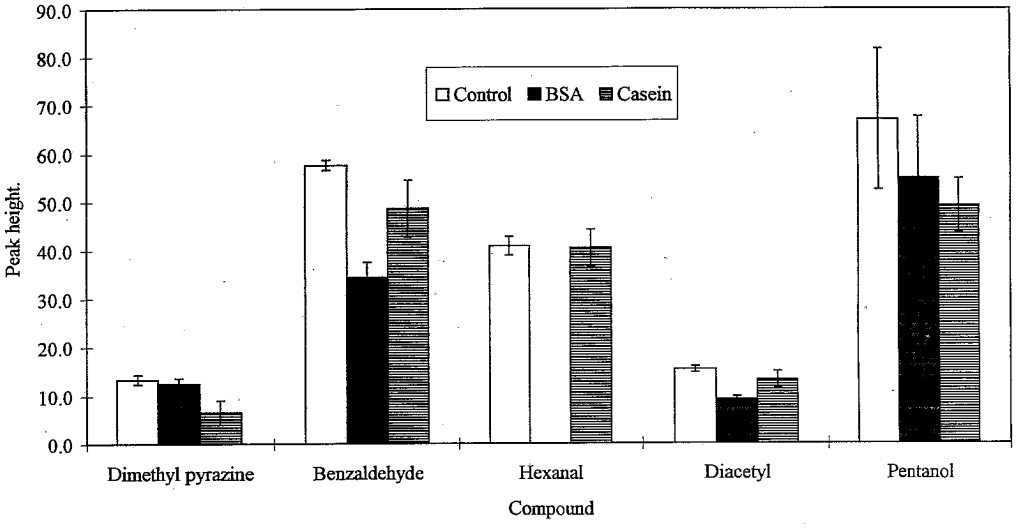

FIG.6. Percentage binding of volatiles by 0.5% protein solutions

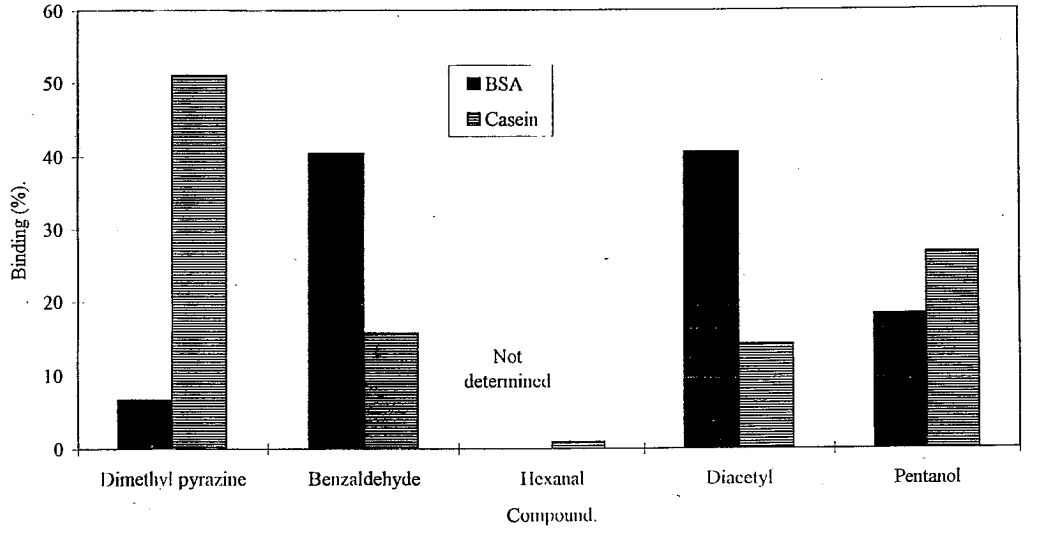

Chimika Chronika, New Series, 26, 487-494 (1997)

STUDY OF PHYSICAL AND MECHANICAL PROPERTIES OF COTTON FIBRES AFTER LOOSE DYEING IN ABSENCE AND PRESENCE OF SOFTENING LUBRICATING AGENTS

A. KEHAYOGLOU*, E. TSATSARONI, S. PEGIADOU - KOEMTZOPOULOU,

I. ELEFTHERIADIS

Laboratory of Organic Chemical Technology, Department of Chemistry, Aristotle University of Thessaloniki, Greece.

U. PANAGIOTALIDIS

Formerly of Hellenic Cotton Board, Textile Technology Research Center, 542 49 Thessaloniki, Greece.

(Received: March 6, 1996 In final form: December 23, 1997)

Summary

Physical (micronaire, fibre length, length uniformity, number and size of neps, short fibre content) and mechanical (tensile strength and elongation at break) properties of long staple cotton before and after loose dyeing at two different liquor ratios were determined. Presence of auxiliary (softening - lubricating) agents (Avivan, Levegal, Sapamin) in various concentrations during loose dyeing resulted in a reduction of the fibres fatigue.

Key words: Cotton loose dyeing, Cotton fibres properties, dyeing auxiliaries

Introduction

Market demand for natural textile materials made of 100 % cotton with different colour effects (melange or jaspe yarns) resulted in an increase of interest in loose cotton dyeing.

Problems met by this dyeing process are mainly related with friction between fibres and other surfaces and between fibres themselves, as well as with electrostatic charges developed during the subsequent fibre processing [1].

In all stages of fibre processing it is of prime importance to achieve a low coefficient of friction between the fibre and other surfaces in order to minimize breakage, abrasion damage of fibres and

static charges built up. Thus the preservation of fibre length should be achieved, as it results in better cotton spinnability, fibre strength, handle, lustre, hairiness and spinning productivity [2].

Fibre to fibre friction is also important to be controlled in order to achieve a minimum level of friction and cohesion to provide good fibre assemblies, lubricity and mobility, to facilitate opening prior to blending and carding etc.

Hence, the friction breakage, abrasion and damage of cotton fibres could be minimized by using softening / lubricating agents during the dyeing of loose cotton fibres.

In addition effects produced by static charges in textile processing, caused by an inadequate conductivity of the material, can interfere with production efficiency and performance of the final product. Thus non - ionic and ionic antistatic agents, providing efficient moisture retention on the surface of the material to ensure dissipation of static charge are used.

In this work the physical (micronaire, fibre length and uniformity, number of neps) and mechanical (tensile strength and % elongation of break) properties of unbleached long staple (Pima, Israel) loose cotton fibres before and after dyeing with a reactive dye (Drimaren Red K4BL) in absence and presence of non - ionic (Avivan SPL, Levegal KNS) and ionic (Sapamine OL) auxiliary agents of softening / lubricating / antistatic action were determined. The choice of Israel cotton fibres was made on the basis that this shows advantages, regarding the length distribution uniformity of the fibres and the maturity of the cotton [3].

Two bath liquor ratios 20: 1 and 7: 1 were used to compare their effect on the above fibre properties. The results obtained for the raw material (cotton fibres) and the dyed one in absence and presence of the above agents are compared and discussed.

Also, the results of the use of the above surfactants are discussed in relation to the reduction of the surface tension of the dyebaths, which favours a better wettability - softening of the fibres.

Experimental

Materials:

The following commercial materials were used. Drimaren Red K4BL (Sandoz) was used as reactive dye. Avivan SPL (Ciba - Geigy), Sapamin OL (Ciba - Geigy) and Levegal KNS (Bayer) were used as auxiliary (softening - lubricating - antistatic) agents.

Determination of physical and mechanical properties:

The samples were conditioned before the measurements at 20 ± 2 °C and 65 ± 2 % relative

humidity for 24 hr. The measurements of micronaire, length (mm 2.5 % and 50 % of fiber amount), % length uniformity, tensile strength (g / tex) and % elongation at break were recorded by using a High Volume Instrument HVI 900 (SPINLAB, USA) [4]. Number of neps / g and mean size of neps (mm) were measured in an AFIS - N system (USTER, Switzerland). Short fibers content % (SFC) was calculated according to the International Textile Manufacturers Federation and SPINLAB, by the Preysch equation [5]

$$SFC = 39.4 + 1.3\ (FB_{2.5\ \%}) - 4.6\ (FB_{50\ \%}) \qquad (1)$$

where: $FB_{2.5\ \%}$ and $FB_{50\ \%}$ the Fibrograph length values for 2.5 % and 50 % of fibre amount, respectively. Six - ten measurements for each sample and property were recorded and standard deviation and variation coefficients % were calculated.

Dyeing:

Cotton treatments and dyeings were carried out in a Rotadyer apparatus (John Jeffreys Ltd, Rochdale Banbury).

Loose cotton fibre samples (25 g or 30 g in a liquor ratio 20: 1 or 7: 1, respectively) were manually packed, inserted in closed rotating steel vessels (500 ml) of the dyeing apparatus and pretreated with water at 90 °C for 1 hr. The water was drained and dyeing was carried out at 40°C, liquor ratio 20: 1 (or 7: 1) and 2.5 % o.w.f. depth of dyeing in absence and presence of 2 - 5 % o.w.f. of the auxiliary agent. After dyeing of 10 min were added: 40 % o.w.f. NaCl; after 40 min: 3 % o.w.f. Na_2CO_3; after 30 min: 3 % o.w.f. NaOH and the dyeing was carried on for 60 min (totally 140 min). The dyed samples were rinsed, boiled in distilled water for 10 min to remove the hydrolyzed dye and dried in an oven at 55 ● 2 °C for 3 hr.

Surface tension coefficients of the initial dye liquors:

They were recorded in a Tensiometer KSV - Sigma 70 using the Wilhelmy plate method at 40°C.

Results and Discussion

The mean values, standard deviation and variation coefficients of measurements of physical (micronaire, fibre length, length uniformity, number of neps / g, size of neps and % short fibre content) and mechanical properties (tensile strength and % elongation at break) for the raw cotton samples and the dyed ones in absence and presence of the three auxiliary (softening – lubricating -

antistatic) agents are given in Tables I and II for a liquor ratio 20: 1 and 7: 1 respectively.

The results in Table I indicate that loose dyeing of the cotton fibres under the described conditions in absence of the softening agents resulted in a significant increase in number of neps / g (almost three times higher value compared to the undyed one) and short fibres content, due to the friction caused during dyeing. However micronaire, fibre length and the mechanical properties (tensile strength and % elongation at break) remained practically the same.

Presence of 3 % o.w.f. of Avivan SPL in the dyebath during the dyeing caused a significant improvement (reduction) of the number of neps and short fibres content % in respect of the results of dyeing in absence of it, whereas no characteristic effect was observed on the other properties.

Also the presence of 3 % o.w.f. of Sapamin OL improved the number and size of neps, but it was less effective than Avivan SPL.

Reduce of the dyeing liquor from 20: 1 to 7: 1 significantly (~ 48 %) decreased the number of neps / g, whereas no change was practically occured on the other properties (Table I, II). The reduce in liquor ratio is also advantageous in the dyeing industry on account of economic and environmental reasons (higher degree of exhaustion etc.) [6,7].

About the same results were observed for the dyeings in presence of 2.% o.w.f. Avivan at a liquor ratio 7: 1 and 3 % at a liquor ratio 20: 1.

An increase of Avivan and Levegal content from 2 to 5 % o.w.f. did not practically show a further improvement of the number of neps, considering the high variation coefficients of the values of this property, nor of the other quality characteristics (Table II). Thus, an optimum concentration of the above auxiliaries seems to be 2 - 3 % o.w.f. Under the same consideration no difference between the effect of Avivan SPL and Levegal KNS auxiliaries on the properties studied was indicated. However Levegal gave better dyeing levelness than Avivan, as that was visually confirmed, but a lower dye exhaustion was respectively observed.

A primary investigation was also attempted to correlate the caused improvement in the neps values of the loose cotton dyed in presence of Avivan or Levegal, with the surface tension reduction of the dyebaths and consequently with the fibre wettability – flexibility. So the surface tension of the initial dye solution at 40°C and those containing in addition 2 or 5 % o.w.f. Avivan or Levegal was measured and the results, as well as these for the corresponding aqueous solution of Avivan and

Table I: M.V., S.D. and C.V. % of the physical and mechanical properties of long staple cotton fibres before and after loose dyeing in absence and presence of various auxiliary agents; liquor ratio 20: 1

Sample	Statistical parameters	Micro-naire	Fibre length (mm, 2.5 %)	Fibre length (mm, 2.5 %)	length unifor-mity	Neps (No / g)	Size of neps (mm)	Short fibres content %	Tensile trength 1 / 8 _ g / tex)	% elonga-tion at break
Initial	M.V.	3.9	34.4	16.64	48.4	177	0.75	7.53	26.2	8.3
cotton	S.D	0.078	0.832		1.678				1.753	0.347
	C.V. %	2.0	2.4		35	18.1	365		6.7	4.2
Dyed	M.V.	3.8	34.1	16.20	47.5	513	0.82	9.21	27.2	8.5
cotton	S.D.	0.086	0.746		2.316	59.61	0.01		0.897	0.255
	C.V. %	2.2	2.2		49	11.61	0.97		3.3	3.0
Dyed in	M.V.	4.0	34.5	16.60	48.1	210	0.75	7.89	25.9	8.8
presence	S.D.	0.130	0.587		2.403	40.96	0.03		2.262	0.369
3%Avivan	C.V. %	3.2	1.7		5.0	19.49	3.10		8.7	4.2
Dyed in	M.V.	3.9	34.2	16.20	47.3	295	0.77	9.34	27.0	8.5
presence	S.D.	0.06	0.672		1.768	35.51	0.02		1.753	0.235
3 % Sa-pamine	C.V. %	1.5	2.0		37	12.03	3.11		6.7	2.7

Levegal, are given in Table III.

The same surface tension values for the two aqueous solutions of different concentrations (same as those in dyeing liquors) for each auxiliary, Avivan and Levegal, indicates that their used concentrations were higher than their critical micelle concentrations. As it is shown in Table III and its footnote, Avivan has a slightly higher surface activity than Levegal. The presence of both decreased the surface tension of the dyebaths at about the same values to those of their aqueous solutions of the same concentration (Table III).

Table II: M.V., S.D. and C.V. % of the physical and mechanical properties of long staple cotton fibres after loose dyeing in absence and presence of various auxiliary agents; liquor ratio 7: 1

Sample	Statistical parameters	Micronaire	Fibre length (mm,2.5 %)	% length uniformity	Neps (No / g)	Tensile strength (1 / 8 " g / tex)	% elongation at break
Dyed	M.V.	3.9	34.3	46.3	264	25.3	7.9
cotton	S.D	0.075	0.845	1.130		1.186	0.117
	C.V. %	1.9	2.5	2.4	11.4	4.7	1.5
Dyed in pre-	M.V.	4.0	34.2	45.8	206	25.0	8.3
sence of	S.D.	0.117	0.303	0.813		1.379	0.172
2 % Avivan	C.V. %	2.9	1.1	1.8	20.4	5.5	2.1
Dyed in pre-	M.V.	4.0	34.3	46.0	220	24.7	8.2
sence of	S.D.	0.049	0.452	1.783		1.454	0.080
5 % Avivan	C.V. %	1.2	1.3	3.9	10.7	5.9	1.0
Dyed in pre-	M.V.	3.8	34.7	46.3	193	25.2	8.2
sence of	S.D.	0.049	0.441	2.583		1.507	0.075
2 % Levegal	C.V. %	1.3	1.3	5.6	25.5	6.0	0.9
Dyed in pre-	M.V.	3.9	34.5	48.1	208	26.1	8.4
sence of	S.D.	0.040	0.674	2.213		1.179	0.136
5 % Levegal	C.V. %	1.0	2.0	4.6	21.3	4.5	1.6

Although the improvement (reduction) of the neps values and short fibre content in the presence of the examined auxiliaries might be attributed to the caused reduction of the surface tension of the dyeing liquors, no consistent relationships between them were found.

Table III: Surface tension values of the dyeing liquors in absence or presence of Avivan SPL and Levegal KNS at various concentrations (ageing time 30 min)

Sample	Concentration of Auxiliary % o.w.f.	Surface Tension dyn / cm, 40 °C
Dyeing liquor [a]	0	39.3
" " plus Avivan [b]	2 (2.85 g / lt)	33.5
" " "	5 (7.13 g / lt)	32.6
" " plus Levegal [c]	2 (2.85 g / lt)	33.9
" " "	5 (7.13 g / lt)	33.7

a: 7: 1 o.w.f., containing 3.57 g / lt dye, 57.14 g / lt sodium chloride, 4.28 g / lt sodium carbonate and 4.28 g / lt sodium hydroxide

b: Surface tension of aqueous solution of 2.85 or 7.13 g / lt Avivan

c: Surface tension of aqueous solution of 2.85 or 7.13 g / lt Levegal

Περίληψη

Μελέτη φυσικών και μηχανικών ιδιοτήτων βαμβακερών ινών βαμμένων απουσία και παρουσία μαλακτικού / λιπαντικού μέσου.

Στην εργασία προσδιορίστηκαν οι φυσικές (micronaire, μήκος της ίνας, ομοιομορφία μήκους, αριθμός και μέγεθος nep, περιεκτικότητα σε κοντές ίνες) και μηχανικές ιδιότητες (αντοχή στον εφελκυσμό και επιμήκυνση στο σημείο θραύσης) του βαμβακιού πριν και μετά τη βαφή σε δύο διαφορετικές σχέσεις λουτρού.

Η παρουσία μαλακτικών - λιπαντικών μέσων ως βοηθητικών βαφής σε διάφορες συγκεντρώσεις στη διάρκεια της βαφής είχε ως αποτέλεσμα την ελάττωση της ίνας.

Aknowledgments

This work was financially supported by a project in the STRIDE HELLAS (20 / 1991) programme in cooperation with K. DOUDOS S. A. (Spinning Mills, Thessaloniki). Thanks are also expressed to Dr. H. Panagiotalidis (Hellenic Cotton Board, Textile Technology Research Center 54249 Thessaloniki, Greece) for technical assistance.

References

1. G. Clarke, "A practical introduction to fibre and tow coloration", The Society of Dyers and Colourists, Bradford, 1982.
2. L. Neuhaus, H. Deusen, "Some thoughts about requirements of cotton for new spinning technologies such as OE rotor spinning, friction spinning and air jet spinning", Bremen Symposium Proceedings, 1984.
3. S. Peles, "Quality controls in cotton production in its relation to the cotton processing industry", Bremen Symposium Proceedings, 1984.
4. ASTM - 4604 - 86, Measurement of Cotton Fibres by High Volume Instrument, 1986.
5. SPINLAB Fibrograph Manual, Knoxwille, USA.
6. K. Bacher, J. S. D. C., **108**, 479 (1992).
7. A. M. Lidyard, A. Woodcock, P. Noone, J. S. D. C., **108**, 501 (1992).

Chimika Chronika, New Series, 26, 495-512 (1997)

THE MECHANISMS OF BILAYER FORMATION ON SUPPORTS AND BIOSENSOR MEMBRANE ELASTICITY CHANGE ACCOMPANYING SUBSTRATUM BINDING

V.I. PASSECHNIK, S.A.IVANOV

Scientific Research Center "Eldis", Institute of Radioengineering and Electronics RAS, Starosadsky per. 8, 101000, Moscow, RUSSIA.

(Received: January 22, 1996 In final form: December 23, 1997)

SUMMARY

Highly stable supported bilayer membranes with incorporated protein molecules are a good model for biosensors. The role of the material of the support and support geometry are investigated. The changes of bilayer elasticity due to substratum binding to the macromolecule are studied. These changes are manifested substantially only for definite concentration of the protein molecules and are affected by the dimensions of the distorted structure zones which are generated around protein molecules.

Key words: Biosensors, lipid membranes, molecular recognition, chemoreception, membrane elasticity

1.INTRODUCTION

Bilayer lipid membrane is a widely spread model of biological membranes [1]. The modification of these membranes, so called supported bilayers formed from lipid solution onto

some flat surface, are proposed to be used as biosensors to measure the ultimately low concentrations of some substances [2,3]. Some bilayer properties can be measured to reveal its interaction with substances under investigation. It was shown that the interaction of some substances with receptor proteins incorporated into the membrane affects membrane elasticity [4]. This phenomenon can be used as the structural basis for a definite type of biosensors [5,6]. The elastic properties of supported bilayers were shown to be a sensitive parameter to determine structure changes of the membranes.

There are various types of supported bilayers. The most stable membranes are formed onto smooth surface of the metal [6], they are called sl-BLM. Beneath the properties of these membranes will be considered.

In order to use sl-BLM as the sensitive biosensors the membrane should have simultaneously (1) high stability and (2) high sensitivity to the substratum. The first property can be achieved by bilayer attachment to the support, high sensitivity and selectivity are achieved by the incorporation of receptor macromolecules into bilayer. So the first problem is the choice of the adjacent metal support, the second one is the analyses of possible changes of bilayer elasticity due to substratum binding. These two problems are considered beneath.

2. METAL SUPPORTS

Metal support can substantially modify the properties of sl-BLM. The support is as a rule a thin (100 nm) Au, Ag or Pt

layer on dielectric polished surface, for example, polished glass. The layer has crystal lattice distortions with the density of about 10^8 cm^{-2}, they induce the formation of basic or acid centers.

3-step mechanism of bilayer formation could have been as follows.

1. Lipid molecules from bulk phase of lipid solution diffuse to the metal, turn their polar or dipole heads to metal surface, substitute solute molecules and interact electrostatically with the ions of the crystal lattice. A physical adsorption takes place.

2. Lipid molecules oriented on the metal surface diffuse laterally to the active centers and bind irreversibly with them. A chemosorption takes place.

3. Lipid molecules diffusing along the metal surface form at first a monolayer and then a bilayer around the chemically adsorbed molecules. The structure of the monolayer adjacent to metal surface is far from ideal one, the second monolayer is more smooth. The bilayer is assembled around each chemosorbed molecule due to physical adsorption.

Sl-BLM nucleates simultaneously in numerous active centers, where the lipid molecules are adsorbed irreversibly, so domain structure is generated. Every lipid domain has its own dimension of about 1÷5 micrometers, the orientations of the crystal structures in the adjascent domains do not correlated with each other (Figure 1, a). The clusters of smaller dimensions can be incorporated in the larger ones.

It should be mentioned that the process of sl-BLM formation is not limited by the diffusion process, because a lateral diffusion coefficient of the lipid molecules onto metal surface is of about $5 \cdot 10^{-8}$ $cm^2 \cdot c^{-1}$, i.e. like that of conventional BLM.

Mosaic structure of sl-BLM and the defects of the support are likely to be responsible for the membrane conductivity and stability. Due to modern theories both phenomena are determined by the pore formation. A narrow pore is a rather stable one and acts as a conductor. If its radius exceeds some limiting value the permanent radius increase takes place and the bilayer ruptures. Mean electric conductance of sl-BLM is of about 100 $pCm \cdot cm^{-2}$, this value is two orders of magnitude as large as that of conventional BLM. This phenomenon can be explained either by increase of the number of pores or by the increase of their diameter.

The potential sources of the pores in the bilayer are the distortions of the bilayer structure either near the surface defects of the metal lattice or at the borders of neighboring dom ains (Figure 1, a). The generation of the pores is more probable in the points, where three borders contact with each other. Because every domain can be generated by the defect of the support, one should expect the surface density of the defects to be the factor determining sl-BLM conductivity as well. A theory of sl-BLM stability should yet be elaborated. A principal distinction of sl-BLM from conventional one is as follows: the bilayer is chemically attached to support in some points, being bound to the surface by forces of physical

adsorption in another points. The stabilization of the large pores by the metal defects is, probably, the reason of high stability of sl-BLM. Sl-BLM stability is increased if the defect density is increased. Thus the increase in bilayer conductance as well as in the membrane stability which are observed experimentally can be rationalized on the basis of the proposed model.

Liquid-crystal properties of the bilayer seem to be also determined, to the great extent, by the surface defects of metal support. For example, the small value of the transversal modulus is determined for the support with the numerous defects (say, cut wire), the value of the modulus value increases for the smooth support. The most dangerous situation for application of sl-BLM as biosensors is the case, when the bilayer distortions are so numerous that the sensitivity of membrane structure to the changes of the structure of the protein macromolecules incorporated into the membrane would be lost.

Some basic physical properties of sl-BLM, unlike conventional BLMs, seem to be determined by the defects of the support structure. Therefore the principle contradiction in biosensor constructing takes place: the increase in sl-BLM stability is connected with its fixation at the support defects, at the same time maximum sensitivity of a biosensor can be obtained if the membrane structure is undisturbed.

To satisfy these contradictory requirements it is necessary to test various types of the support with the controlled density of the surface defects. The appropriate choice of the metal and

the shape of the metal support profile can enable one to change the number of the surface defects. For binding of the bilayer onto the metal it is worthwhile to use sputtering of Pt. Step defects (1) generated onto support surface in this case are likely to be the centers of lipid chemosorption (Figure 1, b). In order to obtain the surface with minimum of the defects the Au sputtering should be used. In this case chemosorption will take place only at the borders of the gold coating (Figure 1, c). So the gold strips should not be too wide in order to maintain stable sl-BLM.

3. MECHANICAL COMPLIANCE OF SL-BLM

During biosensor membrane formation the initial mechanical compliance of the pure bilayer is modified in the distortion zones appearing around the defects by which the bilayer was attached to the support as well as due to the defects generated by the incorporated receptor macromolecules. This modification should depend upon the concentration of the receptors incorporated into the bilayer. After the reaction of binding of the receptor with the substratum under investigation the equilibrium will take place between concentrations of the free receptor macromolecules and of the receptor - substratum complexes in bilayer. This reaction is accompanied by the change in the macromolecule structure as well as in structure of the distortion zones. Respectively, the compliance of the whole bilayer will be changed.

To calculate the change in the membrane compliance some

assumptions should be done:

1. we neglect the influence of the points of bilayer attachment to the support on bilayer elasticity;

2. we consider the receptors macromolecules located in the centers of the quadratic lattice;

3. we let every distortion zone to be of strictly definite size and to be a square in the bilayer plane.

These assumptions will not change qualitatively the results obtained.

The reaction of binding of the substratum S with the receptor can be described by the traditional kinetic scheme

$$N_0 + S \underset{k_2}{\overset{k_1}{\rightleftharpoons}} N_1, \qquad (1)$$

where simbol N_0 denotes free receptor macromolecules in the membrane, their amount being N_0, simbol N_1 denotes receptor - substratum complexes in the membrane, their amount is N_1. The condition $N_0 + N_1 = N$ is valid, where N is the total amount of receptor macromolecules in the membrane. k_1, k_2 are rate constants of the corresponding reactions, the value $K=k_2/k_1$ being the equilibrium constant.

The change in concentration of receptor - substratum complex versus time is described by the equation

$$dN_1/dt=k_1 c\ N_0-k_2 N \qquad (2)$$

where c is the substratum concentration in the solution.

In equilibrium state the amounts of free receptor macromolecules as well as the of the receptor - substratum

complex macromolecules are as follows

$$N_0=N/(1+c/K),\ N_1=N(c/K)/(1+c/K) \qquad (3)$$

Some types of structures coexist in the membrane simultaneously: free bilayer and the distortions of various types. Assuming the validity of the additive scheme, i.e. absence of any additional interactions at the borders of distortion zones , one can after [4] write a formula for membrane compliance M(c) as a function of substratum concentration c

$$M(c) = [M_b(S - \sum_{i=0}^{n} S_i(c)) + \sum_{i=0}^{n} S_i(c)M_i]/S \qquad (4)$$

where M_b is the compliance of the pure bilayer, symbol i denotes the type of the distortion (i=0, 1, 2, ...); S is the membrane area, $S_i(c)$ is the membrane area occupied by the distortions of the i - th type; M_i is the compliance of these pieces of the membrane. It is worthwhile to introduce the area $s_i = S_i/N_i$ generated by one receptor macromolecule in the i-th state, as well as the bilayer area per one macromolecule $\sigma = S/N$.

We consider the dependence of the membrane compliance on substratum concentration in the simplest case when two types of distortions are located in the bilayer: for i=0 one has the distortion zones around free receptor macromolecules, for i=0 one has the distortion zones around receptor - substratum complexes.

The change in substratum concentration changes the relationship between free macromolecules and those in the state of receptor - substratum complex. One can formally derive from

(4) that membrane compliance against values of N_0/N, N_1/N is as follows

$$M = M_b[1 - (s_0/\sigma)(N_0/N) - (s_1/\sigma)(N_1/N)] + M_0(s_0/\sigma)(N_0/N) + \\ + M_1(s_1/\sigma)(N_1/N) \quad (5)$$

Taking into consideration the condition $(N_0/N)+(N_1/N)=1$ one can derive from (5)

$$M(c)=M_b[1-(s_0/\sigma)(1-N_1/N)-(s_1/\sigma)(N_1/N)]+M_0(s_0/\sigma)(1-N_1/N)+ \\ +M_1(s_1/\sigma)(N_1/N). \quad (6)$$

The term in the square brackets is the relative area of the pure bilayer in the membrane. It is evident that it should be positive. So some limitations take place for the permissible values of the parameters s_0/σ and s_1/σ. To derive the corresponding formulae the scheme of the bilayer subdivision into square pieces is presented in Figures 2, a,b. The receptor macromolecules (O) are located in the centers of the quadrats, the areas s_0, s_1 and σ are as follows $s_0=a^2$, $s_1=b^2$ and $\sigma=d^2$. The plane of parameters s_0/σ и s_1/σ is presented in Figure 2, c.

If a small amount N of receptor macromolecules are located in the membrane, the area $\sigma = d^2 = S/N$ per a macromolecule shown by the dotted lines is large, so the zones shown by solid lines for free receptors and by double lines for receptor - substratum complex do not overlap (scheme a), for definiteness the condition $s_0 > s_1$ is taken in the Figure. If the value of N is increased the zone size decreases and the zones overlap. In Figure 2, b the overlap of free receptor zones is shown for definiteness. The parameters plane can be separated into four

regions (Figure 2, c) as follows

1. $s_0/\sigma \leq 1$ and $s_1/\sigma \leq 1$. Separate distortion zones do not intersect each other. In this case the formula (6) describes the function M(c) for all values of c.

2. $s_0/\sigma \geq 1$ and $\sqrt{(s_1/\sigma)} + \sqrt{(s_0/\sigma)} \leq 2$. The distortion zones of free receptors intercept each other, however distortion zones generated by receptor - substratum complex do not intercept. The second limitation as it can be shown from (Figure 2, b) is the sequence of the geometry condition $b/2 \leq d - a/2$.

3. $s_1/\sigma \geq 1$ and $\sqrt{(s_1/\sigma)} + \sqrt{(s_0/\sigma)} \leq 2$. The distortion zones of receptor - substratum complex intercept each other, however distortion zones generated by free receptors do not intercept. The second limitation as it can be shown from the scheme analogous to that of (Figure 2, b) is the sequence of the geometry condition $a/2 \leq d - b/2$.

4. $\sqrt{(s_1/\sigma)} + \sqrt{(s_0/\sigma)} > 2$. The distortion zones generated by both the receptor - substratum complex as well as free receptors intercept each other.

In the regions 2 and 3 the formula (6) for the calculation of the membrane compliance versus substratum concentration c should be modified. In these regions the distortion zones only of one type propagate to the area which is controlled by the neighboring receptor macromolecules. The distortion zone of the second type concentrates around its own receptor macromolecule and does not propagate into nearby located zones, so the definiteness takes place what compliance should be attributed to any piece of the membrane. At the same time in the region 4 some

pieces of the membrane are influenced by the neighboring macromolecules, which are in different states and "try" to generate the distortion zone of their own type. Special study should be conducted to determine which types of structure distortions will be generated in this case (some new type of distortion can also take place). That is why we were obliged to confine the discussion to the regions 2 and 3 where situation is more clear.

Region 2. Pure bilayer is absent. As it is easy to show by analogy with formula (6) the corresponding relationship for compliance in this region $M_2(c)$ is as follows

$$M_2(c)=M_0+ (M_1-M_0)(s_1/\sigma)(N_1/N) \qquad (7)$$

Because $s_1/\sigma<1$ this formula is valid for all values of N_1/N.

Region 3. The the corresponding relationship for compliance in this region $M_3(c)$ can be described by the formulae (6) and (7) with additional conditions. The latter are the mathematical conditions for the areas occupied by pure bilayer or by the zones around incorporated free receptors to be positive.

$$M_3(c)=\begin{cases} M(c), \text{ if } N_1/N\le(1-s_0/\sigma)/(s_1/\sigma-s_0/\sigma) \\ M_2(c), \text{ if } s_1/\sigma\ge N_1/N\ge(1-s_0/\sigma)/(s_1/\sigma-s_0/\sigma) \\ M_1, \text{ if } s_1/\sigma\le N_1/N \end{cases} \qquad (8)$$

In Figures 3, a-b the dependencies of the compliance of the whole membrane, i.e. the values $M(c)$, $M_2(c)$ and $M_3(c)$ for corresponding regions, is shown (the numbers at the curves correspond to the number of the region).

For the region 1 the compliance (curve 1) starts from the

initial value (for zero substratum concentration) which is as follows

$$M(0) = M_b(1-s_0/\sigma) + M_0 s_0/\sigma \quad (9)$$

It is the weighted sum of the compliance M_b of unmodified region of the lipid bilayer and that of M_0 of occupied one. With the rise of substratum concentration the increase ΔM in membrane compliance takes place with the subsequent saturation, half increase being at the concentration c=K.

The compliance for the region 2 (curve 2) starts from the value $M=M_0$ and increases till saturation like the curve 1, the values of the compliance obeying the condition $M(c)<M_1(c)$.

The initial value of the compliance for the region 3 (curve 3) is the same as for the curve 1, however the initial slope is steeper. At the concentration where the first condition in formula (9) for N_1/N is fulfilled the behavior of the curve is somewhat changed and it turns into curve $M_2(c)$ (formula (7)). For higher concentration where second condition takes place the curve 3 goes to the limit value $M=M_1$, which is maintained for the further increase in substratum concentration.

In Figure 3, b the same graphics are plotted but for another row of compliancies $M_0<M_b<M_1$. One can see that the relative change of the compliance is increased. According to the relation between the values M_0, M_b, M_1 the sign of the compliance change can be reversed (Figure 3, c, the row of values $M_0>M_b>M_1$). One should mark the pronounced bend of the curve 3, which appeared for the concentration where the first limiting condition in (8) takes place.

4. DISCUSSION

The analyses conducted in our paper show the the support material as well as the geometry of its separate pieces may play the main role in optimal combination of bilayer stability and the absence of extra quantity of bilayer distortions. Quantitative estimate of this phenomenon needs further investigation.

Our model proposed in the second part of the paper for calculation of membrane compliance versus substratum concentration is very simple. We assume that receptor molecules are located in strictly definite order in lipid bilayer, distortion zones have strictly definite dimensions and shape. We also do not take into consideration the influence of distortion zones which are generated near the points of chemical bilayer attachment to the support and were described in the first part of the paper. However the proposed model enables one to make definite forecasts about the influence of some biosensor parameters on its characteristics. As it follows from our model there is the optimum number of the receptor molecules in the membranes. Since every receptor macromolecule generates the distortion zone around itself the increase in their quantity should increase the measured values of the compliance change ΔM. However the increase in their amount over some critical value when distortion zones begin to intercept may drive either to decrease in the concentration range, where the biosensor is sensitive (region 3 in the scheme Figure 2, c and curves 3 in Figure 3), or to the exit to the region of parameters , where

the dependence of compliance on concentration can't be predicted now (region 4 Figure 2, c).

In the field of parameters where such predictions can be now done the characteristic scale of the substratum concentration is the equilibrium constant K. In the region of parameters 1 and 2 the half of compliance change takes place at the value c=K.

The analysis of the formulae (6 - 8) shows that the sign of the compliance change depends on distortion zones compliance and dimension. One can obtain the maximum range of the compliance change if receptor macromolecules change the compliance of pure bilayer in one direction whereas the receptor - substratum complex changes it in the opposite direction. Perhaps these optimal properties of the biosensor bilayer could be obtained by proportioning of the lipid composition.

ACKNOWLEDGEMENT

The research was supported financially by grant # CIPA-CT94-0231 COPERNICUS awarded by the Commission of European Communities.

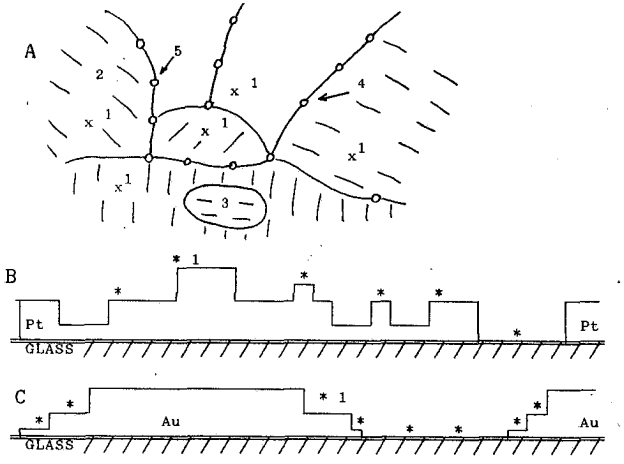

Fig. 1

Figure 1. A scheme of the membrane domains onto the support. a. A possible scheme of s-BLM bilayer domain structure. 1 - the centers of chemosorption, 2 - domains, 3 - a domain incorporated into another one, 4 - the border of adjacent domains, 5 - pores. b. Schematic representation of Pt support surface with the step-like centers of lipid chemosorption; c. Schematic representation of Au support surface with minimum of the defects on the Au surface and the maximum of them at the borders of the gold coating.

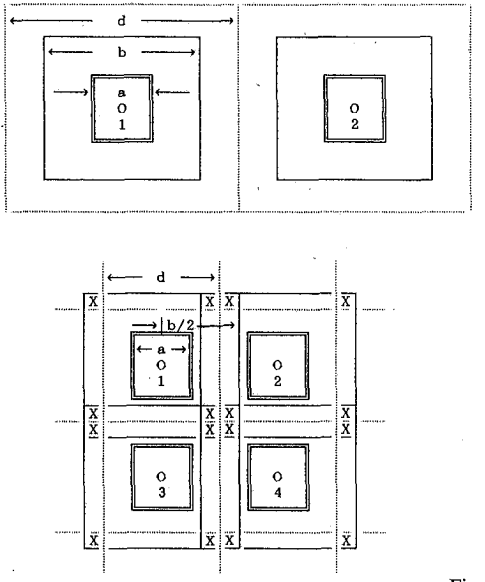

Fig. 2 a,b

Figure 2. The scheme of bilayer subdivision to separate pieces, the receptor macromolecules (O) are located in the centers of the pieces. The borders of square pieces with dimension d are shown with dotted line. Solid lines are the borders of distortion zones generated by the macromolecules of free receptors (their dimension is b), double lines show the borders of the zones, generated by receptor - substratum complex. a. A location of unoverlapping distortion zones generated by two neighboring macromolecules 1 and 2; b. A location of overlapping zones generated by four neighboring macromolecules 1 - 4. The symbols X show the pieces, which are affected by all four macromolecules. The overlap of the zones is shown only for the membrane pieces between the macromolecules. c. The plane of parameters s_0/σ and s_1/σ (c).

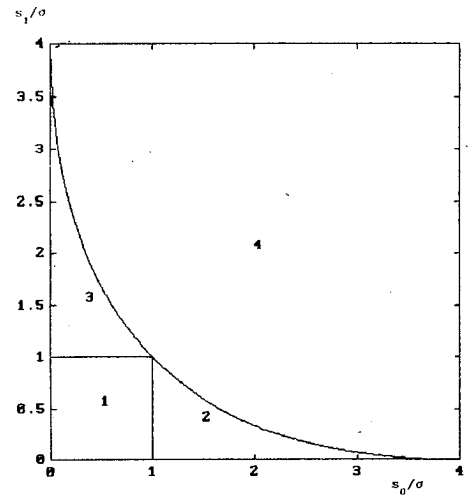

Fig. 2c

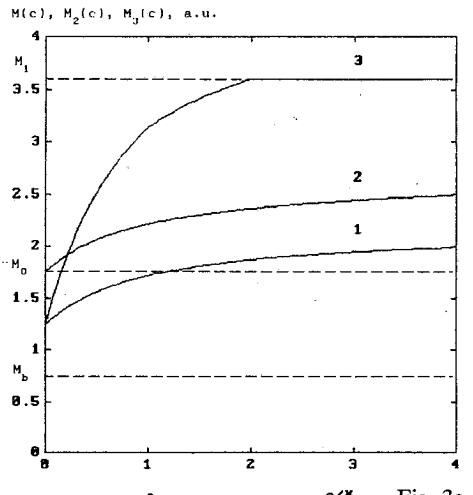

Fig. 3a

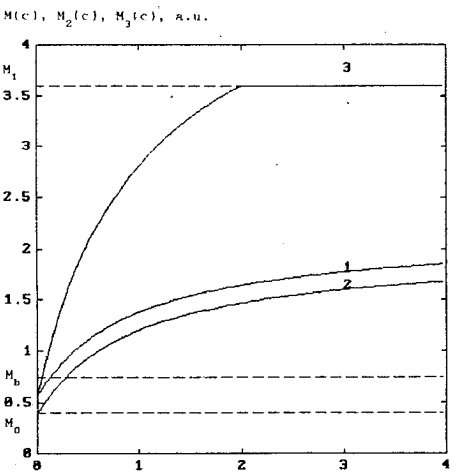

Fig. 3b

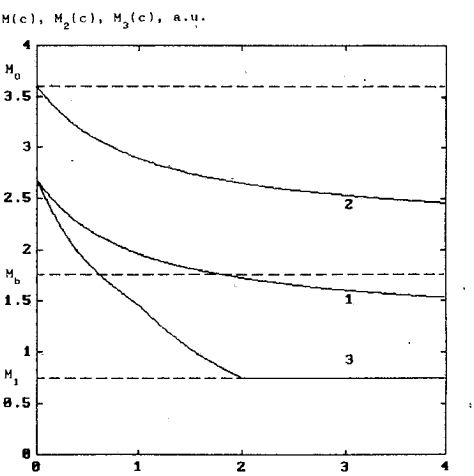

Fig. 3c

Fig. 3. The dependence of membrane compliance M(c), $M_2(c)$, $M_3(c)$ for regions 1-3 respectively on relative substratum concentration c/K for various parameters M_b, M_0, M_1, the number of the curve corresponds to the number of the region in Figure 2.c.

a,b,c. The influence of various relations between the compliances of the pure bilayer M_b, that of the bilayer modified by free receptor molecules M_0, and that of bilayer modified by receptor-substratum complex M_1 on the compliance of the whole membrane. The compliancies are expressed in arbitrary units. The following parameters were used - region 1: $s_0/\sigma=0.5$, $s_1/\sigma=0.5$; region 2: $s_0/\sigma=1.5$, $s_1/\sigma=0.5$; region 3: $s_0/\sigma=0.5$, $s_1/\sigma=1.5$. The values of compliancies M_b, M_0, M_1 are shown by horizontal lines a. A relation between the compliancies is $M_b<M_0<M_1$, for calculation we used: M_b: M_0: M_1=0.75:1. 75:3.6. b. A relation between the compliancies is $M_0<M_b<M_1$, for calculation we used: M_0: M_b: M_1=0.4: 0.75: 3.6. c. The sign inversion of membrane compliance for relation between compliancies as follows $M_0>M_b>M_1$. The ratio between the compliancies is M_0: M_b: M_1=3.6: 1.75: 0.75.

ΠΕΡΙΛΗΨΗ

ΟΙ ΜΗΧΑΝΙΣΜΟΙ ΣΧΗΜΑΤΙΣΜΟΥ ΔΙΠΛΟΣΤΙΒΑΔΑΣ ΕΠΙ ΥΠΟΣΤΗΡΙΓΜΑΤΩΝ ΚΑΙ ΜΕΤΑΒΟΛΗΣ ΤΗΣ ΕΛΑΣΤΙΚΟΤΗΤΑΣ ΤΗΣ ΜΕΜΒΡΑΝΗΣ ΒΙΟΑΙΣΘΗΤΗΡΑ ΠΟΥ ΣΥΝΟΔΕΥΟΥΝ ΤΟ ΔΕΣΜΟ ΤΟΥ ΥΠΟΣΤΡΩΜΑΤΟΣ

Οι υψηλής σταθερότητας μεμβράνες διπλοστιβάδας με ενσωματωμένα μόρια πρωτεΐνης αποτελούν καλό πρότυπο για βιοαισθητήρες. Μελετήθηκαν ο ρόλος του υλικού και η γεωμετρία του υποστηρίγματος καθώς επίσης και οι μεταβολές της ελαστικότητας της διπλοστιβάδας, λόγω του δεσμού του υποστρώματος με τα μακρομόρια που εξετάσθηκαν. Οι μεταβολές αυτές εμφανίζονται, ουσιαστικά, μόνο για συγκεκριμένη συγκέντρωση των μορίων της πρωτεΐνης και επηρεάζονται από τις διαστάσεις των ζωνών διαταραγμένης δομής που παράγονται περί τα μόρια της πρωτεΐνης.

REFERENCES

1 Tien, H.T., Bilayer Lipid Membranes BLM: Theory and Practice, Dekker, New York, 1974.

2 Tien H.T., & Salamon Z., *Bioelectrochemistry and Bioenergetics* 22, 211-218, 1989.

3 Florin, E.L. & Gaub, H.E., *Biophysical Journal* 64, 375-383, 1993.

4 Passechnik, V.I. & Hianik, T., Transversal Elasticity of Lipid Membranes, Veda, Bratislava, 1991.

5 Hianik, T., Dlugopolsky, J. & Gyepessova, M., *Bioelectrochemistry and Bioenergetics* 31, 99-111, 1993.

6 Hianik, T., Passechnik, V.I., Ivanov, S.A., Dlugopolsky, J., Sargent,D.F., *Bioelectrochemistry and Bioenergetics*, 1995. (Submitted for publication)

7 Hianik T., Passechnik V.I., Bilayer lipid membranes: structure and mechanical properties. Kluwer Acad. Publishers, Amsterdam, 1995.

Chimika Chronika, New Series, 26, 513-522 (1997)

AQUEOUS CHEMISTRY OF NIOBIUM AND TANTALIUM. REDUCTION OF NIOBIUM (V) OR TANTALUM (V) IN THE PRESENCE OF OXALATES. DIFFERENCES OF THE RESULTED OXALATO COMPLEXES OF Nb(III) AND Ta(III)

M. Kamariotaki - Paparigopoulou, D. Hatzipanayioti - Stampaki
A. Karaliota - Lymperopoulou

University of Athens
Department of Inorganic Chemistry - Section III
Panepistimioupolis
GR-15771 Athens

(Received: November 7, 1996 In final form: January 26, 1998)

Abstract

Complexation of Nb and Ta in their 3+ oxidation states with oxalates in aqueous media is reported. Differences observed in: i) in the redox behavior of the system (M(V)-oxalate) (M(III)-oxalate) M=Nb or Ta , ii) in the isolation mechanisms of the complexes of M(III) and iii) in various properties of the isolated species, i.e. color, solubility, magnetic properties (magnetic moment, ESR spectra), IR and electronic spectra are attributed to the differenced in coordination number and symmetry adopted by each metal centre.

Introduction

The similarity observed in the properties of the compounds formed by Niobium and Tantalum in their stable oxidation states is attributed to the comparable ionic radii of these two elements.

During our work on the aqueous chemistry of the Niobium and Tantalum in their oxidation states (III) and (IV), we observed significant differences between the two elements, even when they are coupled with the same complexing agents.

The aqueous chemistry of Niobium in its lower oxidation states has experienced significant progress over the last 15 years. The presence of oxo-trinuclear clusters of Niobium in aqueous solutions and in the solids isolated therefrom had been anticipated following a much earlier discovery, [1,2,3,4] namely that relatively stable triangular clusters of reduced Mo or W are present in aqueous solutions and in the crystalline compounds isolated therefrom.

Originally it was presumed that stable Mo(IV) could not be present in aqueous solutions; furthermore, it was presumed that even if this species *was* formed as an intermediate product, it would be highly unstable, and would undergo disproporation reaction: 2 Mo(IV) → Mo(III) + Mo(V). Later, Ardon and Pernick[5] prepared a stable aqua ion of Molybdenum (IV) in aqueous solution: $[Mo_2O_2 (H_2O)_8]^{4+}$. The most striking property of the ion is its remarkable stability to air oxidation. In acid concentration greater than 1M, the concentration of Mo(IV) decreases very slowly upon exposure to the atmosphere. The second unexpected property is the resistance of the ion to disproportionation.

A solution of Mo(IV) prepared by the method of Ardon and Pernick [(5)] was absorbed by a Dowex 5O WX2 cation-exchange column and was eluted with 0.5M oxalic acid. CsCl was added to the eluate and upon slow evaporation of this red-purple solution, red-purple crystals of $Cs_2[Mo_3O_4(C_2O_4)_3 (H_2O)_3] . 4 H_2O . ½ H_2C_2O_4$ **(I)** were formed. [(1,6)]

The formation of the trinuclear oxalato ion is irreversible and this new species is stable indefinitely in aqueous solution without reverting to the Ardon species. The compound **(I)** is the first example of a structurally characterized complex containing Mo(IV) isolated from an aqueous solution of Mo(IV). It is also one of the most stable and easily prepared Mo(IV) complexes known. X-ray crystal structures of **(I)**, together with studies using oxygen-18 labeled solvent water have confirmed that the $[Mo_3O_4]^{4+}$ core present in crystalline samples is retained in solution.

Note that early transition metals have a pronounced tendency to form highly stable trinuclear clusters[(7)]. A. Bino [(8)] discovered that a novel niobium sulfate compound was in fact a bi-oxo-capped cluster, structurally similar to the Mo and W compounds. This gave the first indication that Group 5 metals may also form oxotrinuclear compounds in aqueous solution, with metal ions in their lower oxidation states.

When $Nb_2Cl_6(THT)_3$ (THT=tetrahydrothiophene) dissolved in THF at 0 °C was treated with concentrated aqueous HCl (with O_2 rigorously excluded), a green solution occurred which was then passed through a cation exchange column, where a green band was formed. [(9),(10)] The green cation is of the type $[Nb_3O_4(H_2O)_9]^{N+}$ **(II)**, with low-valent niobium.

Addition of $K_2C_2O_4$ to **II** affords crystals of the eight coordinate complex $K_4 [Nb(C_2O_4)_4] . 3 H_2O$. [(11)] It is useful, to emphasize on the stabilization of the monomer complex Nb(IV) from aqueous solution oxotrinuclear core(II) with addition of oxalate ligand.

A structurally similar green cation **(II)** with charge (+4) has been detected in the solution formed by reducing $NbCl_5$ in concentrated HCl, using Cd as the reductant. [12]

Trinuclear tantalum clusters of the types Ta_3X_{13} and Ta_3X_{17} (X = have been isolated and identified from non-aqueous solutions; [13,14] however, no analogous oxo-clusters have been reported in aqueous solutions.

Tetra-oxalate tantalate (III) has been prepared in aqueous solution, and its diamagnetic pentatribenzylammonium salt has been isolated. [15]

This work, which was done in the context of studying the elements Niobium and Tantalum in aqueous solutions, [15,16] pinpoints the differences we established during the investigation and isolation of oxalato complex derivatives of the metal ions Nb(III) and Ta(III).

Experimental section

All operations were carried out under argon atmosphere using standard inert atmosphere techniques .

Synthesis of K_2 Cd $[Nb(C_2O_4)_3 (HC_2O_4)] . 3 H_2O$(1a).

In a Vycor crucible, 1 g (3.76 mmol) of Nb_2O_5 was fused with 10 g of $KHSO_4$. 4 g (32.25 mmol) of ammonium oxalate and 2 ml of concentrated H_2SO_4 were added to the melt ; water was added to the emulsion to make 80 ml. The solution was degassed and then reduced with metallic cadmium. A clear brown solution was formed, whose coloration became brighter as the reduction proceeded (solution A). This solution was unstable and was instantly decolorized in the presence of O_2, with concomitant oxidation of the metal ion to Nb(V).

When reduction in the reduced solution A was sustained over a 24-hour period, a voluminous precipitate of brown oxalato Nb(III) complex was formed, which was filtered and washed with (degassed) water.

The brown solid was dried at 110 °C. It remained stable when exposed to the atmosphere. The analysis gave the following results for
K_2 Cd $[Nb(C_2O_4)_3 (HC_2O_4)] . 3 H_2O$ (1a)

Calc:	Nb: 13.4	Cd: 16.29	C: 13.91	H: 1.044	K: 11.3
Found:	Nb: 13.4	Cd: 16.45	C: 14.10	H: 1.15	K: 10.95)

IR ν(KBr)cm^{-1} 1740-1660 $\nu_{asym}(CO_2)$ 1450-1400 $\nu_{sym}(CO_2)$

Synthesis of K_6 Cd $[Nb_2(C_2O_4)_7]$. 2 H_2O(1b)

1 g (3.76 mmol) of Nb_2O_5 was fused with 10 g of $KHSO_4$. 4 g (31.7 mmol) of oxalic acid were added to the melt; water was added to the (solution) to make 80 ml. The resulting solution was degassed and then reduced with metallic cadmium. A brown solution of reduced niobium was formed, whose concentration increased with time (solution B). The coloration of solution B was paler than that of solution A. After 24 hours, a precipitate consisting of a complex of reduced niobium was separated from solution B and removed by filtration, washed with (degassed) water and dried to 110 °C. This brown solid complex remained stable when exposed to the atmosphere, unlike solution B, which was unstable. The analysis gave the following results for: K_6 Cd $[Nb_2(C_2O_4)_7]$. 2 H_2O (1b)

Calc:	Nb: 16.18	Cd: 9.75	C: 14.63	H: 0.34	K: 20.43
Found:	Nb: 16.11	Cd: 10.03	C: 14.95	H: 0.6	K: 20.12

IR ν(KBr)cm^{-1} 1680-1580 $\nu_{asym}(CO_2)$ 1450-1400 $\nu_{sym}(CO_2)$

Preparation of $[(Bz_3NH)_5\ Ta(C_2O_4)_4]$. 4 H_2O (Bz = Benzyl) (2)

Preparation of the complex penta-tribenzylammonium tetra-oxalato-tantalate(III) was carried out as described in reference 15b.

Analysis

Niobium was determined quantitatively by precipitating with ammonia. The precipitate was filtered washed with ether, ignited and weighed as Nb_2O_5.

Oxalate were measured by decomposing the complex with ammonia, acidifying and titration with 0,1 N $KMnO_4$.

Potassium determined by Flame photometry Perkin Elmer 146.

Elemental analysis for carbon and hydrogen was performed with a Perkin Elmer 240 Analyzer

Cadmium were also determined by atomic absorption. Spectroscopy Perkin Elmer 305

Oxidation state

The oxidation state of Niobium was determined by titration the complex with dilute permanganate. Since permanganate reacts with oxolate too, Niobium (III) is estimated by difference.

Physical measurements

UV and visible spectra were obtained with Zeiss spectrophotometer and Cary - 17. IR spectra with a Perkin Elmer 337. ESR spectra were recorded at 298K using a Varian E-4 spectrometer.

Results and Discussion

Although the methods used for the preparation of solutions of oxalato-Nb(V) and oxalato-Ta(V) species are similar, the metal : ligand ratio is different in these two instances (Nb : oxalato = 1 : 10; Ta : oxalato = 1 : 130); as a result, the initial solutions contain different species. The aforementioned ratio is the minimum required to effect the reduction which leads to the formation of complexes (1a), (1b), and (2).

The different tendencies for reduction exhibited by the systems Nb(V)-Nb(III) and Ta(V)-Ta(III) are also confirmed, by use of various reducing agents. In particular, oxalato-Nb(V) is reduced by Zn and Cd, while oxalato-Ta(V) is only reduced by Zn, or by reductants of similar reducing potential. The only reduction of oxalato-Nb(V) and oxalato-Ta(V) complexes in aqueous solutions reported is a polarographic one. [17] The same tendency is seen in the reduction of other systems of the type M(V)-X, in which M = Nb or Ta; X = Cl, hydroxy-acids (acyclic and cyclic), alcohols, or pyridine derivatives.

The isolation of the complexes of these elements is different. The high concentration of oxalato-Nb(V) in the initial solution, the high degree of reduction, as well as the presence of cadmium ions (serving as compensatory ions) promote the precipitation of (1a) and (1b) from their aqueous reduced solutions. The oxalato-Ta(III) complex is highly soluble in H_2O under experimental conditions and cannot possibly be isolated from its reduced solution by precipitation. Therefore, it is considered essential to isolate the complex by extraction, using a bulky cation, i.e. that of tribenzylamine.

The diversity in the structures of the isolated complexes results in the emergence of different properties, i.e. color, solubility, magnetic and electronic properties (magnetic moment, ESR spectra). Compounds (1a) and (1b) are brown, while (2) is yellow-green. The presence of tribenzylamine in (2) reduces its solubility in solvents, especially polar ones, i.e. water, alcohols ; the complex is soluble in complexing solvents, i.e. acetyl acetone, where novel complexes are formed.[15a] Complexes (1a) and (1b) are soluble in polar solvents; however, their different solubilities are attrib-

uted to their different structures. Compound (1b), which is a dimer, is less soluble than (1a), which is a monomer.

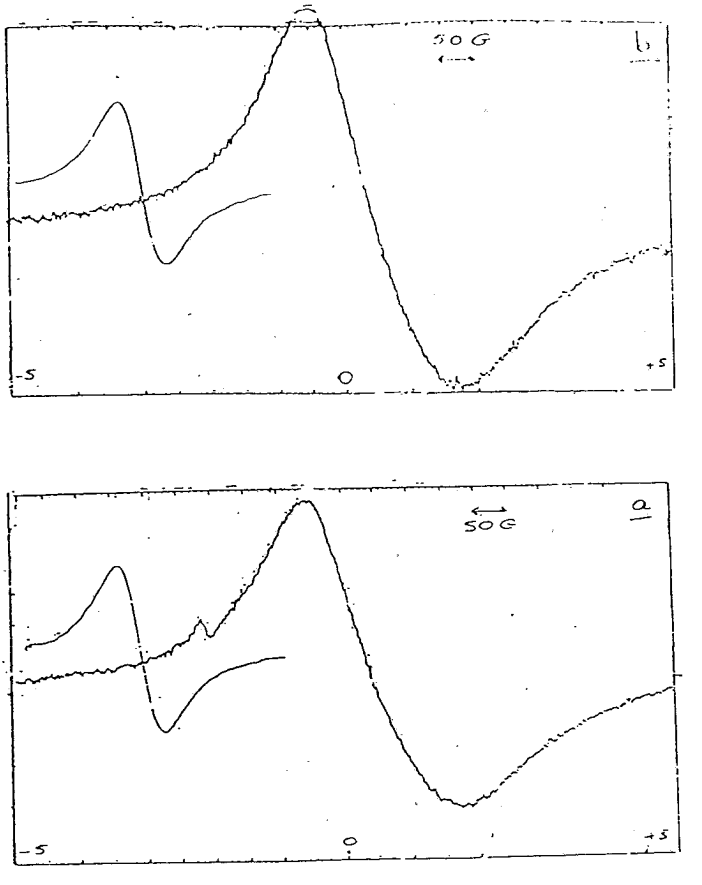

Fig. 1. ESR spectra

1a. K_2 Cd $[Nb(C_2O_4)_3 (HC_2O_4)].3H_2O$

1b. K_6 Cd $[Nb_2(C_2O_4)_7].2H_2O$

A notable difference is seen in magnetic properties. Complexes (1a) and (1b) are seven coordinate paramagnetic complexes and their ESR spectra are shown in Fig.1.

In the case of a seven coordinate complex three possible arrangements are found in nature:

(1) Pentagonal bipyramid D_{5h} symmetry

(2) Monocapped trigonal prism C_{2v} symmetry and

(3) Monocapped octahedro C_{3v} symmetry.

Figure 2 shows 'd'-orbital energy levers. The geometries that may be assumed by seven coordinate molecules have been discussed [18,19,20] concluding that the energetics of the various polyhedra are very similar upon consideration of ligand - ligand repulsions.

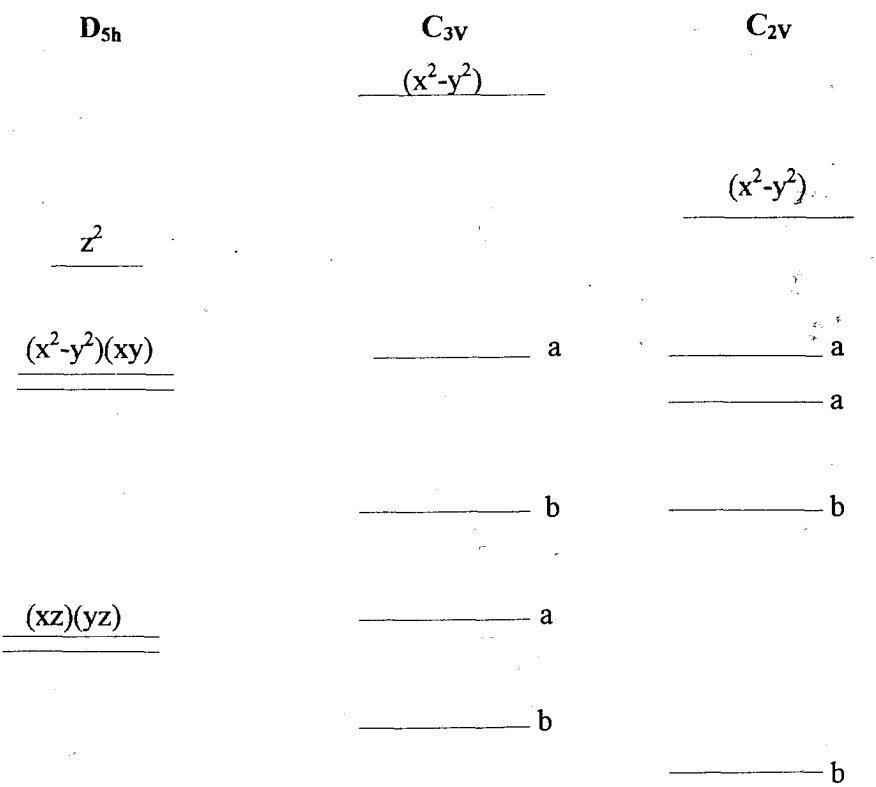

Fig. 2 . 'd'-orbital splitting diagram for seven coordination geometries

a. d_{z^2} , d_{xy} hybrids b.d_{xz} , d_{yz} hybrids

Our results are in agreement with bibliographical data on seven-coordinated complexes of a d^2 metal ion with either D_{5h} (pentagonal

bipyramid) or C_{3v} (monocapped octahedron) symmetry. The idea of a monocapped triangular prism (C_{2v}) is ruled out, given that complexes formed by metal ions with d^2 electronic configuration are diamagnetic[21,22] (Fig.2). Information obtained from ESR spectra (Fig.1) is consistent with a high symmetry (D_{5h}) for (1b) [$g_l = g_{ii} = 2.043$]; a slight disturbance in the symmetry of (1a) was observed [$g_{ii} = 2.2$; $g_l = 2.04$], due to the presence of the monodentate hydrogen oxalate ion, i.e. $(HC_2O_4)^-$. [16]

The complex formed by Ta(III) is diamagnetic and, of course, exhibits no ESR spectrum. Its diamagnetic properties are attributed to the fact that tantalum's coordination number is eight; it is a well-known fact that 8-coordinated complexes of metal ions with electronic configuration d^2 are diamagnetic[23,24,25].

As far as electronic spectra are concerned (see Fig. 3), the pattern of the oxalato-Ta(III) species spectrum is entirely different than that of oxalato-Nb(III), but identical to the spectra obtained from dodecahedral oxalato-Mo complexes, in which the metal ion's electronic configuration is also d^2. [26,27] The absorptivity of the bands exhibited at 32790 cm^{-1} and 26880 cm^{-1}, is 260 $M^{-1}cm^{-1}$ 460 $M^{-1}cm^{-1}$, respectively; this supports the notion of a non-centrosymmetric dodecahedral complex. The spectra recorded for both the solid compound and its solutions demonstrate that this dodecahedral symmetry is retained in the solid compound.

Oxalato-Nb(III) exhibits peaks at 27780 cm^{-1}, 22700 cm^{-1}, and 20830 cm^{-1}, which is in agreement with bibliographic reports. [19] These bands are shifted in comparison to those observed in the electronic spectrum of the d^2-seven-coordinated complex $V(CN)_7^{4-}$, whose symmetry is D_{5h}. This shift is anticipated, due to the difference in the main quantum numbers of the d orbitals[28]. On the other hand the majority of complexes of the form M(unidentate) $(bidentate)_3$ have the Pentagonal Bipyramid geometry with the unidentate ligand in an axial position[29].

The similarity seen in the spectra of compounds (1a) and (1b), combined with the fact that for paramagnetic dimeric 7-coordinated complexes only one type of symmetry (i.e. D_{5h}) yields similar IR spectra, as well as with ESR spectra, lead us to the conclusion that the most probable symmetry for compounds (1a) and (1b) is D_{5h}.

In conclusion, it appears that compounds (1a) and (1b) are seven-coordinated complexes with D_{5h} symmetry, while compound (2) is eight-coordinated, with D_{2d} symmetry or lower, which accounts fully for the differences observed.

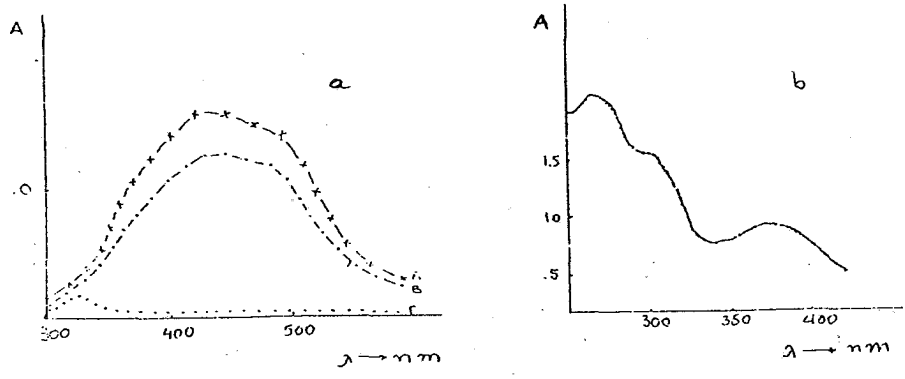

Fig. 3. Electronic spectra of aqueous solutions formed by reduction of complexes.

3a. Nb(III) - oxalate I) immediately after reduction (-x-x-x-) II) after 1 hour (---)
III) after 24 hours (.....)

3b Ta(III) - oxalate immediately after reduction

Acknowledgments

We thank Prof. D.Katakis for helpful discussions

Περίληψη

Στα πλαίσια της μελέτης της υδατικής χημείας των στοιχείων Νιόβιο και Ταντάλιο σε χαμηλές οξειδωτικές καταστάσεις, παρασκευάσθηκαν σύμπλοκα των στοιχείων με οξαλικά στα οποία το μεταλλικό ιόν σταθεροποιείται στην τρισθενή οξειδωτική του κατάσταση. Κατά τη μελέτη διαπιστώθηκαν διαφορές:

α) Στην οξειδοαναγωγική συμπεριφορά του συστήματος
(M(V) - oxal) - (M(III) - oxal)

β) Στη μέθοδο απομόνωσης των συμπλόκων των M(III) - ιόντων και

γ) Σε διάφορες ιδιότητες των απομονωμένων συμπλόκων, όπως χρώμα, διαλυτότητα, μαγν. ιδιότητες, φάσματα IR και ηλεκτρονικά

Τονίζεται ότι τα σύμπλοκα έχουν τον ίδιο συμπλεκτικό παράγοντα και περιέχουν τα μεταλλικά ιόντα στην ίδια ηλεκτρονική διαμόρφωση d^2. Οι παραπάνω διαφορές αποδίδονται κυρίως στο διαφορετικό αριθμό συντάξεως και στη διαφορετική συμμετρία.

References

1. A. Bino, A. Cotton, Z. Dori, *J. Am. Chem. Soc.*, **100**, 5252 (1978).
2. A. Bino, A. Cotton, Z. Dori, *Inorg. Chim. Acta,* **33** L33 (1979).
3. D. Richens, AG. Sykes, *Inorg. Chim. Acta,* **54**, L3 (1981).
4. D. Richens, AG. Sykes, *Inorg. Chem.*, **21**, 418 (1981).
5. M. Ardon, A Pernick, *J. Am. Chem. Soc.*, **95**, 6871 (1973).
6. E. Benory, A. Bino, D. Gibson, F. Cotton, Z. Dori, *Inorg. Chim. Acta,* **99**, 137 (1985).
7. A. Mueller, R. Jostes, and F. Cotton, *Angew. Chem. Int. Ed. Engl.*, **19**, 875 (1980).
8. a) A. Bino, *J. Am. Chem. Soc.*, **102**, 7990 (1980)
   b) A. Bino, *Inorg. Chem.*, **21**, 1917 (1982).
9. Cotton, M. Diebold, R. Llusar, W. Roth, *J. Chem. Soc. Chem. Commun.*, 1276 (1986).
10. S.Minhas and D.Richens, *J. Chem. Soc.* Dalton Trans (1996), 703
11. F.A. Cotton, M. Diebord, and W. Roth, *Inorg. Chem.*, **26**, 2889 (1987).
12. A. Liberopoulou-Karaliota, Doctoral thesis.
13. E. Kibala, F.A. Cotton, M. Shang, *Inorg. Chem.*, **29**, 5148 (1990).
14. Cotton, M. Diebold, X. Feug, W. Roth, *Inorg. Chem.*, **27**, 3413 (1988).
15. a. D. Hatjipanayioti-Stabaki, Doctoral thesis, PhD Athens University (1983).
    b.D. Hatjipanayoti-Stabaki and D. Katakis, *J. Inorg. Nucl. Chem.*, **39**, 995 (1977).
16. Kamariotaki-Paparigopoulou, Doctoral thesis, PhD Athens University (1983).
17. Elson, *J. Am. Chem. Soc.*, **75**, 4193 (1953).
18. J. Gillespie *Can. J. Chem.* **38**, 818 (1960)
19. A. Claxton and G. C. Benson *Can. J. Chem.* **44** 157 (1966).
20. Britton *Can. J. Chem.* **41** 1632 (1963)
21. Speed, J. Perumareddi, and A. Adson, *The Journal of Physical Chemistry*, **72**, 1822 (1968).
22. Hush, *Australian J. Chem.*, **15**, 378 (1962).
23. Kierman and W. Griffith *J. Chem. Soc Dalton* 2489 (1975)
24. Bonds and R. Archer, *Inorg. Chem.* **10** 2057 (1971)
25. Perumaredi A. Liehr and A. Adamson *J. Amer. Chem. Soc.* **85** 249 (1963)
26. Basu, S. Basu, *J. Inorg. Nucl. Chem.*, **31**, 3326 (1969).
27. Figgis, *Introduction to Ligand Field* ed. John Wiley and Sons Inc. New York (1966).
28. Leverson, R. Domingner, *Inorg. Chem.*, **12**, 2342 (1973).
29. Drew, *Progress in Inorganic Chemistry*, Vol. 23 edit S.J.Lippard, Wiley-Interscience New York (1977), p.65

Chimika Chronika, New Series, 26, 523-534 (1997)

NATIONAL IMMUNOASSAY QUALITY CONTROL SCHEME (NIQCS) IN GREECE AND CYPRUS FOR THYROID RELATED HORMONES: A SEVEN YEAR INVESTIGATION

Ion Christofidis*, Nassia Kioukia

*Reprints to Immunoassay Quality Control Laboratory, I.R.R.P, NCSR «DEMOKRITOS», 153 10 Ag. Paraskevi Attikis

(Received: May 31, 1997 In final form: March 20, 1998)

Summary

A National Immunoassay Quality Control Scheme was performed for seven years among 60 laboratories in Greece and Cyprus. Imprecision levels were estimated for standard commercial kits used in the analysis for the thyroid hormones T4, fT4, T3, fT3 and TSH. It is estimated that RIA or IRMA methods/kits are still used by the 55% of the laboratories of this scheme, while a slightly increasing number are using automated non-isotopic methods such as ELISA and MEIA. Despite the invariably lower *within-kit CV%* of the latter, these kits are not extensively preferred due to high costs in reagents and machinery. On the other hand, the gradually lowering effect in *within-kit CV%* in some RIA kits, as on T3 and T4 estimation, or in IRMA kits during TSH estimation seem to control also the *between-kit CV%* (overall kit CV%). This together with the low reagent cost and pre-existent machinery in the latter, defend their high percent use.

Key words

Quality control scheme, thyroid hormones, kit imprecision, isotopic, non-isotopic methods, within-kit, between-kit CV%

Introduction

Accuracy and precision on the analytical estimation of Thyroxine (T4) and free thyroxine (fT4) and other thyroid related hormones, are both crucial for the differential diagnosis of the thyroid diseases. Hyperthyroid subjects are suggested to be monitored continuously for T4 and fT4 levels. Sub-clinical hypothyroid patients are looked for low-normal fT4 levels and above the reference range TSH

values. Besides, T4 levels may clearly be below the reference range due to low binding of fT4 to Thyroid Binding Globulin (TBG) or to other sera proteins (1,2,3,4). In the non-thyroidal illness total T4, free T4 and T3 levels often decrease below physiological but keeping normal TSH (5).

Routine analysis of these hormones is performed daily in analytical laboratories with a wide variety of commercial methods/ kits. It has been previously reported that the level of imprecision increases on estimation of such hormones outside the physiological range, and more emphatically at the functional detection limit, this increase depending also on method/kit used (6,7). Therefore, prior to kit selection the analyst needs to know the expected imprecision level, as well as other details on the kit such as interference effects from proteins, lipids, drugs etc.. Understandably the selection of kit for hormone analysis may also be influenced by other factors, such as the analyst's prior experience with one trade mark, the kit promotion by the firm, and the price of the kit. More importantly, the lack of comparative data on used kits by a particular region, leaves the analyst unassisted. Although data on kit performance may be produced individually by manufacturing companies, these are normally performed at specific expert sites and under the best chosen conditions. More realistic conditions for kits performance may be produced by different routine laboratories subscribed to an external quality control scheme run on national/ international basis. These control schemes ideally aim at discovering the 'state of art' of the kits and at eventually improving their reliability (8,9).

For this reason, we have organised a national external quality control scheme in Greek and Cyprian laboratories for seven years now, to allow comparison between the most used commercial immunoassays referring to the analysis of the thyroid related hormones T4, fT4, T3, fT3 and TSH. The search includes data for a total of 60 laboratories for the period of 1990 till 1996.

Materials and Methods

The National Immunoassay Quality Control Scheme (NIQCS) for thyroid related hormones was organised by the Immunoassay Quality Control Laboratory in DEMOKRITOS. Details on the mode of operation of the National Immunoassay

Quality Control Scheme (NIQCS) have been given already (10). Participation in the scheme was voluntary and strictly confidential. Each year pooled human sera were pre-adjusted to a certain hormone level after exogenous hormone addition. These were dispensed in vials and sent to recipient laboratories under a code name. The examined hormones were estimated with in house RIA T3, T4 and TSH and with fT4 kit of Amersham. The approximate levels were T3≅3nmol/L, T4≅50nmol/L, TSH≅ 5mIU/L and fT4≅30pmol/L. Pooled sera had been checked for contamination by hepatitis B surface antigen and HIV antigen.

The participant laboratories were asked to send their estimations on relative hormones and the necessary data i.e. kit name, methodology, hormone level based on common units etc., up to certain date to DEMOKRITOS. Data were imposed to annual statistical analysis.

A *between-kit mean* (the consensus mean trimmed by ± 2 SD twice) was extracted each year for all laboratory data and all methods/kits per hormone level. A *within-kit mean* (consensus mean trimmed by ± 2SD twice) was derived for data of single method/kit every yearly cycle per hormone level. The overall imprecision was estimated respectively by means of correlation variation percentage (CV%) described as (SD/consensus mean)x100 for the particular hormone levels. Applying the *between-kit mean* or the *within-kit mean* in the above equation, the *between-kit CV%* (overall kit CV%) and the *within-kit CV%* were similarly derived. In this analysis we selected hormone data which coincided with the kits reference range limits. The percent to total number of laboratories using common hormone analysis or methodology group were also calculated.

Results

From 1990 towards 1996 the majority of analytical laboratories included in this investigation were governmental (from 77% to 60%) of which around 73% to 55% used isotopic methods, versus 27% to 45% which used non-isotopic methods (see Table 1). In the present scheme one can also see the rate of laboratories involved in the thyroid hormone measurements.

Table 1: Percent and total number of laboratories classified in the scheme in relation to laboratory identity, method used and hormone analysis per yearly distribution cycle.

Year	1990	1991	1992	1993	1994	1995	1996
Total number of labs	42	44	53	57	54	62	58
Public labs (%)	77.3	67.6	66.7	75.7	61.4	59.7	60.5
Private labs (%)	22.7	32.4	33.3	24.3	38.6	40.3	39.5
Isotopic methods (%)	72.7	73.5	75.8	62.2	66.4	66.4	54.9
Non-isotopic methods (%)	27.3	26.5	24.2	37.8	33.6	33.6	45.1
Total T4 (%)	90.9	85.3	87.9	91.9	80.0	91.1	85.7
Free T4 (%)	68.2	62.0	50.0	50.0	65.0	64.7	53.5
Total T3 (%)	90.9	85.3	88.0	91.9	77.3	91.1	82.1
Free T3 (%)	54.5	32.5	36.4	32.4	47.2	41.2	32.0
TSH (%)	-	88.2	88.7	92.3	86.0	94.5	96.1

The kits used for T4 estimation were the RIA.KODAK, ELISA.BOHERINGER and RIA.DEM. Selecting mean measurement values just below the reference range (Table 2), namely T4≅50nmol/L, Graph 1, the *between-kit CV%* levelled from 15% in 1990 to about 19% in 1993, levelling off to about 11% towards 1996. This pattern is similar to that of the RIA.DEM,- where *within-kit CV%* peaked in 1993 at ~12.5% while the *between-kit CV%* (overall kit CV%) the same year was near 19%. The kits RIA.KODAK and ELISA.BOHERINGER presented rather stable *within-kit CV%* throughout 1990-1996, reaching respective maximum of 8% and 6.5%.

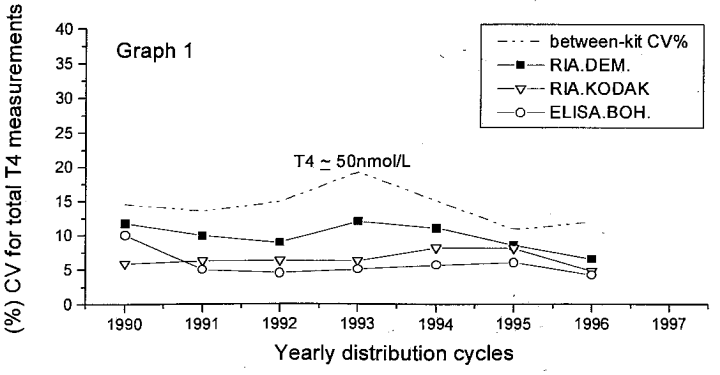

Graph 1: Relationship of between-kit (overall kit CV%) and within-kit CV% to yearly distribution cycles using T4 mean data ~ 50nmol/L. Each point represents CV% for at least 10 mean T4 values. RIA.DEM.= T4 Solid phase RIA, DEMOKRITOS, RIA.KODAK=Kodak Amerlex-M T4 RIA KODAK CL. DIAGN., ELISA.BOHERINGER=Enzymun test T4, BOHERINGER-MANNHEIM.

Table 2: Hormones and relative reference range. The reference range was broadly based on manufacturers data for the used kits.

Hormone	Reference range
Thyroxine (T4)	50-170 nmol/L
Free Thyroxine (fT4)	10-30pmol/L
Triiodothyronine (T3)	0.8-3nmol/L
Free Triiodothyronine (fT3)	3-8pmol/L
Thyroid Stimulating Hormone (TSH)	1-5mIU/L 80/558 I.R.P.

In the kits for free T4 hormone estimation (see Graph 2) CV% was calculated for mean fT4 values ≅30pmol/L. Although both selected kits for fT4 estimation RIA.AMERSHAM and RIA.DPC showed a lowering effect in their *within-kit CV%* from 1993 onwards down to about 7% and 6% respectively, it seems that the increasing *within-kit CV%* up to 16% of MEIA.ABBOTT assisted to keep *between-kit CV%* (overall kit CV%) level at nearly 20% throughout those years. The ELISA.BOHERINGER kit seemed to keep *within-kit CV%* at a low close range, between 2% and 4%.

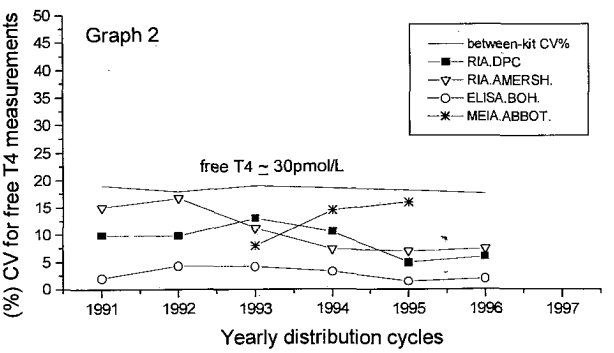

Graph 2: Relation of between-kit (overall kit CV%) and within-kit CV% to the yearly distribution cycles in data of free T4 ~ 30pmol/L. Each point (CV%) accounts for at least 10 mean fT4measurements. RIA.DPC=Coat-a-Count,DPC, RIA.AMERSHAM= Amerlex MAb*,AMERSHAM, ELISA.BOHERINGER=Enzymun test fT4, BOHERINGER-MANNHEIM, MEIA.ABBOTT=IMX fT4, ABBOTT.

Graph 3 allows comparison of the imprecision levels between the RIA.DEM, RIA.JOHNSON, ELISA.BOHERINGER and MEIA.ABBOTT kits for total T3 hormone estimation on values ≅3nmol/L. Interestingly, all four kits showed close

improvement of the *within-kit CV%* this ranging in 1996 between 2.5% and 5% (Graph 3). Similarly decreased the *between-kit CV%* (overall kit CV%) from about 20% in 1991 down to nearly 10% in 1996.

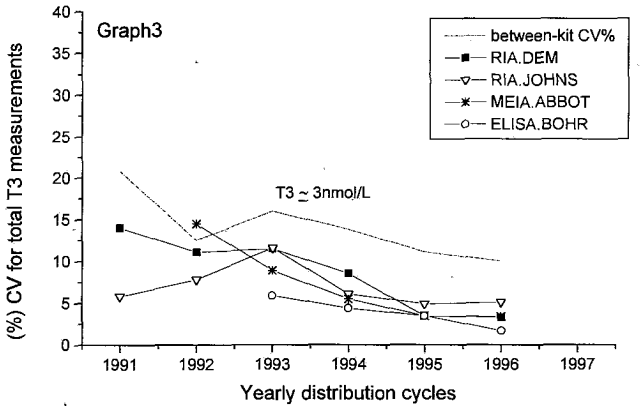

Graph 3: Relationship of between-kit (overall kit CV%) and within-kit CV% with the yearly distribution cycles on measurement of data for T3 ≃ 3nmol/L. Each point (CV%) represents at least 10 mean T3 values. RIA.DEM=T3-solid phase RIA, DEMOKRITOS, RIA.JOHNSON=Amerlex-MT3, JOHN. & JOHNS CL.DIAGN.,MEIA.ABBOTT= IMX TT3, ABBOTT, ELISA.BOHERINGER=Enzymun test TT3, BOHERINGER-MANNHEIM.

In Graph 4 there is an exponential like drop in the *between-kit CV%* (overall kit CV%) from about 30% in 1991 to 6.5% in 1996 for mean TSH measurements ≅5mIU/L (just above physiological) when examining data extracted for the RIA.DEM,

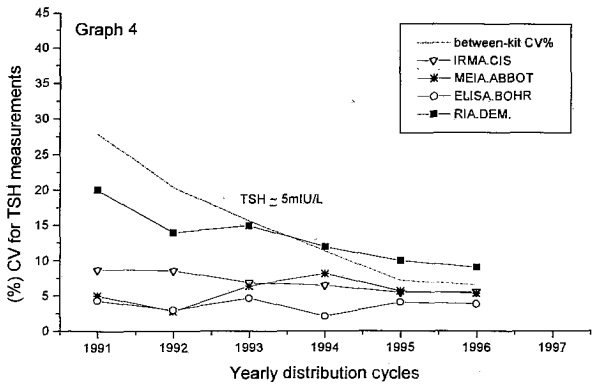

Graph 4: Relationship of between-kit (overall kit CV%) or within-kit CV% with yearly distribution cycles for data of TSH ≃ 5mIU/L I.R.P. 80/558 sera measurements. Each point (CV%) represents at least 10 mean TSH measurements. IRMA.CIS= ELSA2-TSH, CIS, MEIA.ABBOTT= IMX-Ultrasens. hTSH II, ABBOTT, ELISA.BOHERINGER=Enzymun test-TSH, BOHERINGER -MANNHEIM, RIA.DEM= RIA TSH, DEMOKRITOS.

MEIA.ABBOTT, IRMA.CIS and ELISA.BOHERINGER kits. This subtle effect in the *between-kit CV%* seems to derive from the most elevated *within-kit CV%* of RIA.DEM (widely used kit in the scheme), seen to drop from 20% in 1991 to 9% in 1996. In parallel, the MEIA.ABBOTT kit presented low level *within-kit CV%* from about 5% to 7.5%, while data from the IRMA.CIS kit showed *within-kit CV %* to nearly 7.5%. However, the ELISA.BOHERINGER had the lowest *within-kit CV%* ~4.5% from 1991-1996.

Discussion

It is previously said that fT4 quantification may present variance due to interference of serum proteins with the free T4- total T4 balance (11). Besides, the use of indirect methods on fT4 measurement with T4 analogues do not always ensure exclusion of the variance factor (12,13,14). TSH imprecision curves are seen to erode characteristically in their low and high ends of the reference range (11). By another intra-site search *within-kit CV%* was suggested to stay below 6% and 8% for T4 and fT4 kits respectively (15). Moreover, it has been shown that imprecision in kits may be attributed to a combination of factors, such as the human variation on assay operation, the variability of reagents on assessment cycles, protein/lipid interference from the serum matrix, difference of antibody specificity between kits (13, 16).

Variation in data due to kit imprecision may be of major clinical importance, especially in borderline cases of suspected thyroid malfunction (11,16). In this work we have concentrated in variant kit imprecision on hormone estimation especially dealing with the most vulnerable sites of imprecision curve, i.e. nearly outside of the reference range where normally thyroid malfunctions are found and *within-kit CV%* is higher (17,18, 19). The present findings by no means describe overall kit imprecision and this investigation refers to the sample of the present scheme. With this sample we have also partially attempted to explain the reason of analytical laboratories behind their kit selection.

Up to 1992 mainly RIA methodology has been clearly used by the highest percent laboratory number of this scheme for thyroid hormone analysis. Between 1993 and

1995 there was a 10% drop in isotopic methods with a further 10% decrease in 1996 for the given sample of laboratories (see Table 1). Analytically, in T3 and T4 estimation and towards 1996, RIA.DEM, RIA.JOHNSON, RIA.KODAK and RIA.DPC had sufficiently low *within-kit CV%* and close to that of the ELISA.BOHERINGER and MEIA.ABBOTT automated methods (see Graph 3). Characteristically in total T3 kits for values ≅3nmol/L the *within-kit CV%* approached that of ELISA.BOHERINGER by 1996 (Graph 3).

In fT4 measurements the RIA.AMERSHAM, the RIA/DPC kits exhibited similar *within-kit CV% for* free T4 high-normal levels ≅30pmol/L (Graph 2). The ELISA.BOHERINGER as an automated method/kit showed throughout the years low level *within-kit CV%* i.e. between 2% to 3% compared with other current RIA methods. MEIA.ABBOTT, however, an also automated method gave a rather unstable *within-kit CV%* (8-16%) for the same fT4 sera level.

In TSH evaluation, the MEIA.ABBOTT and the IRMA.CIS kits showed similar *within-kit CV%* for the examined hormone levels (i.e.5mIU/L) this being a little higher than that in the automated ELISA.BOHERINGER kit data (about 5%).

From the above it seems the wide use of RIA methodology -or more generally of isotopic methods - for T4 and T3 analysis within the scheme may be justified by the increasingly low *within-kit CV%* of RIA kits over the last years. Such an improvement may be attributed to changes of immunoassay reagents such as more specific antibodies, purer standards and better technology. However, RIA methodology seems to be vanishing from TSH measurement being possibly substituted by the IRMA methodology in kits (data not shown). IRMA.CIS in TSH gave competitively low *within-kit CV%* with the automated MEIA.ABBOTT kit. However, automated methods introduced in T3 and T4 estimation, as for example with the ELISA.BOHERINGER kit they exhibited low kit imprecision, but not very far lower than that of the RIA kits. In the fT4 estimation though, the ELISA/BOHERINGER (also automated technique) *within-kit CV%* was emphatically lower than in the other two RIA kits. The use of MEIA.ABBOTT in TSH estimation is perhaps justified for the low *within-kit CV%* at the examined

estimation level. Interestingly the *within-kit CV%* of MEIA.ABBOTT was unusually high in the fT4 analysis compared with other methods.

In Table 1 it is seen that although the use of non-isotopic methods is being slightly increased from 1990-1996 (from 27% to 45%), still about the 55% of the laboratories use today isotopic methods according to the present scheme. With the increasing use of advanced automated methods such as ELISA.BOHERINGER, MEIA.ABBOTT etc., generally speaking the imprecision levels have been lowered. Switching to these techniques signifies though high capital investment in machinery and relatively usually more expensive reagents. As RIA methods seem to have improved reagents and technology (some of these now apply automation), they can now give sufficiently low imprecision as was seen in the T3 and T4, or fT4 kits. Specifically, in fT4 kits the *between-kit CV%* in borderline values stayed emphatically high compared with other hormones. Besides the IRMA methodology in the TSH kits seemed to be used satisfactorily by the laboratories of our investigation. Conclusively, until higher capital investment is made by the governmental analytical laboratories which seem to represent the main core in this scheme, the introduction of automated and more accurate but surely more expensive methods is delayed.

ΠΕΡΙΛΗΨΗ:

ΕΘΝΙΚΟΣ ΕΛΕΓΧΟΣ ΠΟΙΟΤΗΤΑΣ ΑΝΟΣΟΑΝΑΛΥΣΕΩΝ ΣΤΗΝ ΕΛΛΑΔΑ ΚΑΙ ΚΥΠΡΟ ΓΙΑ ΤΟΝ ΠΡΟΣΔΙΟΡΙΣΜΟ ΤΩΝ ΟΡΜΟΝΩΝ ΤΟΥ ΘΥΡΕΟΕΙΔΟΥΣ : ΕΠΤΑΕΤΗΣ ΕΡΕΥΝΑ

Από το 1990 μέχρι το 1996 το εργαστήριο Ελέγχου Ποιότητας Ανοσοαναλύσεων του Ε.Κ.Ε.Φ.Ε ΔΗΜΟΚΡΙΤΟΣ εκπόνησε ένα πρόγραμμα Εθνικού Ελέγχου Ποιότητας Ανοσοαναλύσεων για τον προσδιορισμό των ορμονών του θυρεοειδούς: Θυροξίνη (T4), Ελεύθερη Θυροξίνη (fT4), Τριιωδοθυρονίνη (T3), Ελεύθερη Τριιωδοθυρονίνη (fT3) και Θυρεοτροπίνη (TSH) σε σύνολο 60 αναλυτικών εργαστηρίων της Ελλάδας και της Κύπρου. Η διαδικασία περιέλαβε διανομή αγνώστων ορών ελέγχου σε αναλυτικά εργαστήρια τα οποία ανέλαβαν να προσδιορίσουν τα επίπεδα των ανωτέρω ορμονών με τις χρησιμοποιούμενες

εμπορικές ανοσοαναλύσεις ρουτίνας. Εκ των αποτελεσμάτων αυτών ακολούθησε ετήσια στατιστική επεξεργασία.

Στην παρούσα ανάλυση ελέγξαμε την διασπορά των τιμών κατά τον προσδιορισμό των παραπάνω θυρεοειδικών ορμονών σε επιλεγμένα επίπεδα μόλις εκτός της φυσιολογικής περιοχής. Μέχρι το 1992 η μεθοδολογία RIA κατελάμβανε το μεγαλύτερο ποσοστό των ανοσοαναλύσεων των ορμονών του θυρεοειδούς στο παρόν πρόγραμμα. Μεταξύ του 1993 και 1995 το ποσοστό των ισοτοπικών μεθόδων γενικότερα έπεσε κατά 10% με επιπλέον 10% μείωση το 1996. Αναλυτικά οι μέθοδοι RIA.DEM, RIA.JOHNSON, RIA.KODAK, RIA.DPC παρουσίασαν αρκετά χαμηλό συντελεστή μεταβλητότητας (CV%), περίπου παρόμοιο με αυτό των αυτοματοποιημένων μεθόδων, όπως των ELISA.BOHERINGER και MEIA.ABBOTT κατά την ανάλυση των επιπέδων T3, T4 ορμονών. Για τον προσδιορισμό της TSH, οι IRMA.CIS και MEIA.ABBOTT μέθοδοι έδωσαν λίγο μεγαλύτερο CV% από αυτό της ELISA.BOHERINGER. Στην fT4 ανάλυση οι μέθοδοι RIA.AMERSHAM, RIA.DPC και MEIA.ABBOTT έδωσαν υψηλότερο CV% (περίπου 6% μέχρι 7%) συγκριτικά με αυτό της ELISA/BOHERINGER (~2%-3%) για τις τιμές ορού fT4≃30pmol/L (υπερθυρεοειδικές).

Από τα παραπάνω προκύπτει ότι η συχνή χρήση RIA μεθοδολογίας ιδιαίτερα κατά την ανάλυση των T3, T4 ορμονών είναι δικαιολογημένη λόγω του παρουσιαζόμενου χαμηλού CV%, γεγονός πού αποδίδει περισσότερο ακριβείς τιμές εκτός φυσιολογικής περιοχής. Στην TSH ανάλυση για τιμές ≃5mIU/L η IRMA.CIS μεθοδολογία φάνηκε να υποκαθιστά την RIA.DEM μέθοδο με χαμηλότερο CV%, παρόμοιο με αυτό της αυτοματοποιημένης MEIA/ABBOTT.

Συμπερασματικά χαμηλές τιμές CV% σε σύγχρονες ισοτοπικές μεθοδολογίες γίνονται αποδεκτές λόγω της βελτιωμένης τεχνολογίας αντισωμάτων, καθαρότητας των προτύπων βαθμονόμησης στις ανοσοαναλύσεις κ.λ.π. Επίσης η αυξανόμενη χρήση αυτοματοποιημένων μεθόδων φαίνεται να οφείλεται σταθερά στην μείωση του CV%.

References

1. Ahmed, J, Smetkhurst, P: Ann. Clin. Biochem. **17**, 241, 1980.
2. Colian, FP, Dutty, MJ, Dutty, GJ, Farell, RJ, Mckenna TJ: Acta Endocrinologica, **306**, 635, 1983.
3. Georgiou, S, Christofidis, I: Journal of Immunoassay, **17**/1, 47, 1996.
4. Dick, M, Watson, F: Med. J. Aust., 115, 1980.
5. Wong, TK, Pekary, AE, Guy Soo Hoo, Bradley, ME, Hershman, JM: Clinical Chemistry, **38**/5, 720, 1992.
6. Spencer, CA, Takendi, M, Kazarosyan, M: Clinical Chemistry, **42**/1, 140, 1996.
7. Pillo, A, Zuchelli, GC, Maltono, R, Clerico, A, Jercasi, G, Signorini, C: Clinical Chemistry, **38**/7, 1345, 1992.
8. Albertini, A, Zuchelli, GC, Chiesa, MR, Bolleli, GF: J. of Clinical Immunoassay, **8**/2, 117, 1985.
9. Pillo, A, Zuchelli, GC, Chiesa, MR, Bolleli, GF, Albertini, A: Clinical Chemistry, **32**/1, 171, 1986.
10. Kioukia, NK, Christofidis, I. Journal of Clinical Ligand Assay, **20**/3, Fall issue, 1997.
11. Nelson, JC, Wilcox, BR: Clinical Chemistry, **42**/1, 146, 1996.
12. Ordonez-Lianos, J, Rodriguez- Espinoza, J, Gomez-Gerique, JA, Solanj-Barri, MD, Ruiz-Minguez, MA: Clinical Chemistry, **30**, 496, 1984.
13. Amino, N, Nishi, K, Nakatani, K, Mizuta, H, Ischihara, K, Tanizawa, O, Miyai, K: Clinical Chemistry, **29**, 321, 1983.
14. Stochigt, JR, DeGaris, M, Csicsman, J, Barlow, JW, White, EL, Hurley, DM: Clin. Endocrin.,**15**,313, 1981.
15. Browning, MCK, Ford, RP, Callaghan, SS, Fraser, CG: Clinical Chemistry, **32**, 902, 1986.
16. Mendel, CM, Frost, PH, Cavalleri, RR: J. Clin. Endocr. Metabol., **63**, 1394, 1986.
17. Bounaud, JY, Bounaud, MP, Begon, F: Clinical Chemistry, **32**/3, 565, 1986.
18. Shishiba, Y, Irie, M, Yamada, H, Kinoshita, F: Clinical Chemistry, **29**/8, 1501, 1983.
19. Zuchelli, GC, Pillo, A, Chiesa, MP, Masini, I: Clinical Chemistry, **40**/10, 1956, 1994.

Chimika Chronika, New Series, 26, 535-544 (1997)

REACTIVITY OF CYANO PHENYLIODONIUM TRIFLATE TOWARDS UNSATURATED HYDROCARBONS IN WET ACETONITRILE

Spyros Nikas, Nestor A. Rodios and Anastasios Varvoglis*

Laboratory of Organic Chemistry, University of Thessaloniki, Thessaloniki 54006, Greece

Aristidis Terzis and Catherine P. Raptopoulou

Institute of Materials Science, Nuclear Research Centre Democritos, Aghia Paraskevi, Athens, Greece

(Received: June 19, 1997 In final form: March 23, 1998)

Summary

The reaction of 2,3-dimethyl-1,3-butadiene with cyano phenyliodonium triflate in wet acetonitrile afforded a mixture of *E*- and *Z*-1,4-bis-acetamido-2,3-dimethyl-2-butene. Other alkenes gave similar adducts (cyclohexene) or products of further transformation (2,3-dimethyl-2-butene, 2,4,4-trimethyl-2-pentene and 1,1-diphenylethylene).

Key words: Acetamidation, cyano phenyliodonium triflate, addition, 2,3-dimethyl-1,3-butadiene

Introduction

A wealth of additions to ethylenic double bonds have been performed through the intermediacy of λ^3-iodanes of the general formula PhILL′. Alkenes and related unsaturated hydrocarbons or other substrates give readily addition products in which the two groups L and L′ are

normally incorporated into the double bond. In this way, the following groups have been added directly, using the appropriate iodane: chlorine (from $PhICl_2$), acetoxy and trifluoroacetoxy (from $PhI(OAc)_2$ and $PhI(O_2CCF_3)_2$) and tosyloxy (from PhI(OH)OTs). Furthermore, several other groups such as azide, thiocyanate, perchlorate, triflate and alkyl (or phenyl)thio were added in the presence of iodanes and a salt or a disulfide. Two different groups may also be added, whereas addition followed by rearrangement is also possible, especially in phenylated alkenes by $PhIF_2$, PhI(OH)OTs and $PhI(O_2CCF_3)_2$. Generally, in all these reactions the outcome may be described as addition of nucleophiles to the double bond which has undergone an umpolung of reactivity by the iodane through formation of another intermediate iodane[1-3].

Cyano phenyliodonium triflate (**1**) is a relatively new iodane, which was obtained from $PhI(O_2CCF_3)_2$ and trimethylsilyl cyanide in the presence of trimethylsilyl triflate[4]. It is a stable compound of intermediate character between that of a covalent iodane and an ionic iodonium salt. The main use of **1** was for the transfer of the phenyliodonium group to nucleophilic sites, resulting in the synthesis of several alkenyl and alkynyl iodonium salts[5-9]. A related heterocyclic iodane is an excellent reagent for the cyanation of the methyl group of *N,N*-dimethylanilines[10].

Results and Discussion

We have chosen to test **1** in reactions with 1,3-dienes in which it was anticipated to show Diels-Alder reactivity, serving as a heterodienophile from its cyano group, by analogy with CH_3SO_2CN[11]. Several dienes, such as cyclopentadiene, furan, anthracene, etc. reacted indeed with **1** but in such a complicated manner which did not permit the isolation of possible Diels-Alder adducts. However, with 2,3-dimethyl-1,3-butadiene (**2**) we have come across a clean solvent-dependent reaction involving 1,4-addition; this type of reactivity was subsequently extended to simpler unsaturated systems, some of which however reacted in a different way.

Reaction of 1 2,3-Dimethyl-1,3-butadiene. Reaction of diene **2** with **1** in wet acetonitrile afforded a mixture of *Z*- and *E*-1,4-bis-acetamido-2-butenes (**3** and **4** respectively) in the ratio 1:2, in a total yield of 71% (Scheme 1).

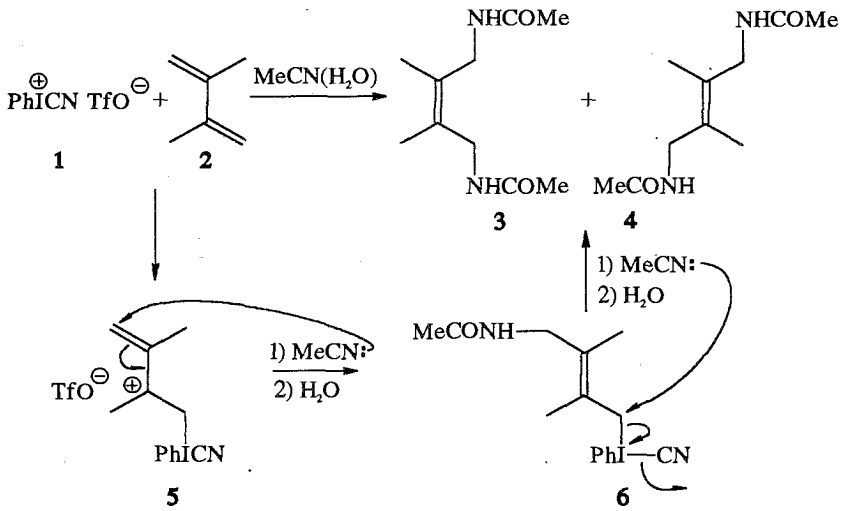

Scheme 1

The formation of these unexpected products may be accounted for by the following sequence of events. Initially, the allylic carbocation **5** results from the addition of $PhI^{+}CN$ to one of the double bonds of the substrate. This then reacts sequentially with acetonitrile and water, furnishing the *E*-acetamido phenyliodonium intermediate **6** along with its *Z*-isomer (not shown). With more acetonitrile, and then water, these iodanes afford the final products **3** and **4**, respectively No amount of 1,2-adduct could be detected. This unusual selectivity may be attributed to steric factors in the intermediate **5**.

The spectroscopic characteristics of the products did not permit a clear distinction between them, despite some slight differences, notably in their mass spectra. However, an unambiguous assignment for the *E*- isomer **4** was provided by a single crystal X-ray structure determination (Figure 1).

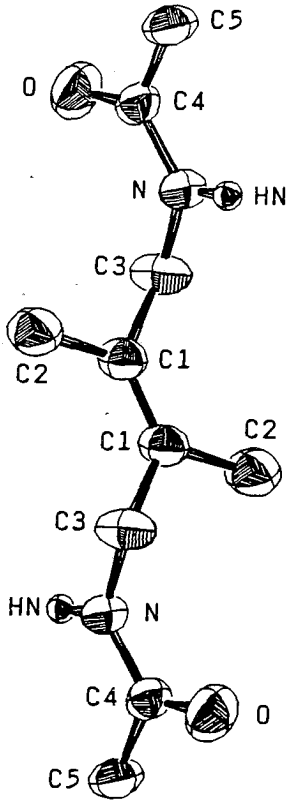

Fig. 1 ORTEP view of bisamide **4**

*Reactions of **1** with other alkenes.* An analogous reaction between **1** and cyclohexene[12], either in equimolecular amounts or with a 10-fold excess of cyclohexene, resulted in 1,2-bis-acetamidation of the alkene. The product obtained was the previously known *trans*-1,2-bis-acetamidocyclohexane[13], which was obtained in 28% yield.

Other alkenes reacted in a different way. The reaction between **1** and 2,3-dimethyl-2-butene (**7**) afforded two types of addition products, each in 23% yield (Scheme 2), that is amides **8** and **9**. Amide **8** was the outcome of a Ritter reaction since the same compound was obtained in an independent reaction[14] between **7** and triflic acid in wet acetonitrile.

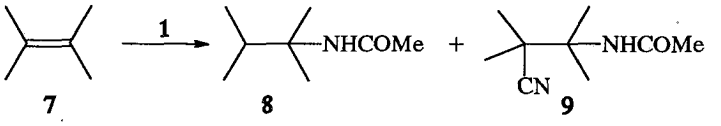

Scheme 2

Amide **9** had the cyano group from **1** added to the vicinal carbon, instead of a proton. It is likely that **9** was formed according to the sequence of events depicted in Scheme 3

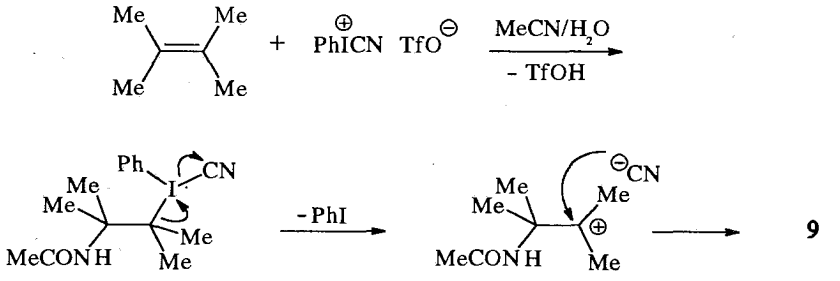

Scheme 3

The major product **12** from the reaction between **1** and 2,4,4-trimethyl-2-pentene (**10**) was of a still different type (Scheme 4). Indeed, **12** may be regarded as an elimination product resulting from an initial carbocationic intermediate analogous to **6** which loses HCN. Two other products were **11**, from a Ritter reaction, and **13**, clearly derived from a complex sequence of events. The identification of these products was based solely on spectroscopic evidence.

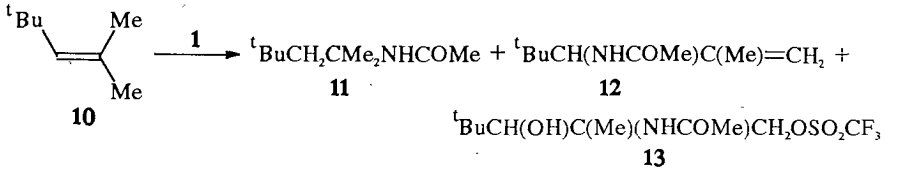

Scheme 4

Finally, when 1,1-diphenylethylene was reacted with **1** the known[15] rearranged product, $PhCOCH_2Ph$ was formed in 70% yield. Since other iodanes have shown the same reactivity, it is likely that **1** may be not specific also for the above mentioned additions, with the exception of the addition leading to the cyanated product **9**.

Experimental

Melting points were determined on a Kofler hot-stage apparatus. IR spectra were recorded with a Perkin-Elmer 297 spectrometer. ^{1}H-NMR and ^{13}C-NMR spectra, reported in δ units, were obtained with a Brucker AM 300 (at 300 and 75.4 MHz respectively) instrument. All NMR spectra were obtained by using TMS as internal standard in $CDCl_3$ or $CDCl_3$+DMSO-d_6 solutions. E.I. mass spectra were obtained at 7o eV with a VG TS-250 spectrometer. Elemental analyses were carried out with a C, H, N Perkin-Elmer 240-B analyser. Column chromatography was carried out on silica gel (Merck 60; 0.063-0.2 mm) eluted with solvent mixtures given in each appropriate experiment.

Reaction of 1 with 2,3-dimethyl-1,4-butadiene. To a stirred suspension of iodonium salt **1** (379 mg, 1 mmol) in commercial acetonitrile (20 ml) , at -15 ° C, was added , under argon, a solution of diene **2** (82 mg, 1 mmol) in acetonitrile (20 ml). After stirring at room temperature for 48 h, the solvent was removed in a rotary evaporator and the residue was chromatographed on a silica gel column, using as eluant hexane-ethyl acetate-methanol (2:2:1). The first eluate was iodobenzene and then followed:

(a) *Z-N,N'-bis-acetyl-2,3-dimethyl-2-butene-1,4-diamine* (**3**) (22 mg, 11%), mp 169-171 °C (chloroform-hexane); ν_{max}(Nujol) 3265, 3065, 1620, 1535, 1280 cm^{-1}; δ_H ($CDCl_3$-DMSO-d_6) 7.89 (2H, unresolved t, NH), 3.79 (4H, d, *J* 5.5 Hz, CH_2) , 1.92 (6H, s, CH_3), 1.65 (6H, s, CH_3); δ_C 169.5 (CO), 127.9 (C=C), 40.6 (CH_2), 22.0 ($COCH_3$), 16.5 (=CCH_3); *m/z* 199 (*M*+1, 22), 139 (90), 97 (86), 96 (100), 82 (60).

(b) A mixture of **3** and **4** (66mg, 35%), in a ratio (by ^{1}H NMR) *ca.* 1:2 and

(c) E-*N,N'-bis-acetyl-2,3-dimethyl-2-butene-1,4-diamine*, **4** (53 mg, 25%), mp 226-227 °C (acetonitrile). Found: C, 60.29; H, 8.98; N, 14.00. $C_{10}H_{18}N_2O_2$ requires C, 60.58; H, 9.15; N, 14.13; ν_{max}(Nujol) 3260, 3070, 1625, 1545, 1285 cm^{-1}; δ_H ($CDCl_3$-DMSO-d_6) 7.85 (2H, unresolved t, NH), 3.67 (4H, d, *J* 5.6 Hz, CH_2), 1.82 (6H, s, CH_3), 1.66 (6H, s, CH_3); δ_C 170.3 (CO), 129.4 (C=C), 42.3 (t, *J* 138 Hz, CH_2), 23.6 (q, *J* 127 Hz, $COCH_3$), 17.4 (q, *J* 126 Hz, $=CCH_3$); *m/z* 199 (*M*+1, 46), 198 (*M*, 4), 140 (52), 139 (65), 98 (51), 97 (62), 82 (100).

Crystal Data for **4**. $C_{10}H_{18}N_2O_2$; triclinic; space group P1; a= 7.52(1), b= 4.85(1), c= 9.63 (2) A; α= 92.63(7)°, β= 112.39(6)°, γ= 113.42(6)°; V= 289.4(9) A^3; Z= 1; D_C= 1.138 $g.cm^{-3}$; μ= 0.080 mm^{-1}; 1019 unique reflections (0- 2θ- 50°) were collected on a Crystal Logic Dual Goniometer diffractometre using graphite monochromated MoK_α radiation; 1019 reflections were used in the structure refinement. The structure was solved by direct methods using SHELXS-86[17] and refined by full-matrix least-squares techniques on F^2 with SHELXL-93[17]. The hydrogen atoms of the methyl groups were introduced at calculated positions as riding on bonded atoms; the rest were located by difference maps and refined isotropically. All non-H atoms were refined anisotropically. All computations for the structure refinement were carried out on a VAX station 3100. Final refinements converged to $R(R_w)$= 0.1201(0.2811), S= 1.023 for I 2σ(I).

Reaction of 1 with 2,3-dimethyl-2-butene (7). Under the same experimental conditions as above, using 758 mg (2 mmol) of **1** and 760 mg (9 mmol) of **7** were obtained, after two chromatographic separations, eluted with mixtures of methylenchloride-methanol 16:1 and n-hexane-ethyl acetate 5:6 respectively, the known compound **8** (mp 63-64 °C, lit[13] mp 65-66 °C), and *3-Acetamido-2,2,3-trimethylbutyronitrile (9)* (77 mg, 23%), mp 172-174 °C (methylene chloride-hexane); Found: C, 64.11; H, 9.41; N, 16.41. $C_9H_{16}N_2O$ requires C, 64.25; H, 9.59; N, 16.65; ν_{max}(Nujol) 3260, 2220, 1650 cm^{-1}; δ_H ($CDCl_3$) 5.43 (1H, s, NH), 1.99 (3H, s, $COCH_3$), 1.52 (6H, s), 1.41 (6H, s); δ_C ($CDCl_3$) 169.9 (CO), 124.1 (CN), 57.8 (HNC), 42.8 (C-CN), 24.9, 23.1, 22.8 (2-CH_3, 3-CH_3 and $COCH_3$); *m/z* 169 (*M*+1, 25), 111 (57), 100 (100), 58 (99).

Reaction of 1 with 2,4,4-trimethyl-2-pentene. Under the same experimental conditions as above (112 mg, 1 mmol of alkene and 379 mg, 1 mmol of **1**) the following products were obtained, after chromatographic separation (n-hexane-ethyl acetate-methanol as eluant):

(a) *N-(1,1,3,3-tetramethyl)butyl-acetamide* ***(11)*** (17 mg, 10%), mp 90-92 °C (lit[15] mp 92-94 °C).

(b) *N-(1-*tert*-Butyl-2-methyl)-2-propenyl-acetamide* ***(12)*** (29 mg, 17%) as an oil; δ_H ($CDCl_3$) 5.65 (1H, bs, NH), 4.97 (1H, m) and 4.84-4.82 (1H, m, $=CH_2$), 4.23 (1H, d, *J* 9.6 Hz, CH), 2.01 (3H, s, $COCH_3$), 1.78 (3H, dd, *J* 1.5 and 1.0 Hz, CH_3), 0.95 (9H, s, $C(CH_3)_3$); δ_C ($CDCl_3$) 169.2 (CO) 143.7 (CHC=), 114.4 ($=CH_2$), 62.1 (CHN), 34.4 (Me_3C), 27.1 ($(CH_3)_3C$), 23.6, 22.2 ($=CCH_3$ and $COCH_3$).

(c) *(2-Acetamido-3-hydroxy-2,4,4-trimethyl)pentyl-trifluoromethyl-sulfonate* ***(13)*** (23 mg, 7%) as an oil; δ_H ($CDCl_3$) 6.25 (bs), 5.61 (bs), 4.25 and 4.18 (2H, two ABd, *J* 12.4 Hz, CH_2), 4.08 (s, 1H, CH), 2.11 (3H, s, $COCH_3$), 1.72 (3H, s, CH_3), 1.15 (9H, s, $C(CH_3)_3$); δ_C ($CDCl_3$) 169.3 (q, *J* 7 Hz, CO), 120 (q, *J* 318 Hz, CF_3), 79.1 (HNC), 77.9 (d, *J* 150 Hz, CHOH), 55.2 (t, *J* 153 Hz, CH_2OSO_2), 33.2 (Me_3C), 25.7 (q, J 125 Hz, $(CH_3)C$), 23.9 (q, J 133 Hz, CH_3CNH), 21.4 (q, 130 Hz, $COCH_3$).

Περίληψη

Η αντίδραση του 2,3-διμεθυλο-1,3-βουταδιενίου με τον κυανο φαινυλοϊωδωνιακό τριφθορομεθανοσουλφονικό εστέρα ($PhI^+CN\ CF_3SO_3^-$) σε έφυγρο ακετονιτρίλιο οδηγεί στο σχηματισμό ενός μίγματος των *E*- και *Z*-1,4-ακεταμιδο-2,3-διμεθυλο-2-βουτενίων. Διακεταμιδίωση του διπλού δεσμού παρετηρήθη επίσης με απλούστερα αλκένια, όπως το κυκλοεξένιο, ενώ από τα αλκένια 2,3-διμεθυλο-2-βουτένιο και 2,4,4-τριμεθυλο-2-πεντένιο ελήφθησαν αντίστοιχα τα μη αναμενόμενα προϊόντα **8** και **9** και **11**, **12** και **13**.

References

1. Varvoglis, A.: *Hypervalent Iodine in Organic Synthesis*, Academic Press, London (1997).
2. Varvoglis, A.: *The Chemistry of Polycoordinated Iodine,* VCH Publishers, New York (1992).
3. Varvoglis, A.: *Tetrahedron* **53**, 1179 (1997).
4. Stang, P. J. and Zhdankin, V. V.: *J. Am. Chem. Soc.* **113**, 4571 (1991).
5. Hinkle, R. J., Poulter, G. T and Stang, P. J.: *J. Am. Chem. Soc.* **115**, 11626 (1993).
6. Stang, P. J., and Ullmann, J.: *Ang. Chem., Int. Ed. Engl.* **30**, 1469 (1991).
7. Zhdankin, V. V., Scheuller, M. C. and Stang, P. J.: *Tetrahedron Lett.* **34**, 6853 (1993).
8. Hinkle, R. J. and Stang, P. J.: *Synthesis* 313 (1994).
9. Stang, P. J. and Ullmann, J.: *Synthesis* 1073 (1991).
10. Zhdankin, V. V., Kuehl, C J., Krasutsky, A .P., Bolz, J. T., Mismash, B., Woodward, J. K. and Simonsen, A. J.: *Tetrahedron Lett.* **36**, 7975 (1995).
11. Griffiths, G. J. and Previdoli, F. E.: *J. Org. Chem.* **58**, 6129 (1993).
12. S. Nikas, Ph. D. Thesis, University of Thessaloniki, 1966.
13. Süess, H. and Hesse, M.: *Helv. Chim. Acta* **62**, 1040 (1979).
14. Oh, S. H., Tamura, K. and Sato, T.: *Tetrahedron* **48**, 9687 (1992).
15. Spyroudis, S. and Varvoglis, A.: *Chimica Chronica, New Series* **12**, 37 (1983).
16. Nagabhuhushanam, K. and Swaminathan, S.: *Org. Mass Spectrometry* **22**, 43 (1987).
17. Sheldrick, G. M.: SHELXS-86: Structure Solving Program, University of Göttingen, Germany (1986).
18. Sheldrick, G. M.: SHELXL-93: Crystal Structure Refinement, University of Göttingen, Germany (1993).

Chimika Chronika, New Series, 26, 545-564 (1997)

Binary and Ternary Complexes of L-Arginine with Lead(II), Indium(III) and cadmium(II). A differential Pulse Polarographic Study

Hussein M. El-Sagher

South Valley university, Faculty of Science, Chemistry Department , Sohag, EGYPT

(Received: September 30, 1996 In final form: March 23, 1998)

Abstract- Differential pulse polarographic study of indium(III)-L-arginine and lead(II)-L-arginine, -glycine and -L-arginine-glycine; was carried out in aqueous 0.10 mol.l^{-1} sodium perchlorate at pH 4.2 and 8.0, respectively. The cadmium (II)-L-arginine system was studied as well under the same conditions at pH 9.2. The overall stability constants and the composition of the formed complexes were calculated with the aid of POLAG-computer programme. It was evident that the reduction of lead(II), cadmium(II), indium(III) and their complexes proceeds via reversible and diffusion-controlled two electrons (three electrons for indium) waves. The results show that lead(II) forms a binary complexes with both L-arginine and glycine and the Pb(II)-L-arginine-glycine ternary complex was also formed. For cadmium(II) it was revealed that at pH 9.2 L-arginine acts as a mixture of two ligands [ArgO.H_2] and [ArgO.H], and a ternary complex was formed. The structures of the detected complexes were discussed on the basis of the dentate sites of the studied ligands.

Key words: Voltammetry, complex, stability, cadmium (II), lead(II), indium(III), arginine, glycine, ternary.

Introduction

The metal complex of L-arginine is of special interest, because it contains a functional group of considerable proton affinity and metal binding properties[1], separated from the chelate ring by three carbon atoms. It is of interest to determine the influence of this structure both in

the protonated and unprotonated forms on the stability of the metal chelate rings involving the α-amino moiety, when the remote group is coordinated or not, to the metal ion.

The metal complexes of L-arginine have been the subjects of several investigations.[2-7] Polargraphic measurements have been employed by Li and Doody[2] to determine the chelate formation constants of the copper(II)-arginine complexes. Goncaves and co-workers have been studied the formation of complexes of Cd(II) and Pb(II) with some natural amino acids.[8-10] Differential pulse polarography has been used to investigate the complex formation of Cd(II) and Zn(II) with L-arginine and vitamin B-6 ligands.[11] Yamauchi and Odani have been collected and critically evaluated the stability constants of the proton and metal complexes of basic α-amino acids(arginine, lysine and ornithine).[12]

Recently, arginine gains a special interest because of its importance to determine the structure of RNA-amino acid arginine-rich peptide complex. The structure demonstrates wayes in which proteins can recognize the major groove of RNA[13]. The binding structure of bis-arginine complexes of copper(II) on highly oriented DNA fibers have been investigated by ESR spectroscopy.[14] Arginine has been used to study the structure and mobility of the complex formed by sodium dodecyl sulfat and gelatin. [15]

The formation constants of L-arginine chelates of some biologically interesting metal ions by various techniques have been reported.[16,17] The stability constants reported by Pettite[17] have been determined from potentiometric titrations. However, quantitative results on the nature and stability of the protonated forms of the metal chelates

of L-arginine at a certain pH's for Cd(II), have not yet been reported in the literature.

As part of a general programme on complex formation between metals and amino acids, this investigation is oriented towards establishing the nature and stability constants of binary and ternary complexes of arginine with lead(II), cadmium(II) and indium(III). The overall stability constants and composition of the complexes investigated have been determined in the non- complexing medium 0.10 $mol.l^{-1}$ sodium perchlorate using differential pulse polarography with the aid of POLAG-computer programme[18].

EXPERIMENTAL

Lead nitrate, cadmium nitrate, indium nitrate and sodium perchlorate were of AR BDH or Merk grade, while L-arginine and glycine were of AR Aldrich grade. Fresh 0.10 $mol.l^{-1}$ $NaClO_4$/ aqueous stock solution was prepared by dissolving sodium perchlorate in carbon dioxide-free bidistilled water. Fresh L-arginine and L-glycine (2.00 $mol.l^{-1}$) were prepared from fresh electrolyte (0.10 $mol.l^{-1}$) in the same day that measurements were taken. The stock standard solutions of cadmium, indium and lead were prepared from their nitrate salts.

Cyclic and differential pulse polarogramms were obtained with the use of the conventional three electrodes cell configuration. An EG & G PAR model SMDE 303A mercury-drop system in the small hanging drop mode was used as working electrode in cyclic voltammetry, while, dropping mercury electrode was used in the defferential pluse polarography. An $Ag/AgNO_3$ (0.10 $mol.l^{-1}$) electrode in 0.10 $mol.l^{-1}$ $NaClO_4$ aqueous solution was utilized as reference electrode. A

platinum wire (1.0 cm^2) was used as auxiliary electrode throughout. All experiments were done at 25°C and the ionic strength was maintained at 0.1 $mol.l^{-1}$ $NaClO_4$. Solutions were purged with pure nitrogen before running the experiment and an atmosphere of nitrogen was maintained above the working solution. The mercury-drop system was equipped with an EG & G PAR model 173 potentiostat / Galvanostat and PAR model 175 universal programer function generator. The electrochemical system was interfaced with Amstrad PC 1640D computer with a mathematical Co-processor. The data were captured, stored and manipulated. In all experiments 500 data points were routinely captured, equally spaced in time. Background data were also stored and were substracted from the experimental data set, minimizing effects such as double-layer charging currents.

METHOD

It has been noted earlier that the most common method of "evaluating" stability constants of binary metal- ligand complexes from polarographic data uses the approach developed by DeFord and Hume[19,20] . The starting equations are:

$$mM + nL \rightarrow M_mL_n \qquad n = 1, 2, ...N \quad m = 1, 2 \qquad (1)$$

$$mM + nL + PL' \rightarrow M_m L_n L'_p ; \quad m, n, p = 0, 1, 2, \ , N (P) \qquad (2)$$

$$F = \exp[nF/ RT(E_{1/2(s)} - E_{1/2(c)})] + \ln (i_{ds} / i_{dc}) \qquad (3)$$

$$F = 1 + C_L \beta_1 + C^2_L \beta_2 + C_L{}^n \beta_N \qquad (4)$$

where the subscripts s and c refer to the uncomplexed and complexed metal ions, respectively. $E_{1/2}$ is the half wave- potential ; i_d is the

diffusion current; C_L is the analytical concentration of the ligand and β_N is the overall stability constant of the Nth complex. For ternary complexes (equilibrium 2) the method of Schaap and McMasters[21,22] is applied directly or with modification[23]. The technique is based on the assumption that $C_L >> C_M$, where C_L is the analytical concentration of the second ligand. The exact form of eqn.(4) is :

$$F = 1 + [L]\beta_1 + [L]^2\beta_2 + [L]^n\beta_N \quad (5)$$

which is derived from :

$$F = C_M / [L] \quad (6)$$

The major problem inherent in the use of the dc polarography are the difficulty in measuring the correct values of the polarographic current and half-wave potentials. It was demonstrated that these problems are to a great extent solved by using the differential pulse polarography[24]. It has been demonstrated earlier that for reversible differential pulse polarographic data, POLAG computer programme[18] is used to calculate reliable estimation of composition and overall stability constants β_N for binary and ternary complexes. POLAG is a non-linear least squares iterative programme that seeks to minimize U, the sum of squares of residuals, i.e.

$$U = \sum_{i}^{j} (F_{calc.} - F_{obs})^2 \quad (7)$$

where j is the number of data points, F_{obs} is given by eqn(3) and represents the experimental data, F_{calc} is obtained from eqn(5). Thus for given values of β_{mnp}, [M], [L] and [L'], F_{calc} depends on the particular combination of m, n and p and the values of β_{mnp}. Therefore, various equilibrium models may be fitted to the polarographic data simply by

changing the input data values of m, n and p together with approximate initial values of β_{mnp}.

RESULTS AND DISCUSSION

Examination of cyclic voltammograms of the metal ions (lead(II), cadmium(II) and indium(III)) complexes of the subject amino acids indicate that the uncomplexed Pb(II), Cd(II) and In(III) ions are reduced at E_{pc} = -0.385, -0.585, and -0.510 V vs Ag/Ag^{+}, respectively. The

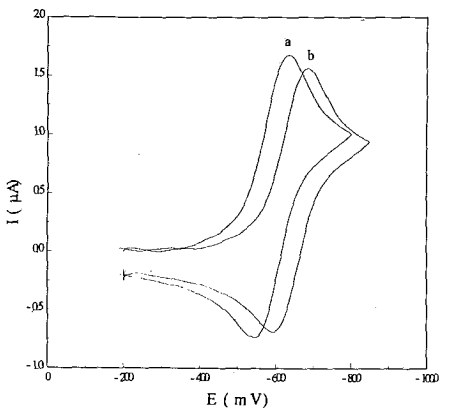

Fig. (1): Cyclic voltammograms of
a) 5 x 10^{-} mol. l^{-1} Cd (II).
b) a + 2 x 10^{-2} mol. l^{-1} arginine

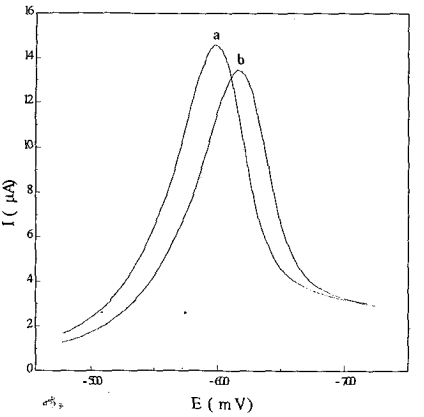

Fig. (2): Differential pulse voltammograms of
a) 5 x 10^{-4} mol. l^{-1}Cd (II).
b) a + 2 x 10^{-2} mol. l^{-1} arginine.

addition of the ligand (arginine or glycine)at the desired pH shifts the CV wave and the differential pluse polarographic peak to more negative potentials and the cathodic peak current decreases relative to that of the labile ion as shown in figures 1 and 2, respectively (as representative examples of the investigated systems). This is an indication of complex formation. All the systems presented here show reversible diffusion-

controlled reduction (the width of the peak half hight almost equal to 96/n mv).

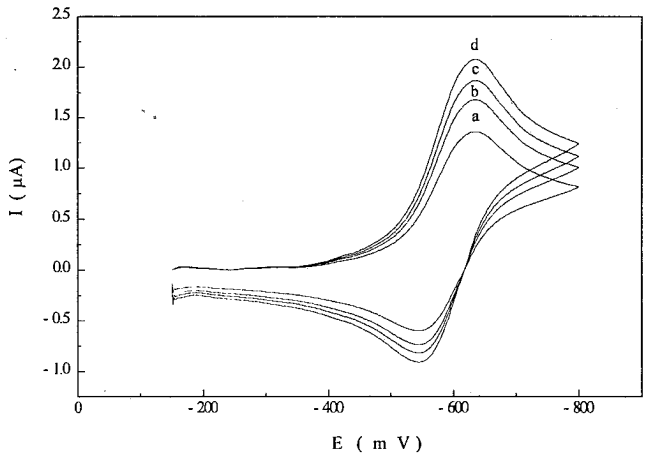

Fig. (3): Cyclic voltammograms of Cd(II)-arginine at different scan rates a) 0.05, b) 0.1, C) 0.2 and d) 0.5 mVs^{-1}.

The cyclic voltammograms show reversible reduction waves of n electrons (n=2 for Pb(II) and Cd(II) and n=3 for In(III)). Figure 3 shows that the anodic and the cathodic peak current potentials, E^a_p and E^c_p are independent on the scan rate used (20-1000 mv/sec.). E^a_p-E^c_p and E_p-$E_{p/2}$ are of 59.1/n±2 mV and 56.5/n±1 mV , respectively and the anodic to cathodic peak current ratio, i^a_p/ i^c_p, approches unity[25]. The overall stability constants β_N and the composition of the complexes are evaluated using the differential pulse polarographic data as input for the POLAG Programme. To calculate the overall stability constants of the systems under consideration, all the reasonable stoichiometries (species) between the metal ion and the ligand, taking into account the coordination number of the metal and whether the ligand is mono, di or terdentate, as well as, all the mathematical combinations of these species

as input sets were examined making use of the programme. Many of these sets were rejected when the statistical output (σ_{DATA}, the standard deviation of fit and U the sum of squares of residuals) are large or when constants have large standard deviation of, $\sigma(\log \beta)$. Furthermore, the effect of variation in the value of protonation, hydrolysis on the chosen binary and ternary models were examined.

I) Binary systems

a) Lead(II) - L-arginine

It is well known that L-arginine, abbreviated $Arg^{+}O^{-}$, is potentially tridentate ligand with three ligating sites. The carboxyl group, -COOH, ($H_2Arg \rightleftharpoons H_2ArgO$, $pK_{a1} = 6.1$), the protonated amino nitrogen group, $-N^{+}H_3$, ($H_2ArgO \rightleftharpoons HArgO$, $pK_{a2} = 9.36$) and the guanidinium group, $-NHC(=N^{+}H_2)NH_2$, ($HArgO \rightleftharpoons ArgO$, $pK_{a3} = 11.5$)[1] are available for complexation. However, in solutions of pH > 11.5, three species for arginine are considered to be the possible ligands for chelation. They are H_2ArgO, HArgO and ArgO. The Lead(II)-L-arginine chelates are studied at pH 8.0 by DPP and the voltammetric data are depicted in Table 1. At pH 8.0 L-arginine behaves as monodentate and the predominant species at the given pH is $[H_2ArgO]$. The equilibrium concentrations of this species and the others if present are evaluated from the knowledge of the analytical concentration of L-arginine, C_{arg}, pK_{a2} and pK_{a3} values utilizing the following relations.[26]

$$[H_2ArgO] = \frac{[H]^2}{K_{a2}K_{a3} + K_{a2}[H] + [H]^2} \times C_{arg} \qquad (8)$$

$$[\text{HArgO}] = \frac{K_{a2}[H]^2}{K_{a2}K_{a3} + K_{a2}[H] + [H]^2} \times C_{arg} \quad (9)$$

$$[ArgO] = \frac{K_{a2}K_{a3}}{K_{a2}K_{a3} + K_{a2}[H] + [H]^2} \times C_{arg} \quad (10)$$

Table (1): Voltammetric data for Pb(II)-L-arginine system, $[Pb^{2+}]$ = $1x10^{-4}$ mol.l^{-1}, at I = 0.10 mol.l^{-1} $NaClO_4$, 25°C and pH = 8.00.

C_{arg} (m mol)	$[H_2ArgO]$ (m mol)	[HArgO] (m mol)	[ArgO.] (m mol)	$-E_p$ (mv)	I_p (μA)
50	48	1.80	0.00	460	21.00
100	96	3.60	0.01	475	22.00
150	144	5.80	0.02	480	21.50
200	192	7.60	0.03	485	24.50
300	240	11.20	0.04	495	23.50
450	288	16.60	0.06	500	22.50

Table 2 comprises some of the proposed models. It seems that some of the two species models are not accepted and execution terminated. Models C and D are rejected due to high values of σ log β. Of the single species models converged, model A, matches well the formed complex between lead(II) and the diprotonated arginine $[H_2ArgO]$. The diprotonated arginine $[H_2ArgO]$ acts as a monodentate ligand, in which the α–amino and quanidinium groups still protonated, ligating lead(II) through the carboxylate group. Accordingly one can expect that the proposed formula of the complex would be $[Pb(H_2ArgO)]$.

Table (2): Overall stability constants of Pb-L-arginine binary complexes at I = 0.10 mol.l^{-1} $NaClO_4$, 25°C and pH = 8.00. p = [H_2ArgO], q = Pb(II) and r = OH.

Model	Pqr	Log β(σ)	10^3 σ_{DATA}	10^5 U
A	110	4.15(0.06)	4.30	9.40
B	210	4.85(0.13)	4.30	4.36
C	01-1 210	5.24(0.15) 4.62(0.09)	4.28	7.32
D	110 210	3.99(0.12) 4.24(0.03)	3.79	5.74

b) **Lead(II)-glycine**

The formation of a complex between lead(II) and -glycine is studied at pH 8.0 using DPP. The system is shown to be a reversible two electrons reduction. It is well known that glycinate functions as a bidentate NO ligand; Five-membered metal chelates are assumed to be formed.

The statistically accepted models are depicted in Table 3. It can be seen that the formation of more than one species is rejected (models D and E). Only binary species of the type $[PbL_n]$ and $[PbL_{(n-1)}OH_j]$, where n=1, 2 and j=1, 2 can be formed, however, the best model to represent the formation of a complex between lead(II) and glycine is C.

Table (3): Overall stability constants of Pb-L-glycine binary complexes at I = 0.10 mol.l^{-1} $NaClO_4$, 25°C and pH = 8.00.

p = g;ly., q = Pb(II) and r = OH.

Model	Pqr	Log β(σ)	10^3 σ_{DATA}	10^5 U
A	210	4.88(0.04)	2.70	3.70
B	211	3.12(0.04)	2.70	3.70
C	212	11.12(0.04)	2.20	1.98
D	210 310	4.55(0.24) 4.79(0.06)	2.20	1.98
E	211 310	3.21(0.06) 4.55(0.24)	2.20	1.98

It is worth while to compare the binary complexes of lead(II) with L-arginine and glycine. It is revealed that lead forms more stable complex with glycine (logβ= 11.12±0.04) than with L-arginine (logβ = 4.15±0.06). Because of the presence and protonation of the strongly basic guanidinium group, L-arginine can function as a Zwetterionic species.[1, 2, 5] The lower stability constant obtained for lead complex formation with L-arginine is attributed to the inductive effect of guanidinium group.

c) **Indium(III) -L-arginine**

Indium complexes of L-arginine are studied by DPP at pH 4.2 in the non-complexing medium 0.10 mol.l^{-1} $NaClO_4$. The statistical data and the overall stability constants of the system are represented in Table 4.

Table (4): Overall stability constants of In-L-arginine binary complexes at I = 0.10 mol.l^{-1} $NaClO_4$, 25°C and pH = 4.20.
p = [H_2ArgO], q = In(III) and r = OH.

Model	Pqr	Log β(σ)	10^3 σ_{DATA}	10^5 U
A	01-1	2.01(0.41)	17.00	126.00
B	01-2	6.38(0.49)	21.55	185.00
C	110	2.92(0.27)	11.96	57.23
D	210	3.66(0.18)	7.70	24.02
E	310	2.64(0.31)	24.11	197.00

Of the different models proposed (Table 4), the only acceptable model is D from the statistical point of view on one hand and on the other hand since arginine at such a lower pH value (< 9.5) will form the diprotonated species [H_2ArgO], the α–amino and the guanidinium groups still protonated. If so, the only center available for complexation might be the carboxylate group. Model E is rejected not only for statistical outputs, but for the bigger molecule of arginine that hinders the formation of this species. It is found that models with more than single species as well as the hydroxo species are not converged.

II- TERNARY SYSTEMS

a) Lead(II)-L-arginine-glycine system

As just stated above that lead(II) forms binary complexes with both L-arginine and glycine of varying stability constants. The lead(II)-l-arginine-glycine ternary system is investigated. This is done by varying the concentration of glycine, gly., while the concentration of arginine and

leadI(II) is kept constant at their analytical concentration. The DPP technique is used to study the system. The peak potentials are shifted to more negative upon addition of glycine (c.f. Table 5). This indicates the formation of ternary complexes. The overall stability constants are determined by POLAG computer programme.

Table (5): Voltammetric data for Pb(II)-L-arginine-glycine ternary system, $[Pb^{2+}] = 1x10^{-4}$ mol.l^{-1}, at I = 0.10 mol.l^{-1} $NaClO_4$, 25°C and pH = 8.00.

$[H_2ArgO]$ (m mol)*	[Gly.] (m mol)	$-E_p$ (mv)	I_p (μA)
	0.00	475	28.00
	100	488	27.00
	200	500	27.50
	300	510	28.00
	400	515	29.00
	500	520	28.00
	700	528	27.50
	900	535	29.00

* L-arginine is representated as $[H_2ArgO]$ and its fixed concentration at 28.8 m mol is calcuulated from eqn.(9).

Table 6 comprises the most acceptable models, however, all single species models are rejected because of high σ_{DATA} values. An inclusion of a second species has improved the value of σ_{DATA} as well as the standard deviation of logβ. Model K is presumably the most likely one to be considered with respect to all the statistical values. It is clear that lead-

l-argininate-glycinate ternary complex $[Pb(H_2ArgO)(Gly.)(OH)_2]$ is present together with lead-glycinate binary complex $[Pb(gly.)(OH)_2]$, as the two species have perfectly close overall stability constants of 11.69±0.08 and 12.37±0.02, respectively.

Table(6): overall stability constants of Pb(II)-L-arginine-glycine ternary complexes at I = 0.10 $mol.l^{-1}$ $NaClO_4$, 25°C and pH = 8.00.
p = $[H_2ArgO]$, q = Gly., r = Pb(II) and s = OH

Model	Pqrs	Log β(σ)	10^3 σ_{DATA}	10^5 U
A	1110	4.93(0.07)	5.39	14.50
B	111-1	3.05(0.08)	5.39	14.50
C	111-2	11.05(0.06)	5.39	14.50
D	111-1 0210	3.69(0.06) 3.63(0.03)	0.69	0.19
E	111-1 0310	3.30(0.03) 3.62(0.07)	1.20	0.56
F	111-1 021-1	3.69(0.08) 3.37(0.08)	0.69	0.19
G	111-1	3.39(0.08)	0.69	0.19
H	111-2 0210	11.69(0.08) 3.63(0.03)	0.69	0.19
I	111-2 0310	11.30(0.04) 3.62(0.05)	1.20	0.58
J	111-2 021-1	11.69(0.08) 4.37(0.03)	0.69	0.19
K	111-2 021-2	11.69(0.08) 12.37(0.03)	0.69	0.19

b) **Cadmium(II)-L-arginine ternary system**

The structure of L-arginine, $Arg^{+}O^{-}$, is written $H_2N\text{-}C(=N^{+}H_2)\text{-}NH\text{-}(CH_2)_3\text{-}CH(NH_2)COO^{-}$[27]. Potentiometric titration of arginine indicates that a stepwise dissociation reaction takes place[1]. It is found that dissociation of the proton from the α–amino group (-$CH(NH_2)$-COOH) takes place prior to the dissociation of the proton from the terminal basic group (-$NHC(=N^{+}H_2)NH_2$). Consequently, arginine is potentially terdentate if the terminal group takes part in chelation. However, it is found that arginine function as bidentate ligand for metal chelates, in which the ligating sites are the carboxylate and the α–amino groups. In solutions of lower pH's (< 9.2), the species (H_2ArgO) reasonably exists and acts as monodentate ligand through the carboxylate group. In the pH range 9.2 up to < 11.0 the carboxylate and α-amino groups become available for chelation and the predominant species [HArgO], which acts as bidentate ligand, will be present together with the monodentate species [H_2ArgO].

The cadmium(II)-L-arginine system is studied at pH 9.2 by DPP. The equilibrium concentrations of the species [H_2ArgO], [HArgO] and [ArgO.] are evaluated following the same procedure described above (c.f. Pb(II)-arginine system) from eqns (8) , (9) and (10) . The studies are performed at pH = 9.2, at constant concentration of Cd (II) by varying the analytical concentration of arginine, $C_{arg.}$, so that [H_2ArgO] and [HArgO.] vary considerably with C_{arg} . The voltammetric data of the subject system are summarized in Table 7. Examination of these data reveals that at such conditions the [H_2ArgO] and [HArgO] species are of considerable concentrations and are the most likely ligands to be present. It is also clear that the concentration of [ArgO.] species is too small to

be neglected. Again this confirms that L-arginine in such medium can not behave as a terdentate ligand. Thus, the Cd (II)-L-arginine system has to be examined as a mixed ligand complex.

Table (7): Voltammetric data for Cd(II)-L-arginine system, $[Cd^{2+}]$ = $5x10^{-4}$ mol.l^{-1} , at I = 0.10 mol.l^{-1} $NaClO_4$, 25°C and pH = 9.20.

C_{arg} (m mol)	$[H_2ArgO]$ (m mol)	[HArgO] (m mol)	[ArgO.] (m mol)	$-E_p$ (mv)	I_p (μA)
50	29.50	20.30	0.02	660	11.50
100	59.00	40.70	0.03	690	14.50
150	86.00	61.10	0.05	705	16.00
200	118.00	81.60	0.07	715	16.50
250	148.00	102.00	0.09	718	17.50
300	177.00	122.30	0.10	725	18.00
350	207.00	142.70	0.12	728	18.00
400	236.00	163.10	0.14	732	22.00

The calculation of the overall stability constants and the composition of such a unique ternary system are achieved with the aid of POLAG- computer programme. The results are collected in Table 8. From these results, it may be concluded that, the choices are correct with errors in the values of overall stability constants within the standard deviation. Examination of these results in Table 8 reveals that, when only one species *viz*, model A, is considered the best statistical fit give results of high statistical output. Considering model B increases significantly the standard deviation of log β with the same values of σ_{DATA}, and U as in model A.

Table(8): overall stability constants of Cd(II)-L-arginine ternary complexes at at I = 0.10 mol.l^{-1} $NaClO_4$, 25°C and pH = 9.20.
p = [H_2ArgO], q = [HArgO] , r = Cd(II) and s = OH

Model	Pqrs	Log β(σ)	10^3 σ_{DATA}	10^5 U
A	1110	7.71(0.04)	2.50	3.20
B	111-1	1.49(0.35)	2.50	3.20
C*	1110 111-1	-	-	-
D	111-2	10.69(0.04)	2.50	3.20
E*	1110	-	-	-

* Execution terminated.

Examination of the rest models in Table 8 indicates that the best model to represent this ternary system is D, which is statistically accepted in such experimental conditions. Two species models, C and E, were not converged and execution terminated. As already stated, L-arginine has two ligating sites, the carboxylate and the α-amino groups. The species [Cd(H_2ArgO)(HArgO)] implies that [H_2ArgO] may act as monodentate ligand with protonated α-amino and guanidinium groups and the ligating site presumably being the carboxylate groups. [HArgO] species may be bidentate ligand with protonated guanidinium group and offering the carboxylate and α-amino group as ligating sites for cadmium(II).

ΠΕΡΙΛΗΨΗ

ΔΙΑΔΙΚΑ ΚΑΙ ΤΡΙΑΔΙΚΑ ΤΕΤΡΑΣΘΕΝΗ ΣΥΜΠΛΟΚΑ L-ΑΡΓΙΝΙΝΗΣ ΜΕ ΜΟΛΥΒΔΟ (II) ΙΝΔΙΟ (II) ΚΑΙ ΚΑΔΜΙΟ (II). ΔΙΑΦΟΡΙΚΗ ΠΑΛΜΙΚΗ ΠΟΛΑΡΟΓΡΑΦΙΚΗ ΜΕΛΕΤΗ

Η διαφορική παλμική πολαρογραφική μελέτη της ινδιο (III)-L-αργινίνης, -γλυκίνης και -L-αργινίνης-γλυκίνης πραγματοποιήθηκε σε υδατικά διαλύματα υπερχλωριώδους νατρίτου 0,10 mol l^{-1} σε pH 4.2 και 8.0, αντιστοίχως. Το σύστημα της καδμιο (II)-L-αργινίνης μελετήθηκε, επίσης, υπό τις ίδιες συνθήκες σε pH 9.2. Οι συνολικές σταθερές σταθερότητας και η σύσταση των συμπλόκων που σχηματίσθηκαν υπολογίσθηκαν με τη βοήθεια προγράμματος POLAG. Ήταν προφανές ότι η αναγωγή του μολύβδου (II), καδμίου (II), ινδίου (III) και των συμπλόκων τους προχωρεί μέσω αντιστρεπτών και ελεγχόμενων από τη διάχυση κυμάτων δύο ηλεκτρονίων (τριών ηλεκτρονίων για το ίνδιο). Από τ' αποτελέσματα φαίνεται ότι ο μόλυβδος (II) σχηματίζει δυαδικά σύμπλοκα με την L-αργινίνη και γλυκίνη και ότι σχηματίσθηκε, επίσης, το τριαδικό σύμπλο Pb(II)-L-αργινίνη-γλυκίνη. Για το κάδμιο (II) βρέθηκε ότι σε pH 9.2 η L-αργινίνη λειτουργεί ως μίγμα δυο δεσμών συναρμογής [ArgO·H_2] και [ArgO·H] και σχηματίζεται τριαδικό σύμπλοκο. Οι δομές των συμπλόκων που ανιχνεύθηκαν συζητούνται επί τη βάση των μονοσχιδών θέσεων των δεσμών συναρμογής που μελετήθηκαν.

REFERENCES

1. E. R. Clark and A. E. Martell J. Inorg . Nucl. Chem. 1970 , **39**, 911.

2. N. C. Li and Doody, J. Am. Chem. Soc. 1952, **74**, 4184.

3. D. J. Perkins, J. Biol. Chem. 1953, **55**, 649.

4. S. P. Datta and A . K . Grzybowski, J. Chem . Soc . 1959, 1091.

5. C. Tanford and W. S. Shore , J . Am. Chem . Soc 1953, **75** , 816.

6. D. D. Perrin , J. Chem . Soc. 1958, 3125 ; 1959, 290.

7. S. Pelletier, Doct. Diss., Univ. of Paris 1960.

8. M. L. S. Simoes Goncalves and M.M. Correia Dos Stantos , J. Electroanal. Chem., 1984, **132**, 315.

9. M. L. S. Simoes Goncalves and M.M Correia Dos Stantos , J. Electroanal. Chem., 1985, **187**, 333.

10. M. M. Correia Dos Stantos and M. L. S. Simoes Goncalves, J. Electroanal. Chem., 1986, **137**, 208.

11. F. Khan, J. Indian Chem. Soc., 1997, **73**, 171.

12. O. Yamauchi and A. Odani, Pure& Applied Chemistry, 1996, **68**, 469.

13. D.D. Miller, W. Lenhart, B.J. Antalek, A.J. Williams and J.M. Hewitt, Langmuir, (1994), **10**, 68.

14. M. Chikira, M. Inoue, R.Nagane, W. Harada and H. Shindo, Journal of Inorganic Biochemistry, 1997, **66**, 131

15. J.D. Puglisi, L. Chen, S. Blanchard and A.D. Frankel, Science, 1995, **270**(5239), 1200.

16. M. Nair, Sivasankarani and M. Santappa, India J. Chem.,Sec. A., 1982, **21**(A), 58.

17. Gleann Brookers and Leslie D. Pettit , J.C.S Dalton, 1972, 42.

18. D. J. Leggett, Talanta, 1980, **27**, 787.

19. D.D. Defored and D.N. Hume, J. Am. Chem. Soc., 1951, **73**, 5321

20. D. N. Hume, D. D. Defored and G. C. B. Cave, J.Am. Chem. Soc., 1951, **73**, 532

21. D. L. McMasters and W. B. Schaap , Proc. Indian Acad. Sci., 1958, **67**, 11.

22. W. B. Schaap and D. L. McMasters , J. Am. Chem., 1961 , **83**, 4699.

23. K. Momoki, H. Ogawa and H. Sato, Anal. Chem., 1969, **41**, 1826.

24. J. I. Mayer and J. E . Banman , J. Am. Chem., 1970, **92** , 4210.

25. R. S.Nichlson and I. Shain, Anal. Chem., 1964, **36**, 706.

26. J. C. K. Placeres, M. T. S. Alacjos and F. J. G. Montelong, 1992, **39**, 649.

27. E. J. Cohn and L. T. Edsall, "Proteins, Amino Acids and Peptides," Reinhold publishing Corp., New York, N. Y. ,1943, PP. 103-104.

Chimika Chronika, New Series, 26, 565-596 (1997)

A NEW CHARACTERIZATION METHOD FOR SOLID CATALYSTS - COMPARISON WITH THE OLD ONES

F. Roubani-Kalantzopoulou*[a], A. Kalantzopoulos[a] and N. A. Katsanos[b]

[a] Department of Chemical Engineering, National Technical University, 157 80 Zografou, Athens, Greece

[b] Physical Chemistry Laboratory, University of Patras, 265 00 Patras, Greece

(Received: November 3, 1997 In final form: April 10, 1998)

An application of the Reversed-Flow Gas Chromatographic technique (RF-GC) for the characterization of catalysts, and the calculation of many physicochemical parameters pertaining to heterogeneous reactions, is proposed. A new relevant mathematical model is derived on the basis of a non-linear experimental adsorption isotherm. Experimental results are presented concerning the behaviour of four metal oxides, as catalysts for the reactions of olefin isomerization-polymerization and hydrogenation-dehydrogenation of hydrocarbons. One oxide has a *p*-type conductivity (Cr_2O_3), two are of a *n*-type (ZnO and Fe_2O_3), and one is an amphoteric conductor (PbO). A comparison is made of the proposed new method for the characterization of catalysts with the old ones, which have been based either on a linear adsorption model or on the well known and widely used adsorption isotherms of Langmuir and BET. The superiority of the new method with its many advantages is described.

Key words: Reversed-Flow, Catalyst characterization, Physicochemical parameters, Adsorption isotherms.

Introduction

A thorough understanding of the structural and mechanistic details of a catalyzed heterogeneous reaction leads, both directly and indirectly, to the development of new and better catalysts. One of the main objectives in the science of catalysis is the

study of the nature of adsorption and the number of active sites [1, 2]. Furthermore, dealing with ordinary supported metal catalysts, the estimation of the support surface uncovered by the active ingredients, as it is known, may be obtained by the difference between the total surface area, as measured usually by the BET method, and the metal surface area measured by chemisorption methods. This is done e.g. in supported metal oxide catalysts [3]. The number of cases where chemisorption measurements [4, 5] have been successfully applied to this end has increased in recent years, e.g., the hydrotreatment of petroleum feed stocks [6]. The most detailed investigations designed to study the interaction between the surface and chemisorbed probe molecules are the pioneer works of Garner and co-workers [7, 8] in England, who studied the rates and heats of adsorption, and the conductivity changes occuring with oxides as ZnO and Cr_2O_3. Other examples of selective surface area measurements in two-component oxide systems are provided by Voltz and Weller [9], and by Maclver and Tobin [10], who used the amount of oxygen to estimate the specific surface area of chromia in supported catalysts. More recently, much work upon chemisorption of different (CO_2, CO and NO) probes [11] on metal oxide catalysts, within the framework of the NO+CO removal from the exhaust gases of car engines, was done by the Ford Motor Co in U.S.A. The chemisorption of such molecules as pyridine, ammonia, hydrogen sulfide and boron trifluoride [12] is specific for certain types of adsorbents, this behaviour being generally related to the occurrence of specific surface sites (acidic or basic) which are present in a surface concentration that is not known. Data of this kind are useful for the identification and estimation of specific types of adsorption sites [13].

Standard methods for catalytic surface area determination formally exist for a few supported-metal catalysts. However, there is not a general acceptance of such methods for supported-metal oxides [3]. There are inherent difficulties in selecting any method as a standard for surface area measurements, since catalyst manufacturers throughout the world prepare their materials from different precursors and in different ways. These differences can cause marked variations in the procedure required to measure accurately the surface area of metal oxides. No

doubt, the chemisorption of suitable probe molecules is the method of choice for such purposes. It is also of great interest to combine the chemisorption measurements with appropriate surface spectroscopies or other techniques in order to determine precisely the stoichiometry between the probe and the surface sites. A remaining question is that of the proportionality between the surface area of the supported metal oxides and the number of sites responsible for a given reaction. The answer to this question is most often positive, but contrary examples exist in the literature. It is therefore obvious that one should not select a catalyst on the basis of an invalid test, and that other physicochemical quantities may be required to be measured for more correct results. Many empirical or semi-empirical equations have been found to be useful, but have limited applicability; the most important of these are the Langmuir, Freundlich, Frumkin-Temkin and the Brunauer-Emmett-Teller (BET) isotherm equations. The Langmuir model is sometimes a good approximation for adsorption on solids with nearly uniform surfaces, but it usually fails to provide an accurate representation when the adsorbent is an inorganic solid of the kinds used as catalysts [14-15]. The assumption of uniformity of the surface sites is invalid for metal oxides [15]. The nonuniformity of the surface sites is usually the major reason for the model's inadequacy. One adsorption isotherm is of great value in determining surface areas of catalysts, the BET isotherm [14, 16]. In contrast to the Langmuir isotherm, it accounts for multilayer adsorption and therefore gives a much better representation of physisorption than the Langmuir isotherm. Even the BET model, however, which is both well known and the most used one is catalytic works, is inexact and the surface areas determined by that are to some degree arbitrary.

The above raises the question of what mathematical formulations do a better job in representing experimental results. In the present paper an answer to this question is attempted, by the method of Reversed-Flow Gas Chromatography (RF-GC). Using this method, many phenomena relating to catalytic reactions have been succesfully studied [17-40]. However, all calculations so far were based on linear adsorption isotherms [33-35]. Now, a simple determination of direct experimental isotherms over a wide range of concentrations is possible [40], without

specifying *a priori* an isotherm equation. Incorporating this important development into the mathematical models, non-linear isotherms are automatically taken care of leading to the calculation of adsorption, desorption and surface reaction rate constants under the real experimental isotherm. In this work a valid and adequate model for both, the chemisorption of probe molecules and the specific surface area (SSA) studies of a new-catalyst is developed. After a proper modification of the RF-GC experimental set-up for obtaining conveniently better and realistic results from catalytic studies, one can quantitatively and accurately follow the surface reaction and the desorption of a reversibly adsorpted reactant, together with the local adsorption parameter pertaining to the isotherm. From this, the real experimental isotherm can be plotted directly without the need of an *a priori* isotherm equation, like the ones mentioned before.

Theoretical

The calculation of the physicochemical parameters adopting the linear model is based on the theoretical analysis already published [34-35] and includes the rate constants for adsorption (k_1), desorption (k_{-1}) and possible first-order surface reaction (k_2), the overall mass transfer coefficient of the gas to the solid surface (K_G), and the adsorption equilibrium constant (K). A brief description of this analysis is given here. By plotting the height H of the extra chromatographic peaks obtained by the reversal of the flow direction of the carrier gas as a function of time t, measured from the injection of the reactant into the solid bed (cf. Fig. 1), one obtains the so-called *diffusion band*. The mathematical analysis of this by means of a PC programme already published [33] gives the function of time describing $H = f(t)$, as the sum of two exponential functions:

$$H^{I/M} = N_3\left(1 + \frac{Z}{Y}\right)\exp\left(-\frac{X+Y}{2}t\right) + N_3\left(1 - \frac{Z}{Y}\right)\exp\left(-\frac{X-Y}{2}t\right) \qquad (1)$$

where N_3 is a constant depending on the experimental conditions, X, Y and Z are defined by the relations

$$X = \frac{\alpha_1}{1+V_1} + \frac{V_1 k_1}{1+V_1} + k_{-1} + k_2 \tag{2}$$

$$\frac{X^2 - Y^2}{4} = \frac{\alpha_1 (k_{-1} + k_2)}{1+V_1} + \frac{V_1 k_1 k_2}{1+V_1} \tag{3}$$

$$Z = X - 2(k_{-1} + k_2) \tag{4}$$

while

$$\alpha_1 = 2D_1/L_1^2 \tag{5}$$

$$V_1 = 2\frac{V'_G(\text{empty})\varepsilon}{V_G} + \frac{L_2^2}{L_1^2} \tag{6}$$

D_1 being the diffusion coefficient of the analyte in section L_1, and V_G and V'_G denoting the gaseous volumes of empty sections L_1 and L_2, respectively (cf. Fig. 1) and ε the external porosity of the solid bed.

From the values of the two pre-exponential factors and the two exponential coefficients of time of Eq. (1), together with α_1 and V_1, one can easily find the values of the three physicochemical parameters k_1, k_{-1} and k_2, together with K_G and K from the relations

$$K_G = k_1 \frac{V'_G}{A_s} \quad \text{and} \quad K = \frac{k_1}{k_{-1}} \cdot \frac{\varepsilon}{1-\varepsilon} \tag{7}$$

where A_s is the total surface area of the solid. More details can be found in the original publication [34].

The non-linear isotherm model is now based on a recent significant advancement, namely a simple determination of the experimental adsorption isotherm of a gaseous substance on the surface of a solid, defining a local adsorption parameter k_1 of the isotherm, without using an *a priori* isotherm equation, like that of Langmuir, BET, *et al.* The detailed theoretical analysis, the

experimental set-up, and several sample isotherms so determined are given in the original publication [40]. Together with the isotherm parameter k_1, the method gives the value of the desorption rate constant k_{-1}, of the gas from the surface of the solid, the rate constant k_2 of a possible first-order or pseudo-first-order surface reaction of the adsorbed analyte, and the chromatographic detector calibration factor g for the pollutant.

In the present work, the experimental arrangement of ref. [33] was used, repeated in Fig. 1.

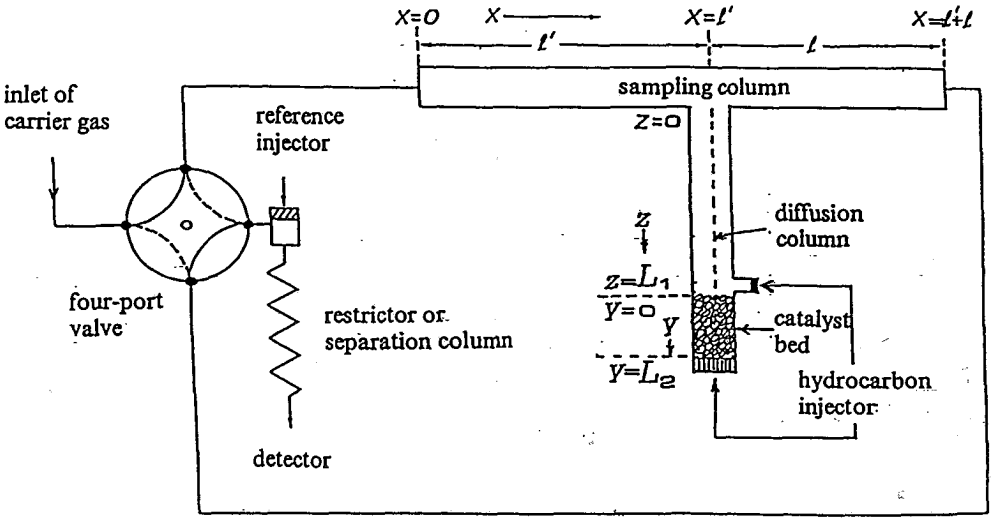

FIGURE 1. Schematic representation of columns and gas connections for characterization of solid catalysts by Reversed-Flow Gas Chromatography.

The mathematical modelling now was considerably different than before, [40], but the solution of the resulting partial differential equations led again to mathematical relations for the calculation of the same physicochemical parameters, namely:

(a) The local adsorption parameter k_1 (s^{-1}) of the gas A and its experimental isotherm on the surfaces of the solid.

(b) The rate constant of desorption k_{-1} (s^{-1}) from the surface.

(c) The rate constant k_2 of a possible first- or pseudo-first-order surface reaction.

It is noteworthy that the equations derived here were the same for two different ways of introducing the gaseous analyte onto the solid bed (cf. Fig. 1).

The main lines of the necessary mathematical analysis based on the arrangement of Fig. 1 are given below, by assuming a non-linear adsorption isotherm. For this purpose, it is not necessary to determine the isotherm equation. Only the basic definition of the local adsorption equation is adopted, thus incorporating the non-linear isotherm in the mathematical calculations. The non-linearity is automatically taken care of. The above definition is

$$c_s^* = \frac{a_y}{a_s} k_1 \int_0^t c_y(\tau)\mathrm{d}\tau \quad \text{or} \quad c_s^* = \frac{m_s}{a_s}\delta(y - L_2) + \frac{a_y}{a_s} k_1 \int_0^t c_y(\tau)\,\mathrm{d}\tau \tag{8}$$

depending on whether the pollutant A is injected as an instantaneous pulse (delta fuction, δ) at $z = L_1$ (left-hand side of Eq.(1)) or at $y = L_2$ (right-hand side of Eq.(1)).

The symbols above are

c_s^*	equilibrium adsorbed concentration of analyte at time t, mol/g.
m_s	initially adsorbed concentration of analyte, mol.
a_s	amount of solid adsorbent per unit length of column bed, g/cm.
y	length coordinate along section L_2, cm.
c_y	gaseous concentration of the analyte in region y, mol/cm^3.
a_y	cross sectional area of the void space in region y, cm^2.
$\delta(y - L_2)$	Dirac's delta fuction describing the initial condition of the bed, when the analyte is introduced as an instantaneous pulse at the point $y = L_2$, cm^{-1}.
k_1	local adsorption parameter transforming into c_s the area under the curve of the gaseous concentration c_y in region y vs time at any later time t, s^{-1}.
τ	dummy variable for time.

The mass balance equation in the filled region y of the diffusion column is

$$\frac{\partial c_y}{\partial t} = D_2 \frac{\partial^2 c_y}{\partial y^2} - k_{-1} \frac{a_s}{a_y}(c_s^* - c_s) \tag{9}$$

where

D_2 diffusion coefficient of the analyte in section L_2, cm^2/s.

k_{-1} rate constant of desorption from the bulk solid, s^{-1}.

c_s concentration of analyte adsorbed on the solid at time t, mol/g.

The rate of change of the adsorbed concentration is described by the relation

$$\frac{\partial c_s}{\partial t} = k_{-1}(c_s^* - c_s) - k_2 c_s \tag{10}$$

where k_2 (s^{-1}) is the rate constant of a possible first-order or pseudofirst-order surface reaction of the adsorbed gas.

The initial conditions are

$$c_y(0, y) = \frac{m}{a_y}\delta(y - L_2) \quad \text{and} \quad c_s(0, y) = 0 \tag{11}$$

where m is the amount (mol) of analyte introduced as a pulse.

In gaseous region z the diffusion equation for the analyte is

$$\frac{\partial c_z}{\partial t} = D_1 \frac{\partial^2 c_z}{\partial z^2} \tag{12}$$

where

z length coordinate along section L_1, cm.

c_z gaseous concentration of analyte in z, mol/cm^3.

The system of partial differential equations, (9), (10) and (12) is solved by using double Laplace transforms of all terms with respect to time and length coordinates, under the initial conditions (11) and $c_z(z, 0) = 0$, the isotherm equation (8), and subject to the appropriate boundary conditions at the junctions L_2/L_1 and $x = l'$ (cf. Fig. 1). The result, by means of certain approximations [38], leads to the expression

$$H^{1/M} = A_1 \exp(B_1 t) + A_2 \exp(B_2 t) + A_3 \exp(B_3 t) + A_4 \exp(B_4 t) \tag{13}$$

The physical meaning of the exponential coefficients of time B_1, B_2 B_3 and B_4 are as follows:

$$\alpha_2(1 + V_1) + k_{-1} + k_2 = -(B_1 + B_2 + B_3 + B_4) = X \tag{14}$$

$$\alpha_2(1 + V_1)(k_{-1} + k_2) + \alpha_1\alpha_2 + k_1k_{-1} = B_1B_2 + B_1B_3 + B_1B_4$$

$$+ B_2B_3 + B_2B_4 + B_3B_4 = Y \tag{15}$$

$$\alpha_1\alpha_2(k_{-1} + k_2) + \alpha_2V_1k_1k_{-1} + k_1k_{-1}k_2 =$$

$$-(B_1B_2B_3 + B_1B_2B_4 + B_1B_3B_4 + B_2B_3B_4) = Z \tag{16}$$

$$\alpha_2V_1k_1k_{-1}k_2 = B_1B_2B_3B_4 = W \tag{17}$$

where α_1 and V_1 are given by Eq. (5) and (6), respectively, and $\alpha_2 = 2D_2/L_2^2$.

By entering the pairs of H (peak height), t (time of reversal) in the DATA lines of the PC program listed in the Appendix, the exponential coefficients B_1, B_2 and B_3 of Eq.(13) are computed. From these, using Eqs.(14)-(17), k_1, k_2 and k_{-1} can be calculated.

Instead of using diffusion coefficients in Eq.(5) from other sources, one can use a steady-state approximation for c_s in Eq.(10), $dc_s/dt = 0$, leading to

$$k_{-1}(c_s^* - c_s) - k_2c_s = 0 \tag{18}$$

Using this in place of (10), there results

$$H^{1/M} = A_5\exp(B_5 t) + A_6\exp(B_6 t) + A_7\exp(B_7 t) \tag{19}$$

instead of Eq.(13), with B_5, B_6 and B_7 having the content:

$$\alpha_2(1+V_1) = -(B_5+B_6+B_7) = X_1 \tag{20}$$

$$\alpha_1\alpha_2 + \frac{k_1k_{-1}k_2}{k_{-1}+k_2} = B_5B_6 + B_5B_7 + B_6B_7 = Y_1 \tag{21}$$

$$\frac{\alpha_2V_1k_1k_{-1}k_2}{k_{-1}+k_2} = -(B_5B_6B_7) = Z_1 \tag{22}$$

Thus, the same experimental pairs H, t can be used on the basis of three exponential functions of time (19) to give the values of B_5, B_6 and B_7. From the seven auxilliary parameters X, Y, Z, W, X_1, Y_1 and Z_1, one can calculate the three main physicochemical parameters k_1, k_{-1} and k_2, without the use of D_1 and D_2, assuming only that they are equal. The PC programme in GW BASIC of the Appendix A has been written for this purpose, giving directly k_1, k_{-1} and k_2.

From these parameters the deposition velocity V_d of the gaseous analyte on the surface of the solid, and the reaction probability γ with that are calculated by the simple mathematical formulae

$$V_d = \frac{k_1V'_G(\text{empty})\varepsilon}{A_s}\cdot\frac{k_2}{k_{-1}+k_2} \tag{23}$$

$$\frac{1}{\gamma} = \left(\frac{R_gT}{2\pi M}\right)^{1/2}\cdot\frac{1}{V_d}+\frac{1}{2} \tag{24}$$

where R_g is the ideal gas constant, T the absolute temperature and M the molar mass of the gaseous analyte. The values of these two additional parameters, V_d and γ, are also displayed by running the PC programme of the Appendix.

It is clear from the definition of V_d by Eq.(23) and the relation of γ with it (Eq.(24)), that both parameters are independent of molecular diffusion, being related only to the local adsorption isotherm (k_1), the desorption rate constant (k_{-1}) and the surface reaction rate constant (k_2).

The calculation of the isotherms is carried out as described elsewhere [40], using the following equations:

$$\frac{\partial c_s^*}{\partial c_g} = k_1 \frac{a_y \sum_{i=1}^{3} A_i \exp(B_i t)}{a_s \sum_{i=1}^{3} A_i B_i \exp(B_i t)} \tag{25}$$

$$c_s^* = -\frac{k_1 a_y}{g a_s} \sum_{i=1}^{3} A_i \exp(B_i t)/B_i \tag{26}$$

$$c_g = \frac{1}{g} \sum_{i=1}^{3} A_i \exp(B_i t) \tag{27}$$

where A_i and B_i are the pre-exponential factors and the exponential coefficients of Eq.(19), and g (cm/mol cm^{-3}) is the proportionality constant between peak height H (cm) and gaseous concentration of the analyte c_g (mol cm^{-3}). One can consider t in the above equations as a dummy independent variable and calculate, for chosen arbitrary values of t, both the differential isotherm $\partial c_s^*/\partial c_g$ and c_s^*, together with the corresponding values of c_g. Plotting $\partial c_s^*/\partial c_g$ or c_s^* against c_g for each chosen t, independent experimental isotherms are obtained. By entering an initial time T_1 and a final time T_2 in the 330 and 340 INPUT lines of the PC programme given in the Appendix, this calculates and prints $\partial c_s^*/\partial c_g$, c_s^* and c_g, together with the other parameters mentioned before.

Experimental

Chemicals. All gases used including the carrier gas were obtained from Air Liquide (Athens, Greece) and had a purity of 99.000-99.999%. The oxides used were pro-analysi from Merck.

Apparatus. The experimental arrangement has been described elsewhere [34, 35] and is schematically outlined in Fig. 1.

The geometrical characteristics of the cells used in the experiments are given in Table 1, together with the mass, external porosity and specific surface are of the solids.

Procedure. After the injection of 1 cm^3 of each gas at atmospheric pressure and waiting for the monotonously rising concentration - time curve to appear in the

TABLE 1

Lengths and Volumes of the Cell Used to Obtain the Diffusion Bands, together with the Solid's Amount, External Porosity and specific Surface Area

Solid	L_1 (cm)	L_2 (cm)	V_G (cm^3)	V'_G (cm^3)	a_s (g cm^{-1})	ε	SSA/cm^2 g^{-1}
Cr_2O_3	51.6	2.9	10.15	13.50	4.517	0.7252	33400
ZnO	51.2	3.3	8.65	15.00	3.152	0.3840	17316
Fe_2O_3	22.0	2.9	2.12	0.279	0.1000	0.7988	23400
PbO	21.7	3.5	2.09	0.337	0.4171	0.5551	300

TABLE 2

Adsorption, Desorption and Surface Reaction Parameters for C_xH_y on Cr_2O_3, at 323.2 K, based on a Linear and Non-Linear Isotherm Model

C_xH_y	k_1 (10^{-4} s^{-1})	k_1 (10^{-4} s^{-1})	k_{-1} (10^{-4} s^{-1})	k_{-1} (10^{-3} s^{-1})	k_2 (10^{-5} s^{-1})	k_2 (10^{-5} s^{-1})	K_G (10^{-10} cm s^{-1})	V_d (10^{-10} cm s^{-1})	K	γ (10^{-14})
	Linear	Non-linear	Linear	Non-linear	Linear	Non-linear	Linear	Non-linear	Linear	Non-linear
C_2H_2	6.76	15.5	2.69	9.99	3.40	3.83	1.96	1.32	8.61	1.51
C_2H_4	7.55	14.2	2.38	16.7	2.70	3.85	2.19	0.733	10.8	0.839
C_2H_6	6.06	9.40	3.04	8.15	2.11	4.29	1.76	1.10	6.82	1.26
C_3H_6	3.94	9.02	2.20	6.25	0.16	1.33	1.14	0.428	6.12	0.490
1 - C_4H_8	4.91	2.63	1.08	3.34	2.18	8.05	1.42	1.38	15.5	1.58

TABLE 3

Adsorption, Desorption and Surface Reaction Parameters for C_xH_y on ZnO, at 323.2 K, based on a Linear and Non-Linear Isotherm Model

C_xH_y	k_1 (10^{-4} s^{-1})	k_1 (10^{-4} s^{-1})	k_{-1} (10^{-4} s^{-1})	k_{-1} (10^{-4} s^{-1})	k_2 (10^{-5} s^{-1})	k_2 (10^{-5} s^{-1})	K_G (10^{-10} cm s^{-1})	V_d (10^{-10} cm s^{-1})	K	γ (10^{-14})
	Linear	Non-linear	Linear	Non-linear	Linear	Non-linear	Linear	Non-linear	Linear	Non-linear
C_2H_2	11.8	6.90	3.52	54.3	2.11	9.36	4.40	3.74	2.43	2.91
C_2H_6	7.76	7.80	2.85	124	3.70	6.95	2.95	1.37	2.02	1.14

TABLE 4

Adsorption, Desorption and Surface Reaction Parameters for C_xH_y on Fe_2O_3, at 323.2 K, based on a Linear and Non-Linear Isotherm Model

C_xH_y	k_1 (10^{-4} s^{-1})	k_1 (10^{-4} s^{-1})	k_{-1} (10^{-4} s^{-1})	k_{-1} (10^{-4} s^{-1})	k_2 (10^{-4} s^{-1})	k_2 (10^{-4} s^{-1})	K_G (10^{-8} cm s^{-1})	V_d (10^{-8} cm s^{-1})	K	γ (10^{-12})
	Linear	Non-linear	Linear	Non-linear	Linear	Non-linear	Linear	Non-linear	Linear	Non-linear
C_2H_2	1.56	16.0	3.51	47.8	6.17	21.6	1.64	1.63	1.76	1.27
C_2H_4	131	0.0182	1.26	397	3.41	444	138	0.0561	414	0.0454
C_2H_6	92.0	13.4	4.99	11.3	3.25	20.3	96.9	2.83	73.2	2.37
C_3H_6	1.47	0.0094	3.16	521	4.13	560	1.54	0.0448	1.84	0.0444
1 - C_4H_8	2.64	527	2.94	0.0821	2.67	0.338	2.78	228	3.56	261

TABLE 5

Adsorption, Desorption and Surface Reaction Parameters for C_xH_y on PbO, at 323.2 K, based on a Linear and Non-Linear Isotherm Model

C_xH_y	$k_1(10^{-4}\,s^{-1})$	$k_1(10^{-4}\,s^{-1})$	$k_{-1}(10^{-4}\,s^{-1})$	$k_{-1}(10^{-4}\,s^{-1})$	$k_2(10^{-4}\,s^{-1})$	$k_2(10^{-4}\,s^{-1})$	$K_G(10^{-8}\,cm\,s^{-1})$	$V_d(10^{-7}\,cm\,s^{-1})$	K	$\gamma\,(10^{-11})$
	Linear	Non-linear	Linear	Non-linear	Linear	Non-linear	Linear	Non-linear	Linear	Non-linear
C_2H_2	0.180	5739	0.280	0.0322	4.52	28.9	2.12	2448	0.820	1909
C_2H_6	45.3	10.0	11.9	64.5	3.18	15.9	525	0.845	4.74	0.708
C_3H_6	0.510	6.37	7.61	35.2	3.33	14.9	5.85	0.810	0.080	0.803
$1 - C_4H_8$	1.51	5.11	3.59	5.75	2.13	23.6	13.8	2.89	0.45	3.31

detector signal, the chromatographic sampling procedure was started by reversing the direction of the carrier gas flow for 10 s, which is a shorter time period than the gas hold-up time in both column sections l and l'. Examples of sample peaks created by the flow reversals have been given elsewhere [38]. First, the diffusion coefficient of each gas into the carrier gas was determined, by using an empty glass vessel. Then, by using the same vessel filled with a solid catalyst, the various physicochemical parameters described in the Theoretical section were determined. In all experiments, the pressure drop along all columns was negligible. The carrier gas was nitrogen with a flow rate of 0.44 $cm^3 s^{-1}$. Conditioning of each catalyst was carried out *in situ* at 473.2 K for 24 h with nitrogen flowing continuously through the sampling column at the same flow rate.

Results and Discussion

Some experimental results are now presented in Tables 2-5. They are based on the linear model, together with the corresponding output for the non-linear one, for comparison. One sees that the values of some physicochemical parameters are significantly different and so it is obvious that for an inorganic solid of the kinds used as catalysts the linear isotherm model is inadequate, due obviously to the nonuniformity of the surface [14]. The linear model is a first approximation when dealing with inorganic oxides, either used as catalysts or not, and the physicochemical parameters so obtained are to some degree arbitrary, while the new characterization method of catalysts seems more valid.

Two physicochemical parameters characterizing any newly-prepared catalyst are the adsorption and desorption rate constants, k_1 and k_{-1}, respectively. These constants can be measured easily and accurately and from their values a safe criterion of catalyst characterization can be drawn. That is why one can state that the RF-GC method without an *a priori* acceptance of an adsorption isotherm equation is preferable to the Langmuir or the BET one for this purpose. Any new quantity of a catalyst can be tested through adsorption-desorption rate constants values before utilization. Besides, the adsorption rate constant k_1 describes the local

adsorption isotherm in a dynamic non-equilibrium way, and this, is another safe criterion, simultaneously determined. Thus, the adsorption equilibrium constant of the linear model can be replaced by the local adsorption parameter k_1 of the non-linear one for catalytic studies.

The deposition velocity V_d (cf. Eq.(23)) based on k_1 is completely analogous to the overall mass transfer coefficient of the gas to the solid surface, K_G [35], except for the correction factor $k_2/(k_{-1} + k_2)$. The important difference between the parameters k_1, K_G, k_{-1} and k_2 of the previous work [35], introduced for measurement of building pollution, and the parameters k_1, V_d, k_{-1} and k_2, defined here for the characterization of catalysts, is that the first were based on a supposedly linear adsorption isotherm, while here the true experimental isotherm is employed, without specifying an *a priori* isotherm equation like that of Langmuir, B.E.T., etc. An example of the isotherm determination, as described in the Theoretical section, is given in Table 6. The surface reaction rate constant k_2 for the heterogeneous process between the gas and the solid corresponds also to the real experimental isotherm, not necessarily linear. Together with the deposition velocity V_d of the gas onto the catalyst, the overall reaction probability γ (cf. Eq.(24)) can be determined.

From the Tables 2-5, it is obvious that some values obtained from the non-linear isotherm model are 1-2 orders of magnitude higher than those corresponding to the linear model, except of k_{-1} and k_2 which are of the same order of magnitude in most cases, independently of the model.

All above physicochemical quantities intend to characterize any newly-prepared catalyst, on the basis of accurately defined physicochemical concepts. Of course the whole mathematical model uses certain approximations, but to calculate the extent of the contribution of these approximations to the final results is difficult, if not impossible

Comparison of the Chemisorption Methods. The extent of gas adsorption is a basic quantity required in adsorption studies. Either the equilibrium amount adsorbed or the rate of adsorption (adsorbed amount vs time) is measured as a function of temperature and time. The amount adsorbed may be calculated from the variation of the gas pressure in a calibrated volume or from the variation of the

TABLE 6

Sample Isotherms at 323.2 K for the Adsorption of Ethyne on PbO

Dummy variable (min)	$\partial c_s^*/\partial c_g$ ($cm^3\ g^{-1}$)	c_s^* (10^{-7} mol g^{-1})	c_g (10^{-8} mol cm^{-3})
10	1.55	6.116	1.716
15	7.323	5.748	2.804
20	48.97	5.278	3.120
25	-41.17	4.788	3.095
30	-22.15	4.316	2.926
35	-17.86	3.875	2.701
40	-16.10	3.471	2.462
45	-15.20	3.104	2.227
50	-14.67	2.773	2.005
55	-14.34	2.476	1.808
60	-14.12	2.209	1.612
65	-13.97	1.970	1.442
70	-13.86	1.757	1.289
75	-13.78	1.566	1.150
80	-13.72	1.396	1.027
85	-13.68	1.244	0.9158
90	-13.64	1.108	0.8166
95	-13.62	0.9876	0.7280
100	-13.60	0.8799	0.6489

weight of the catalyst sample in a static or continuous-flow apparatus. An adsorption apparatus may be static when the gas is brought into contact with the catalyst sample in successive doses, either directly (classical volumetric method) or through a capillary (flow method). In a dynamic apparatus the gas flows over the catalyst sample for all the duration of the experiment. All known methods can be classified in four categories:

1. Volumetric Methods [3]
2. Gravimetric Methods [3]
3. Continuous Flow Method [41, 42]
4. Pulse Flow Method [43, 44].

The Pulse technique, derived from the flow technique, is referred in the literature as the best technique for describing both its mathematical and experimental aspects in considerable detail. The basic relation in this method is

$$L/t_m v_l = K_a^{-1}$$

where L is the length of the packed column, t_m is the retention time of the pulse maximum, v_l is the linear gas velocity (velocity that would result if the column were completely empty), and K_a is the adsorption equilibrium constant. K_a is directly proportional to the slope of the adsorption isotherm, and is a true constant only for those systems with Henrian (linear) adsorption isotherms.

As mentioned in the Introduction, the linear model is inadequate for the metal oxides and the major reason of this inadequacy is the nonuniformity of sites on their surface [14]. Besides, steric and/or ligand effects caused by the absorbate may come into play and then the inadequacies extend to the Langmuir model which, though it is a non-linear one it is ivalid for these inorganic substances. The BET equation is based on the same assumptions made by Langmuir, but with the presumption that multilayers of adsorbate are allowed to exist on top of the monolayer. The BET model is still an oversimplification, but it represents many experimental results very well and is widely used. The BET model is inexact [14] and the surface areas are to some degree arbitrary but as the BET equation is

almost universally used, the internal consistency of results obtained in many laboratories is assured.

The RF-GC technique [36] has the following advantages in relation to the above mentioned adsorption isotherms: (1) the diffusion and resistance to mass transfer are not neglected, (2) the sorption effect in dynamic systems is non-existent, (3) the pressure gradient is negligible along the solid bed, (4) the isotherm can be determined in the presence of a surface reaction of the adsorbate, and (5) above all, this method does not requires a specification of an *a priori* isotherm equation, as it leads directly to a local experimental isotherm. This is very important when dealing with catalysts.

Conclusion

It is often difficult to reproduce a catalyst preparation exactly and it is well known that after any catalyst preparation a physicochemical characterization process must follow. Thus, the prepared catalysts are generally characterized through the study of their specific surface areas by means of adsorption-desorption isotherms, from which the pore size distrubutions can also be found. Besides the catalyst surface acidity, if there is any, can be determined by means of desorption measurements of some basic probe molecules. These and many other determinations based on Chemisorption must follow every catalyst preparation, especially when dealing with metal oxides as supported or unsupported catalysts. Since surface areas vary from batch to batch, the implication is that before an experimental isotherm is available, it is hardly possible to make meaningful quantitative comparisons of activities, acidities etc. of various catalysts. Without the development of such an experimental isotherm method, quantitative comparisons of activities of high-surface area catalysts are not feasible.

The present paper attends to solve this problem by giving an answer that seems to be more correct and accurate than any other one mentioned in the literature.

ΝΕΑ ΜΕΘΟΔΟΣ ΧΑΡΑΚΤΗΡΙΣΜΟΥ ΣΤΕΡΕΩΝ ΚΑΤΑΛΥΤΩΝ ΚΑΙ ΣΥΓΚΡΙΣΗ ΜΕ ΠΑΛΑΙΟΤΕΡΕΣ

Η τεχνική της αεριο-χρωματογραφίας αναστρεφομένης ροής (RF-GC) εφαρμόσθηκε για τον χαρακτηρισμό καταλυτών και τον υπολογισμό φυσικοχημικών παραμέτρων ετερογενών αντιδράσεων. Χρησιμοποιήθηκε νέο μαθηματικό πρότυπο με βάση μη γραμμική πειραματική ισόθερμο προσροφήσεως του αντιδρώντος. Η μέθοδος εφαρμόσθηκε σε τέσσερα οξείδια μετάλλων, (Cr_2O_3, ZnO, Fe_2O_3, PbO) ως καταλυτών των αντιδράσεων ισομερισμού-πολυμερισμού και υδρογονώσεως-αφυδρογονώσεως υδρογονανθράκων. Γίνεται σύγκριση της προτεινομένης μεθόδου χαρακτηρισμού των καταλυτών με παλαιότερες μεθόδους, οι οποίες είχαν στηριχθεί είτε σε γραμμική ισόθερμο προσροφήσεως, είτε στις ισοθέρμους Langmuir και BET. Περιγράφονται τα πλεονεκτήματα της νέας μεθόδου.

Acknowlendgments

The authors wish to thank the DG-XII of the European Commission for the financial support under contract EV 5V-CT94-0537. They also thank Miss Anna Malliori for the typescript preparation.

Appendix A

```
10 REM Non-Linear Regression Analysis of Function:
20 REM H^(1/M)=A1*EXP(B1*T)+S*A2*EXP(B2*T)+P*A3*EXP(B3*T)+X*A4*EXP(B4*T)
30 REM H^(1/M)=A5*EXP(B5*T)+S*A6*EXP(B6*T)+P*A7*EXP(B7)
40 REM Calculation of kinetic parameters with non-linear isotherms and
       experimental set-up of Chromatographia 41,227(1995),with injection
        of one or two gaseous substances, at y=0 or y=L2.
50 REM    N2    = Minimum number of points of first exponential function
60 REM    MAX   = Square of maximum correlation coefficient
70 REM    OPT   = Final optional choice of variables when OPT=1
80 REM    J     = Number of points of first exponential function
90 REM    G     = Number of points of second exponential function
100 REM    F     = Number of points of third exponential function
110 REM   K,L   = First and last point of linear regression in subroutine
120 REM   SA,SB = Standard errors of A and B in each linear regression
130 REM   Y(I)  = Ordinate for each linear regression in the subroutine
140 REM   U(I)  = Variable remaining by  removal of the previous one, two or
                  three exponential functions
150 REM   D(I)  = Function for calculating the correlation coefficient
160 INPUT "Total number of pairs H,T=";N
170 DIM H(N),T(N),Y(N),U(N),D(N)
180 INPUT "Response factor=";M
190 INPUT "Factor to divide H(I)=";H1
200 INPUT "Temperature in K=";T
210 INPUT "Lenth L1(cm) of Section z=";L1
220 INPUT "Length L2(cm) of Section y=";L2
230 INPUT "Gaseous Volume VG1(cm^3) of Empty Section L1=";VG1
240 INPUT "Gaseous Volume VG2(cm^3) of Empty Section L2=";VG2
250 INPUT "External Porosity of the Solid bed,E=";E
260 INPUT "Cross Sectional Area AY(cm^2) of Void Space in Region y=";AY
270 INPUT "Amount of Adsorbent per Unit Length of Bed AS(g/cm)=";AS
280 INPUT "Specific Surface Area of Solid SSA(cm^2/g)=";SSA
290 INPUT "Molar Mass MB(kg/mol) of Analyte B=";MB
300   FOR I=1 TO N
310     READ H(I),T(I)
320     H(I)=H(I)/H1
330   NEXT I
340 N2=INT(N/7+.5)
350 MAX=0:OPT=0
360 REM Calculation of A1 and B1 with H,T pairs ranging from N2 to N-2*N2-3
370 FOR J=N2 TO N-2*N2-3
380    K=N-J+1
390    L=N
400    FOR I=K TO L
410       Y(I)=(1/M)*LOG(H(I))
420    NEXT I
430    GOSUB 2380      :REM Subroutine for linear regression analysis
440    A1=EXP(A)
450    B1=B
460    SA1=SA
470    SB1=SB
480    IF OPT=1 THEN  520
490 REM Calculation of A2 and B2 with H,T pairs ranging from N2 to N-J-N2-3
       ,and both prefixes -1 or +1
500    FOR S=-1 TO +1 STEP 2
510       FOR G=N2 TO N-J-N2-3
520          K=N-J-G+1
530           L=N-J
540          FOR I=K TO L
550             U(I)=S*H(I)^(1/M)-S*A1*EXP(B1*T(I))
560             Y(I)=LOG(ABS(U(I)))
570          NEXT I
580          GOSUB 2380     :REM Subroutine for linear regression analysis
590          A2=EXP(A)
600          B2=B
610          SA2=SA
620          SB2=SB
```

```
630          IF OPT=1 THEN 670
640 REM Calculation of A3 and B3 with H,T pairs ranging from N2 to N-J-G-3
      and both prefixes -1 or +1
650          FOR P=-1 TO +1 STEP 2
660             FOR F=N2 TO N-J-G-3
670                K=N-J-G-F+1
680                 L=N-J-G
690                FOR I=K TO L
700                   U(I)=P*(H(I)^(1/M)-A1*EXP(B1*T(I))-S*A2*EXP(B2*T(I)))
710                   Y(I)=LOG(ABS(U(I)))
720                NEXT I
730                GOSUB 2380    :REM Subroutine for linear regression analysis
740                A3=EXP(A)
750                B3=B
760                SA3=SA
770                SB3=SB
780                IF OPT=1 THEN 810
790 REM Calculation of A4 and B4 with H,T pairs ranging from 1 to N-J-G-F,and
      both prefixes -1 or +1
800                FOR X=-1 TO +1 STEP 2
810                   K=1
820                   L=N-J-G-F
830                   FOR I=K TO L
840                      U(I)=X*(H(I)^(1/M)-A1*EXP(B1*T(I))-S*A2*EXP(B2*T(I))-P*
                            A3*EXP(B3*T(I)))
850                      Y(I)=LOG(ABS(U(I)))
860                   NEXT I
870                   GOSUB 2380  :REM Subroutine for linear regression analysis
880                   A4=EXP(A)
890                   B4=B
900                   SA4=SA
910                   SB4=SB
920                   IF OPT=1 THEN 1120
930                   C1=0
940                   C2=0
950                   C3=0
960                   FOR I=1 TO N
970                      D(I)=H(I)^(1/M)-A1*EXP(B1*T(I))-S*A2*EXP(B2*T(I))-P*A3*
                            EXP(B3*T(I))-X*A4*EXP(B4*T(I))
980                      C1=C1+D(I)^2
990                      C2=C2+H(I)^(2/M)
1000                      C3=C3+H(I)^(1/M)
1010                   NEXT I
1020                   R=1-C1/(C2-C3^2/N)
1030                   IF R>MAX THEN MAX=R:SMAX=S:PMAX=P:XMAX=X:JMAX=J:GMAX=G:
                         FMAX=F
1040                NEXT X
1050             NEXT F
1060          NEXT P
1070       NEXT G
1080    NEXT S
1090 NEXT J
1100 S=SMAX:P=PMAX:X=XMAX:J=JMAX:G=GMAX:F=FMAX:OPT=1
1110 GOTO 380
1120 LPRINT "Intercept Ln(A1) and its Standard error =";LOG(A1*H1) "+-"SA1
1130 LPRINT "Slope B1 and its Standard error=";B1 "+-"SB1
1140 LPRINT
1150 LPRINT "Intercept Ln(A2) and its Standard error=";LOG(A2*H1) "+-"SA2
1160 LPRINT "Slope B2 and its Standard error=";B2 "+-"SB2
1170 LPRINT
1180 LPRINT "Intercept Ln(A3) and its Standard error=";LOG(A3*H1) "+-"SA3
1190 LPRINT "Slope B3 and its Standard error=";B3 "+-"SB3
1200 LPRINT
1210 LPRINT "Intercept Ln(A4) and its Standard error=";LOG(A4*H1) "+-"SA4
1220 LPRINT "Slope B4 and its Standard error=";B4 "+-"SB4
1230 LPRINT
```

```
1240 LPRINT "Square of maximum correlation coefficient r^2=";MAX
1250 LPRINT "Optimum values of points for 1st, 2nd , 3rd and 4th exponential
          functions, respectively=";JMAX","GMAX","FMAX"and"N-JMAX-GMAX-FMAX
1260 LPRINT "Values of S,P and X,respectively ="; SMAX","PMAX"and"XMAX
1270 LPRINT
1280 N2=INT(N/6+.5)
1290 MAX=0:OPT=0
1300  REM Calculation of A5 and B5 with H,T pairs ranging from N2 to N-N2-3
1310 FOR J=N2 TO N-N2-3
1320    K=N-J+1
1330    L=N
1340    FOR I=K TO L
1350       Y(I)=(1/M)*LOG(H(I))
1360    NEXT I
1370    GOSUB 2380          : REM Subroutine for linear regression analysis
1380    A5=EXP(A)
1390    B5=B
1400    SA5=SA
1410    SB5=SB
1420    IF OPT=1 THEN  1460
1430  REM Calculation of A6 and B6 with H,T pairs ranging from N2 to N-J-3 and
        both prefixes -1 and +1
1440    FOR S=-1 TO +1  STEP 2
1450       FOR G=N2 TO N-J-3
1460          K=N-J-G+1
1470          L=N-J
1480          FOR I=K TO L
1490             U(I)=S*H(I)^(1/M)-S*A5*EXP(B5*T(I))
1500             Y(I)=LOG(ABS(U(I)))
1510          NEXT I
1520          GOSUB 2380      : REM Subroutine for linear regression analysis
1530          A6=EXP(A)
1540          B6=B
1550          SA6=SA
1560          SB6=SB
1570          IF OPT=1 THEN 1600
1580  REM Calculation of A7 and B7 with H,T pairs ranging from 1 to N-J-G,
        with both prefixes -1 and +1
1590          FOR P=-1 TO +1 STEP 2
1600             K=1
1610             L=N-J-G
1620             FOR I=K TO L
1630                U(I)=P*(H(I)^(1/M)-A5*EXP(B5*T(I))-S*A6*EXP(B6*T(I)))
1640                Y(I)=LOG(ABS(U(I)))
1650             NEXT I
1660             GOSUB 2380     : REM Subroutine for linear regression analysis
1670             A7=EXP(A)
1680             B7=B
1690             SA7=SA
1700             SB7=SB
1710             IF OPT=1 THEN 1890
1720             C1=0
1730             C2=0
1740             C3=0
1750             FOR I=1 TO N
1760                D(I)=H(I)^(1/M)-A5*EXP(B5*T(I))-S*A6*EXP(B6*T(I))
                        -P*A7*EXP(B7*T(I))
1770                C1=C1+D(I)^2
1780                C2=C2+H(I)^(2/M)
1790                C3=C3+H(I)^(1/M)
1800             NEXT I
1810             R=1-C1/(C2-C3^2/N)
1820             IF R>MAX THEN MAX=R:SMAX=S:PMAX=P:JMAX=J:GMAX=G
1830          NEXT P
1840       NEXT G
1850    NEXT S
```

```
1860 NEXT J
1870 S=SMAX:P=PMAX:J=JMAX:G=GMAX:OPT=1
1880 GOTO 1320
1890 LPRINT "Intercept Ln(A5) and its Standard error=";LOG(A5*H1) "+-"SA5
1900 LPRINT "Slope B5 and its Standard error=";B5 "+-"SB5
1910 LPRINT "Intercept Ln(A6) and its Standard error=";LOG(A6*H1) "+-"SA6
1920 LPRINT "Slope B6 and its Standard error=";B6 "+-"SB6
1930 LPRINT "Intercept Ln(A7) and its Standard error=";LOG(A7*H1) "+-"SA7
1940 LPRINT "Slope B7 and its Standard error=";B7 "+-"SB7
1950 LPRINT
1960 LPRINT "Square of maximum correlation coefficient r^2=";MAX
1970 LPRINT "Optimum values of points for 1st, 2nd and 3rd exponential
          functions,respectively=";JMAX","GMAX"and"N-JMAX-GMAX
1980 LPRINT "Values of S and P, respectively =";SMAX"and"PMAX
1990 LPRINT
2000 DATA 8704,3,21760,5,29440,7,34560,9,37888,11,39680,13,39424,15,39168,17,391
68,19,37376,21,36864,23,35840,25,34816,27,33536,29,32256,31,30976,33,29696,35,28
672,37,27648,39,25600,41,25344,43,25088,45,23296,48,22528,50,21504,52
2010 DATA 20736,54,20096,56,19200,58,18432,60,17664,62,17152,64,16384,66,15744,6
8,14848,70,14592,72,14080,74,13312,76,12928,78,12288,80,12160,82,11648,84,11136,
86,10752,88,10240,90,9856,92,9600,94,9216,96,8832,98,8576,100,8192,102
2020 DATA 7808,104,7488,106,7232,108,7040,110,6656,112,6208,117,5984,119,5760,12
1,5440,123,5280,125,5056,127,4864,129,4736,131,4544,133,4352,135,4192,137,3968,1
39,3904,141,3712,143,3712,145,3488,147,3264,149,3264,151,3136,153
2040 DATA
2050 DATA
2060 X=-(B1+B2+B3+B4)/60
2070 Y=(B1*B2+B1*B3+B1*B4+B2*B3+B2*B4+B3*B4)/60^2
2080 Z=-(B1*B2*B3+B1*B2*B4+B1*B3*B4+B2*B3*B4)/60^3
2090 W=(B1*B2*B3*B4)/60^4
2100 X1=-(B5+B6+B7)/60
2110 Y1=(B5*B6+B5*B7+B6*B7)/60^2
2120 Z1=-(B5*B6*B7)/60^3
2130 V1=2*VG2*E/VG1+(L2^2/L1^2)
2140 SK(1)=X-X1:SK(2)=W/Z1:SK(3)=(SK(1)+SK(2))/2:REM  SK=k_1+k2
2150    FOR I=1 TO 3
2160 AV=X-SK(I)
2170 A2V1=AV*V1/(1+V1)
2180 A2=AV/(1+V1)
2190 K1K3=(Y-AV*SK(I)-Z/SK(I)+W/A2V1/SK(I))/(1-A2V1/SK(I))
2200 K1K3=ABS(K1K3)
2210 K2=W/A2V1/K1K3
2220 K3=SK(I)-K2
2230 K1=K1K3/K3
2240 A11 =(Y-AV*SK(I)-K1K3)/A2
2250 A12=(Z-A2V1*K1K3-K1K3*K2)/SK(I)/A2
2260  VD=K1*VG2*E*K2/(SSA*AS*L2*SK(I))
2270  G1=SQR(1.32321*T/MB)/VD*100+.5
2280  G2=1/G1
2290  LPRINT "k1 in 1/s=";K1
2300  LPRINT "k_1 in 1/s=";K3
2310  LPRINT "k2 in 1/s=";K2
2320  LPRINT "Deposition velocity in cm/s=";VD
2330  LPRINT "Reaction probability =";G2
2340  LPRINT "a2(1+V1) in 1/s=";AV",a2 in 1/s=";A2",a1 in 1/s=";A11","A12
2350  LPRINT
2360 NEXT I
2370 END
2380  REM Linear regression of Y(I) = A + B T(I)
2390 S1=0
2400 S2=0
2410 S3=0
2420 S4=0
2430 S5=0
2440    FOR I=K TO L
2450    S1=S1+T(I)
```

```
2460     S2=S2+T(I)^2
2470     S3=S3+Y(I)
2480     S4=S4+Y(I)^2
2490     S5=S5+T(I)*Y(I)
2500 NEXT I
2510 Z=L-K+1  :REM Number of points for the linear regression analysis
2520 M1=S5-S1*S3/Z
2530 M2=S2-S1^2/Z
2540 M3=S4-S3^2/Z
2550 A=(S3-S1*M1/M2)/Z
2560 B=M1/M2
2570 SYT=SQR(ABS(S4-A*S3-B*S5)/(Z-2))
2580 SA=SYT*SQR(S2/Z/M2)
2590 SB=SYT/SQR(M2)
2600 RETURN
```

Appendix B

```
10   REM Non-Linear Regression Analysis of Functions:
20   REM H^(1/M)=A1*EXP(B1*T)+S*A2*EXP(B2*T)+P*A3*EXP(B3*T)
30   REM H^(1/M)=A4*EXP(B4*T)+S*A5*EXP(B5*T)
40   REM Calculation of non-linear isotherms with the experimental
       set-up of Chromatographia 41,227(1995), and injection
       at z=L1 or y=L2 of single substances
50   REM VARIABLES
60   REM    N2    = Minimum number of points of first exponential function
70   REM    MAX   = Square of maximum correlation coefficient
80   REM    OPT   = Final optional choice of variables when OPT=1
90   REM    J     = Number of points of first exponential function
100  REM    G     = Number of points of second exponential function
110  REM   K,L    = First and last point for linear regression analysis in
                    the subroutine
120  REM   SA,SB  = Standard errors of A and B in each linear regression
130  REM   Y(I)   = Ordinate for each linear regression in the subroutine
140  REM   U(I)   = Variable remaining by removal of the previous
                    exponential functions
150  REM   D(I)   = Function for calculating the correlation coefficient
160  INPUT "Total numbers of pairs H,T=";N
170  DIM H(N),T(N),Y(N),U(N),D(N)
180 INPUT "Response factor=";M
190 INPUT "Factor to divide H(I)=";H1
200 INPUT "Flow Rate in cm^3/s=";F
210 INPUT "Amount of Analyte injected in mol=";NB
220 INPUT "Initial Time in min for the Calculation of the Isotherm=";T1
230 INPUT "Final Time in min for the Calculation of the Isotherm=";T2
240 FOR I=1 TO N
250    READ H(I),T(I)
260    H(I)=H(I)/H1
270 NEXT I
280 N2=INT(N/6+.5)
290 MAX=0:OPT=0
300  REM Calculation of A1 and B1 with H,T pairs ranging from N2 to N-N2-3
310 FOR J=N2 TO N-N2-3
320    K=N-J+1
330    L=N
340    FOR I=K TO L
350       Y(I)=(1/M)*LOG(H(I))
360    NEXT I
370    GOSUB 2070         : REM Subroutine for linear regression analysis
380    A1=EXP(A)
390    B1=B
400    SA1=SA
410    SB1=SB
420    IF OPT=1 THEN  460
430  REM Calculation of A2 and B2 with H,T pairs ranging from N2 to N-J-3 and
       both prefixes -1 and +1
440    FOR S=-1 TO +1  STEP 2
450       FOR G=N2 TO N-J-3
460          K=N-J-G+1
470          L=N-J
480          FOR I=K TO L
490             U(I)=S*H(I)^(1/M)-S*A1*EXP(B1*T(I))
500             Y(I)=LOG(ABS(U(I)))
510          NEXT I
520          GOSUB 2070      : REM Subroutine for linear regression analysis
530          A2=EXP(A)
540          B2=B
550          SA2=SA
560          SB2=SB
570          IF OPT=1 THEN 600
580  REM Calculation of A3 and B3 with H,T pairs ranging from 1 to N-J-G,
       with both prefixes -1 and +1
590          FOR P=-1 TO +1 STEP 2
600             K=1
```

```
610             L=N-J-G
620             FOR I=K TO L
630                U(I)=P*(H(I)^(1/M)-A1*EXP(B1*T(I))-S*A2*EXP(B2*T(I)))
640                Y(I)=LOG(ABS(U(I)))
650             NEXT I
660             GOSUB 2070    : REM Subroutine for linear regression analysis
670             A3=EXP(A)
680             B3=B
690             SA3=SA
700             SB3=SB
710             IF OPT=1 THEN 910
720             C1=0
730             C2=0
740             C3=0
750             FOR I=1 TO N
760                D(I)=H(I)^(1/M)-A1*EXP(B1*T(I))-S*A2*EXP(B2*T(I))
                       -P*A3*EXP(B3*T(I))
770                C1=C1+D(I)^2
780                C2=C2+H(I)^(2/M)
790                C3=C3+H(I)^(1/M)
800             NEXT I
810             R=1-C1/(C2-C3^2/N)
820             IF R>MAX THEN MAX=R:SMAX=S:PMAX=P:JMAX=J:GMAX=G
830 PRINT MAX
840 REM When satisfied with the MAX value reached,Ctrl Break and GO TO 1010
850          NEXT P
860       NEXT G
870    NEXT S
880 NEXT J
890 S=SMAX:P=PMAX:J=JMAX:G=GMAX:OPT=1
900 GOTO 320
910  LPRINT "Intercept Ln(A1) and its Standard error=";LOG(A1*H1) "+-"SA1
920  LPRINT "Slope B1 and its Standard error=";B1 "+-"SB1
930  LPRINT "Intercept Ln(A2) and its Standard error=";LOG(A2*H1) "+-"SA2
940  LPRINT "Slope B2 and its Standard error=";B2 "+-"SB2
950 LPRINT "Intercept Ln(A3) and its Standard error=";LOG(A3*H1) "+-"SA3
960 LPRINT "Slope B3 and its Standard error=";B3 "+-"SB3
970 LPRINT "Square of maximum correlation coefficient r^2=";MAX
980 LPRINT "Optimum values of points for 1st, 2nd and 3rd exponential
          functions,respectively=";JMAX","GMAX"and"N-JMAX-GMAX
990 LPRINT "Values of S and P, respectively =";SMAX"and"PMAX
1000 LPRINT
1010 B1=B1/60:B2=B2/60:B3=B3/60
1020 A1=A1*H1:A2=S*A2*H1:A3=P*A3*H1
1030 A=A1/B1+A2/B2+A3/B3
1040 G3=-F*A/NB
1050 LPRINT "Calibration Factor of Detector g'in cm per mol/cm^3=";G3
1060 LPRINT
1070 LPRINT TAB(1);"Time(min)";TAB(17);"dCS/dCR";TAB(35);"CS";TAB(50);"CG"
1080 T1=T1*60:T2=T2*60
1090 FOR T=T1 TO T2 STEP 300
1100    DCS=K1*AY*(A1*EXP(B1*T)+A2*EXP(B2*T)+A3*EXP(B3*T))/(A1*B1*EXP(B1*T)
           +A2*B2*EXP(B2*T)+A3*B3*EXP(B3*T))/AS
1110    CS=-(K1*AY/AS/G3)*(A1*EXP(B1*T)/B1+A2*EXP(B2*T)/B2+A3*EXP(B3*T)/B3)
1120    CG=(A1*EXP(B1*T)+A2*EXP(B2*T)+A3*EXP(B3*T))/G3
1130 LPRINT TAB(1);T/60;TAB(15);DCS;TAB(30);CS;TAB(45);CG
1140 NEXT T
2000 DATA
2010 DATA
2020 DATA
2030 DATA
2040 DATA
2050 DATA
2060 END
2070  REM Linear regression of Y(I) = A + B T(I)
2080 S1=0
```

```
2090 S2=0
2100 S3=0
2110 S4=0
2120 S5=0
2130    FOR I=K TO L
2140    S1=S1+T(I)
2150    S2=S2+T(I)^2
2160    S3=S3+Y(I)
2170    S4=S4+Y(I)^2
2180    S5=S5+T(I)*Y(I)
2190 NEXT I
2200 Z=L-K+1  :REM Number of points for the linear regression analysis
2210 M1=S5-S1*S3/Z
2220 M2=S2-S1^2/Z
2230 M3=S4-S3^2/Z
2240 A=(S3-S1*M1/M2)/Z
2250 B=M1/M2
2260 SYT=SQR(ABS(S4-A*S3-B*S5)/(Z-2))
2270 SA=SYT*SQR(S2/Z/M2)
2280 SB=SYT/SQR(M2)
2290 RETURN
```

References

1. Pepe, F., and Stone, F. S., *J. Catal.* **56**, 160 (1979).
2. Kim Du Soung, Wachs, I. E., and Segawa, K., *J. Catal.* **146**, 268 (1994).
3. Fierro, J. L. G., and Gardia de la Banda, J. F., *Catal. Rev. Sci. Eng.* **28** (2-3), 265 (1986).
4. Juszczyk, W., Karpiński, Z., Lomot, D., Pielaszek, J., and Sobczak, J. W., *J. Catal.* **151**, 67 (1995).
5. Miller, J. T., Meyers, B. L., Barr, M. K., Modica, F. S., and Koningsberger, D. C., *J. Catal.* **159**, 41 (1996).
6. Merlen, E., Beccat, P., Bertolini, J. C., Delichère, P., Zanier, N., and Didillon, B., *J. Catal.* **159**, 178 (1996).
7. Garner, W. E., *J. Chem. Soc.* 1239 (1949).
8. Garner, W. E., Stone, F. S., and Tiley, P. F., *Proc. R. Soc. London* **A211**, 472 (1952).
9. Voltz, S. E., and Weller, S. W., *J. Am. Chem. Soc.* **75**, 522 (1953).
10. MacIver, D. S., and Tobin, H. H., *J. Phys. Chem.* **64**, 451 (1960).
11. Damyanova, S., Daza, L., and Fierro, J. L. G., *J. Catal.* **159**, 150 (1996).
12. Lietti, L., and Forzatti, P., *J. Catal.* **147**, 241 (1994).
13. Jacobs, P., *in* "Characterization of Heterogeneous Catalysts" (F. Delannay, Ed.), Dekker, New York, 1984.
14. Gates, B., "Catalytic Chemistry" John Wiley and Sons Inc, New York, 1992.
15. Kalinitchev, A. I., *Russian Chemical Reviews* **65**(2), 95 (1996).
16. Allen, D., and Hayhurst, A. N., *J. Chem. Soc., Faraday Trans.* **92**(7), 1227 (1996).
17. Katsanos, N. A., *J. Chem. Soc., Faraday Trans.1* **78**, 1051 (1982).

18. Karaiskakis G., Katsanos N. A., Georgiadou I., and Lycourghiotis A., *J. Chem. Soc., Faraday Trans.1*, **78**, 2017 (1982).

19. Karaiskakis, G., Lycourghiotis, A., and Katsanos, N. A., *Chromatographia* , **15**, 351 (1982).

20. Kotinopoulos, M., Karaiskakis G., and Katsanos, N. A., *J. Chem. Soc., Faraday Trans. 1*, **78**, 3379 (1982).

21. Karaiskakis, G., Katsanos N. A., and Lycourghiotis A., *Can. J. Chem.* **61**, 1853 (1983).

22. Katsanos N. A., and Karaiskakis, G., *Adv. Chromatogr.* **24**, 125 (1984).

23. Katsanos, N. A., Karaiskakis G., and Niotis, A., "Proc. 8th Intern. Congress on Catalysis", Vol. III, p.143, West Berlin, 1984.

24. Karaiskakis, G., and Katsanos, N. A., "Proc. 3rd Mediterranean Congress on Chemical Engineering", p. 68, Barcelona, Spain, 1984.

25. Katsanos, N. A., and Kotinopoulos, M., *J. Chem. Soc., Faraday Trans.1* **81**, 951 (1985).

26. Katsanos, N. A., Karaiskakis, G., and Niotis, A. *J. Catal.* **94**, 376, (1985).

27. Dalas, E., Katsanos, N. A., and Karaiskakis, G., *J. Chem. Soc., Faraday Trans.1*, **82**, 2897, (1986).

28. Katsanos, N. A., "Symposium on New Methods of Catalyst Preparation and Characterization", RSC, Brunel University, 1987, *Catalysis Today* **2**, 605 (1988).

29. Ioffe, B. V., Katsanos, N. A., Kokovina, L. A., Marinichev, A. N., and Stolyarov, B. V., *Kinetika i Kataliz* **28**, 805 (1987).

30. Kapolos, J., Katsanos, N. A., and Niotis, A., "17th Intern. Symposium on Chromatography", Vienna, 1988, *Chromatographia* **27**, 333 (1989).

31. Katsanos, N. A., Karaiskakis, G., and Vassilakos, Ch., "Intern. Symposium on Surface Chemistry, Adsorption and Chromatography", Moscow, USSR, 1988, *Pure Appl. Chem.* **61**, 2057 (1989).

32. Katsanos, N.A., and Kapolos, J., "Hydrotreating Catalysts, Proc. Annual Intern. AIChE Meeting", Washington DC-U.S.A. 1988 (Occelli, M. L., and Anthony, R. G., Eds.), p. 211, Elsevier, Amsterdam, 1989.

33. Niotis, A., and Katsanos, N. A., *Chromatographia* **34**, 398 (1992).

34. Topalova, I., Niotis, A., Katsanos, N. A., and V. Sotiropoulou, *Chromatographia* **41**, 227 (1995).

35. Katsanos, N. A., and Vassilakos, Ch., *J. Chromatogr.* **557**, 469 (1991).

36. Kalantzopoulos, A., Roubani-Kalantzopoulou, F., Kapolos, I., and Katsanos, N. A., "Proc. 4th Panhellenic Symposium on Catalysis", p. 45, Papigo, Greece, 1995.

37. Arvanitopoulou, E., Katsanos, N. A., Metaxa, H., and Roubani-Kalantzopoulou, F., *Atmos. Environ.* **28**, 2407 (1994).

38. Katsanos, N. A., Roubani-Kalantzopoulou, F., *J. Chromatogr. A* **710**, 191 (1995).

39. Sotiropoulou, V., Katsanos, N. A., Metaxa H. and Roubani-Kalantzopoulou, F., *Chromatographia* **42**(No 7/8), 441 (1996).

40. Sotiropoulou, V., Vassilev, G. P., Katsanos, N. A., Metaxa, H., and Roubani-Kalantzopoulou, F., *J. Chem. Soc. Faraday Trans.* **91**, 485 (1995).

41. Gruber, H. L., *Anal. Chem.* **34**, 1828 (1962).

42. Gaworska-Galas, Z., and Wrzyszcz, J., *Int. Chem. Eng.* **6**, 604 (1966).

43. Eberly, P. E. Jr., and Spencer, E. H., *Trans. Faraday Soc.* **57**, 287 (1961).

44. Eberly, P. E. Jr., *J. Phys. Chem.* **65**, 68 (1961).

CONTENTS

Author Index (Volume 26, 1997)

Key Words (Volume 26, 1997)

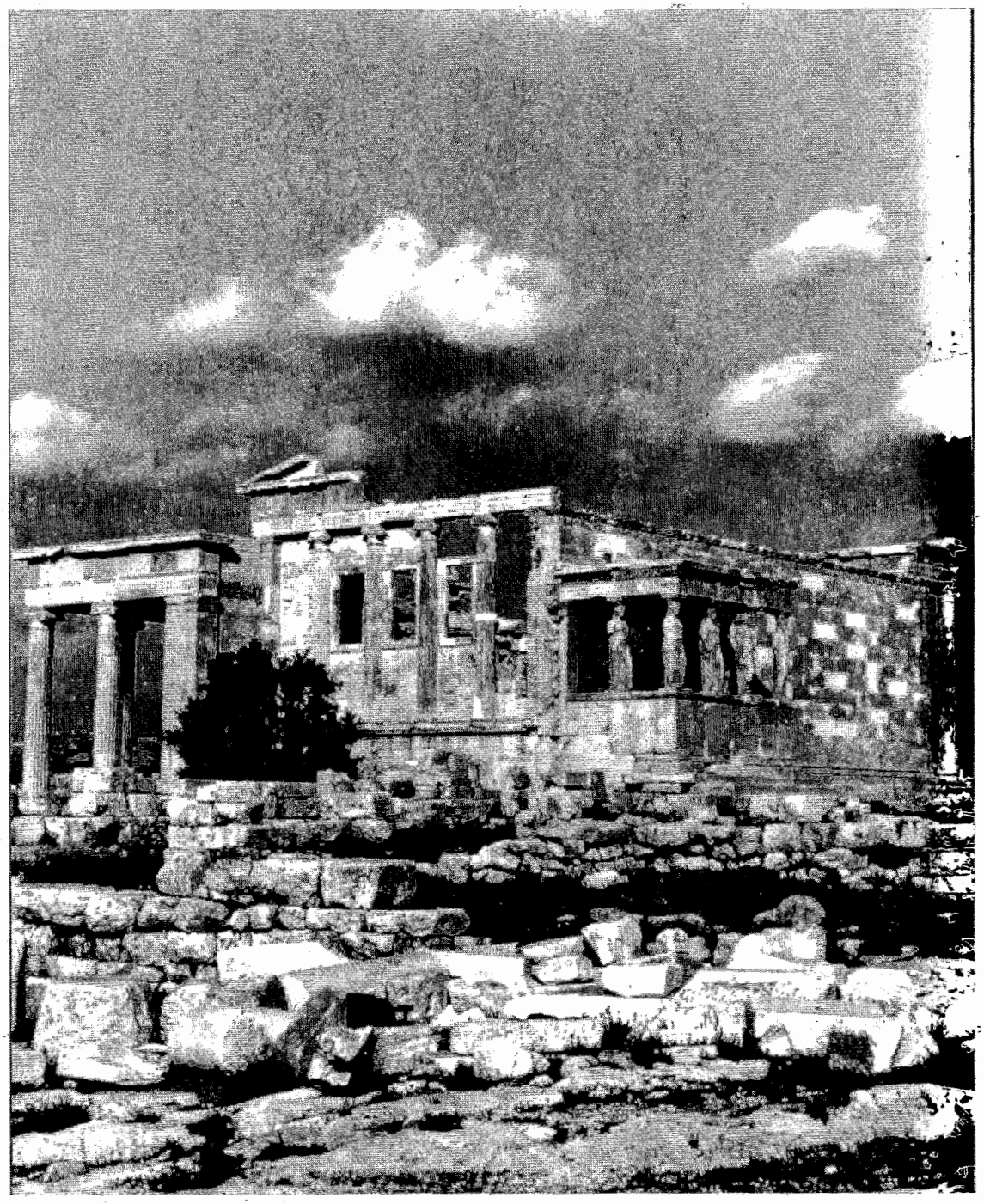

ΕΡΕΧΘΕΙΟΝ

ΟΛΥΜΠΙΑΚΗ ΑΕΡΟΠΟΡΙΑ

Hellas

ΕΛΛΗΝΙΚΟΣ ΟΡΓΑΝΙΣΜΟΣ ΤΟΥΡΙΣΜΟΥ